NOTICE

The quality of this microform is heavily dependent upon the quality of the original thesis submitted for microfilming. Every effort has been made to ensure the highest quality of reproduction possible.

If pages are missing, contact the university which granted the degree.

Some pages may have indistinct print especially if the original pages were typed with a poor typewriter ribbon or if the university sent us an inferior photocopy.

Reproduction in full or in part of this microform is governed by the Canadian Copyright Act, R.S.C. 1970, c. C-30, and subsequent amendments.

AVIS

La qualité de cette microforme dépend grandement de la qualité de la thèse soumise au microfilmage. Nous avons tout fait pour assurer une qualité supérieure de reproduction.

S'il manque des pages, veuillez communiquer avec l'université qui a conféré le grade.

La qualité d'impression de certaines pages peut laisser à désirer, surtout si les pages originales ont été dactylographiées à l'aide d'un ruban usé ou si l'université nous a fait parvenir une photocopie de qualité inférieure.

La reproduction, même partielle, de cette microforme est soumise à la Loi canadienne sur le droit d'auteur, SRC 1970, c. C-30, et ses amendements subséquents.

Gas Adsorption With Molecular Sieve Zeolites

Georgia Apolonatos

A thesis submitted to the Department of Chemical Engineering
at the University of Ottawa
in partial fulfillment of the requirements
for the degree of M. A. Sc. in Chemical Engineering

ISBN 0-315-68039-3

UNIVERSITÉ D'OTTAWA
UNIVERSITY OF OTTAWA

Abstract

Adsorption kinetics and equilibrium of CH_4, CO and N_2 gases were studied on various molecular sieve zeolites. Ethylene was also tested, yet was found to be incompatible with the molecular sieves under consideration. The gas chromatographic technique was chosen as the method of studying the adsorption by which equilibrium and kinetic parameters are derived by matching the response peak to appropriate mathematical models.

It was found that the synthetic zeolites (H-Mordenite, 4A zeolite, 5A zeolite) rather than naturally occurring Chabazite had a higher capacity for the adsorption of all three gases. Pure and binary gas isotherms of CH_4 and CO with molecular sieve 5A were also studied for the separation of these gases. These isotherms indicated that under the present conditions CO is preferentially adsorbed on the 5A zeolite and the adsorption capacity of the sieve increases with decreasing temperature.

Acknowledgement

The author would like to express her sincere gratitude to Dr. H. Tezel for her insight, guidance and assistance throughout the course of this study. She would also like to extend a thank-you to Dr. W. Hayduk for his encouragement in pursuing the degree of M.A.Sc in Chemical Engineering at the University of Ottawa.

The help and collaboration of Mr. J. Gasperetti, Mr. L. Tremblay and Mr. A. Bonaldo of the machine shop was also greatly appreciated as was the assistance of fellow graduate students.

Contents

List of Tables

List of Figures

Nomenclature

The various symbols used in this work are summarized below.

Symbols

A_{-1}, A_0, A_1, A_2, A_3	Coefficients of equation 4.30 and 4.31
B_0, B_1, B_2	Coefficients of equation 4.28 and 4.32
C_0, C_1, C_2	Coefficients of equation 4.29 and 4.33
c	Sorbate concentration in macropores
C	Sorbate concentration in bulk phase
D_c	Micropore diffusivity
D_L	Axial dispersion coefficient
D_M	Molecular diffusivity
D_p	Macropore diffusivity
D_0	Temperature independent constant ($D_c = D_0 \exp(-E_a/RT)$)
E_a	Diffusional activation energy

Nomenclature

ΔH_0	Limiting heat of adsorption
k	External mass transfer coefficient
K	Equilibrium constant based on sorbate concentration in a pellet of sieve (Binary Isotherms) (dimensionless)
K_c	Sorption equilibrium constant based on sorbate concentration in zeolite crystal (dimensionless)
K_p	Equilibrium constant based on sorbate concentration in a pellet of sieve (dimensionless)
K_p'	Apparent equilibrium constant based on sorbate in a pellet of sieve (Pure Isotherms) (dimensionless)
K_0	pre-exponential factor in $K_p = K_0 exp(-\Delta U_0/RT)$
L	Length of chromatographic column
m_n	n^{th} moment integral defined by equation 4.13
MW	Molecular weight
N_{Sh}	Sherwood number
p	Laplace transform variable
P	Total pressure
p_i	Partial pressure of component i (i=1, 2)
q	Local sorbate concentration in a zeolite crystal
$\overline{q}$	Average sorbate concentration for a crystal

q_i	Amount of component i adsorbed in pellet (i=1, 2)
Q	Sorbate concentration in a pellet
$\overline{Q}$	Sorbate concentration averaged over a pellet
r	Radial coordinate for zeolite crystal
R	Radial coordinate for zeolite pellet
r_c	Radius of zeolite crystal
R_p	Pellet radius
t	Time
T	Temperature
ΔU_0	Internal energy change of sorption
v	Interstitial velocity
w	Volume fraction of zeolite crystals to total solid material in a pellet
x	Number of silica molecules found in a unit cell of zeolite
X_i	Mole fraction of component i in adsorbed phase Mixed Carrier Gas Systems)
y	Number of water molecules found in a unit cell of zeolite
Y_i	Mole fraction of component i in bulk gas phase Mixed Carrier Gas Systems)
z	Distance measured from bed entrance

Greek Letters

β	Parameter in equation 4.34
$\delta(t)$	Pulse function
ϵ	Void fraction of bed
θ	Void fraction of pellet
μ	First moment of response peak
ρ_b	Bed density
ρ_p	Pellet density
σ^2	Second moment of response peak
τ	Tortuosity factor

Chapter 1

Introduction

Determination of transport properties and gas-solid adsorption equilibria is a crucial step in designing gas separation units and heterogenous chemical reactors. Kinetic and equilibrium parameters have to be determined before any design calculations can be carried out. The objective of this study is to determine equilibrium constants, diffusivities, as well as pure and binary isotherms of gases with solid adsorbents.

Commercial adsorbents which exhibit ultraporosity and which are generally used for separation of gas and vapor mixtures include the activated carbons, activated clays, inorganic gels and activated alumina. These materials however, do not possess an ordered crystal structure and consequently the pores are non uniform. The distribution of pore diameters may be narrow (20-50Å) or it may range widely (20 to several thousand Å) as is the case for some activated carbons. Molecular sieve zeolites, on the other hand, have pores of uniform size (3Å-10Å) [6].

The adsorptive properties of naturally occurring zeolites were initially investigated by Barrer in the 1930's [25]. As a direct result of his research Linde Company, a division of Union Carbide became interested in the application of natural zeolites

to the company's gas-separation operations. However, it soon became apparent that although the zeolites performed the desired separations, the availability of the natural zeolites was inadequate for any large scale commercial application. By the mid fifties the scientists at the Linde company had successfully embarked on a program to synthesize molecular sieve zeolites. Some of these zeolites were analogous to the naturally occurring ones while others had completely new compositions, 'tailor made' for a particular separation. The advantage of these synthetic zeolites was that they could be produced in abundance at a fairly economical cost [39].

Even though initial interest in molecular sieve zeolites was high it was not until the early and mid seventies that they began being considered as possible adsorbents. Such companies as Procter & Gamble and Texaco began using zeolites for such diverse applications as the replacement of polyphosphates in detergents to n-paraffin separation for the improvement of octane number in gasoline [34]. By the late seventies zeolitic materials were being used extensively in the petroleum industry. By 1977 an excess of four million barrels of oil per day were produced in the United States using cracking catalysts containing molecular sieve zeolites [6]. Interest lay mainly with large port zeolites, in particular the faujasite-type (zeolites X and Y) that were proving to have a widespread application in the gas and oil industry, not only in catalytic operations but also for hydrocarbon separation and purification processes [26]. In the early eighties the potential of zeolites for air pollution abatement began being investigated. Such zeolites as the mordenites and type A were suggested as possible adsorbents for the removal of CO_2, SO_2 and NO_x from industrial streams [36]. Molecular sieve zeolites have also found applicability in the separation of industrial streams such as the oxygen enrichment of air by the selective adsorption of nitrogen [33].

Zeolites have gained a wider acceptance in industry due to their following adsorptive properties [33]:

1. large adsorption capacity
   - these materials all have a high internal surface area available for adsorption due to the pores which uniformly penetrate the entire volume of the solid. The external surface area of the adsorbent contributes only a small amount (approximately 0.5%) to the total available surface area [18].
2. adequate adsorption and desorption rates
3. selective adsorption of molecules based on molecular dimensions
4. highly preferential adsorption of polar molecules
5. highly hydrophilic surface
6. variation of properties by ion exchange

In addition they exhibit:

1. thermal, hydrothermal and chemical stability
2. low catalytic activity (without ion exchange)

3. physical strength

4. attrition resistance

5. good ability to be regenerated and reused

More important though, is that the use of zeolites as adsorbents in existing plant equipment requires little or no modification to the processes thus making the economics favorable.

This study concentrates primarily on testing four different zeolites (H-Mordenite, 4A zeolite, 5A zeolite and Chabazite) for the separation of CH_4, CO, and N_2 gases.

Chapter 2

Zeolites

2.1 Stucture and Chemistry

Molecular sieve zeolites are crystalline, hydrated aluminosilicates of Group I and Group II elements (i.e. sodium, potassium, magnesium, calcium, strontium and barium). They consist of a well developed, uniform intracrystalline pore structure (micropores) that is in turn bonded together into granules providing a second type of pore distribution (macropores). They are thus described by a bidispersed pore model as illustrated in Figure 2.1 [29]. Molecular sieve pellets used industrially consist of particles of the zeolite crystal embedded in a matrix of clay. These pellets have approximately a 1 mm radius. They consist of crystals whose radii generally range between 50-100 microns. These crystals are in turn composed of channels with radii in the angstrom level. Adsorption in the crystals is preceded by mass transfer in the macropores and by transport through the micropore network [23]. Extensive studies performed by Ruthven and Loughlin [47] on the sorption and diffusion of n-butane in Linde 5A molecular sieve suggest that there is no significant difference between the sorptive properties of pelleted zeolite and Linde 5A zeolite crystals. The

clay binder acts merely as an inert diluent with no effect on either the equilibria or kinetics of the sorption process.

The primary structural units of zeolites are the tetrahedra of silicon and aluminum. These units are assembled into secondary polyhedral building units such as cubes, hexagonal prisms, octahedra and truncated octahedra. The silicon and aluminum atoms are located at the corners of the polyhedra and are joined by a shared oxygen atom. The final zeolite structure is an assemblage of the secondary units in a regular, infinitely extending, three-dimensional, crystalline network.

Each aluminum atom in the framework introduces one negative charge which is balanced by an exchangeable cation. A unit cell of a zeolite may therefore, be represented by the empirical formula [9]:

$$M_{2/n}\ O\ -\ Al_2O_3\ -\ xSiO_2\ -\ yH_2O$$

where M is the compensating cation in the system with valency n.

Various factors influence the adsorption properties of zeolites. Among these are:

1. the size of the pore channels

2. the type of channel network

3. the silica-alumina ratio of the zeolite

The inner atoms in the windows of the intracrystalline channel structure are generally oxygen, thus the size of the windows is in part determined by the number of oxygen atoms in the ring. Intracrystalline diffusivity and hence kinetic selectivity are mainly determined by the free diameters of these windows. Though, due to the effects of vibration of both the diffusing molecule and the crystal lattice, these

windows may be penetrated by molecules with critical kinetic diameters greater than the free diameter of the window. The adsorptive properties of a particular zeolite are also determined by the nature of the cation present in the crystal network, their number per unit cell and by the positions they occupy. Studies conducted by Tsitshvilli and Andronikashvili [58] on types A, X and Y zeolites in part indicated that the adsorption capacity for H_2O vapor decreased linearly as the sodium ion was replaced by thallium in the type A zeolite whereas an equal replacement of sodium ions by lanthanum ions had little effect. Zeolites X and Y showed a reverse trend, the presence of lanthanum ions promoted an increase of water vapor adsorption. They concluded that in the type A zeolite the cations occupy positions in the entering windows decreasing the effective diameter, thus causing a decrease in the adsorption capacity and diffusion coefficients. In zeolites X and Y a decrease of cation density takes place because of the decationization of certain positions by ion exchange thus providing larger openings to the windows.

The interactions between the cations in the cage and the gas molecules is also an important factor that affects the diffusional resistance. Work performed by Ma and Mancel [36] has shown that the effective diffusion coefficient for NO_2 is approximately the same in 5A and 13X sieves while that of CO_2 is smaller in the 13X sieve than it is in the 5A sieve. It would be expected that as the pore size increased from the 5A zeolite to the 13X zeolite the diffusion coefficients would also increase. It was concluded that the observed results were due to the interaction between the surface and the gases.

Though zeolites, both natural and synthetic have a strong affinity for water, the silica to alumina ratio (SiO_2/Al_2O_3) in each framework determines whether the adsorbent will have a hydrophobic or hydrophilic surface. A study performed by Chen [10] showed that the dealuminization of mordenite caused the zeolite to become hydrophobic. Dealuminized mordenites with a SiO_2/Al_2O_3 ratio $\geq$ 80 adsorbed little

or no water at all. Thus the silica-alumina ratio determines the preferential adsorption of certain molecules.

Another factor that affects the performance of zeolites is the type of channels that are present. Zeolites may have one-, two-, or three- dimensional channels. A one dimensional system consists of channels that are parallel and permit flow in one direction. A two dimensional system consists of main channels linked together by smaller channels, thus permiting flow in two directions. There are two types of three dimensional, intersecting channels. In one type the channels are equidimensional, that is the free diameter of all channels is equal regardless of direction. The second type of system consists of three-dimensional, intersecting channels whose free diameter depends on crystallographic direction.

The type of channels present has an effect on both the diffusivity of a molecule in a perspective zeolite and the zeolite's adsorption capacity. For example, ideally, large three-dimensional channels of equal diameter would permit very rapid diffusion [7]. In the petroleum industry where coke formation on the zeolite pores is sometimes a problem, one would prefer a three-dimensional channel network to a one-dimensional network. The adsorption capacity of a one-dimensional zeolite would become hindered very rapidly by the coke formation.

A diagrammatic representation of two different types of zeolite channels is given in Figure 2.2 [43]. The first sketch represents the three dimensional channel structure of zeolite ZSM-5 and the second sketch illustrates the two dimensional channel network of molecular sieve ZSM-11.

Thus by an appropriate choice of framework structure, SiO_2/Al_2O_3 ratio and cationic form, zeolites not only offer a class of adsorbents with widely different adsorptive properties but they also offer the possibility of tailoring the adsorptive properties to achieve the selectivity required for a particular separation.

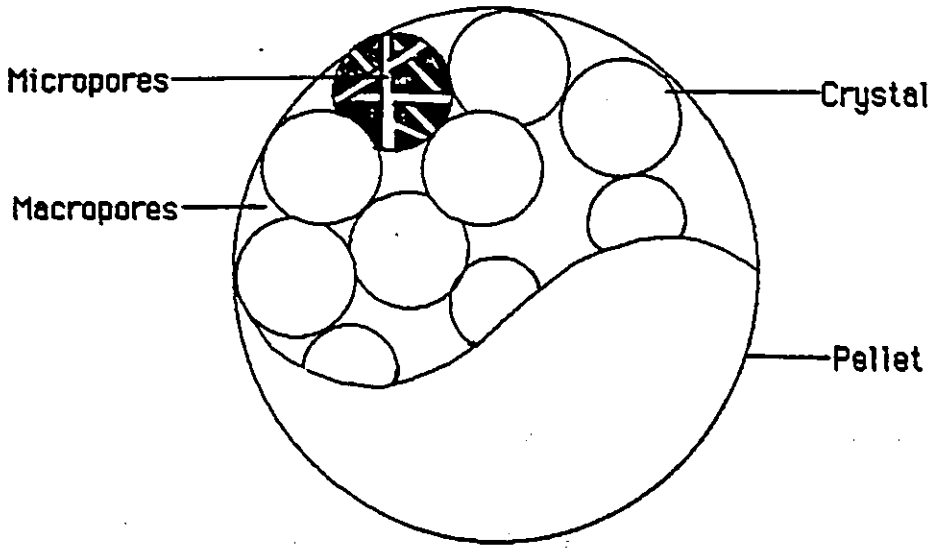

Figure 2.1: Schematic representation of zeolite pellet (Bidispersed Pore Model)

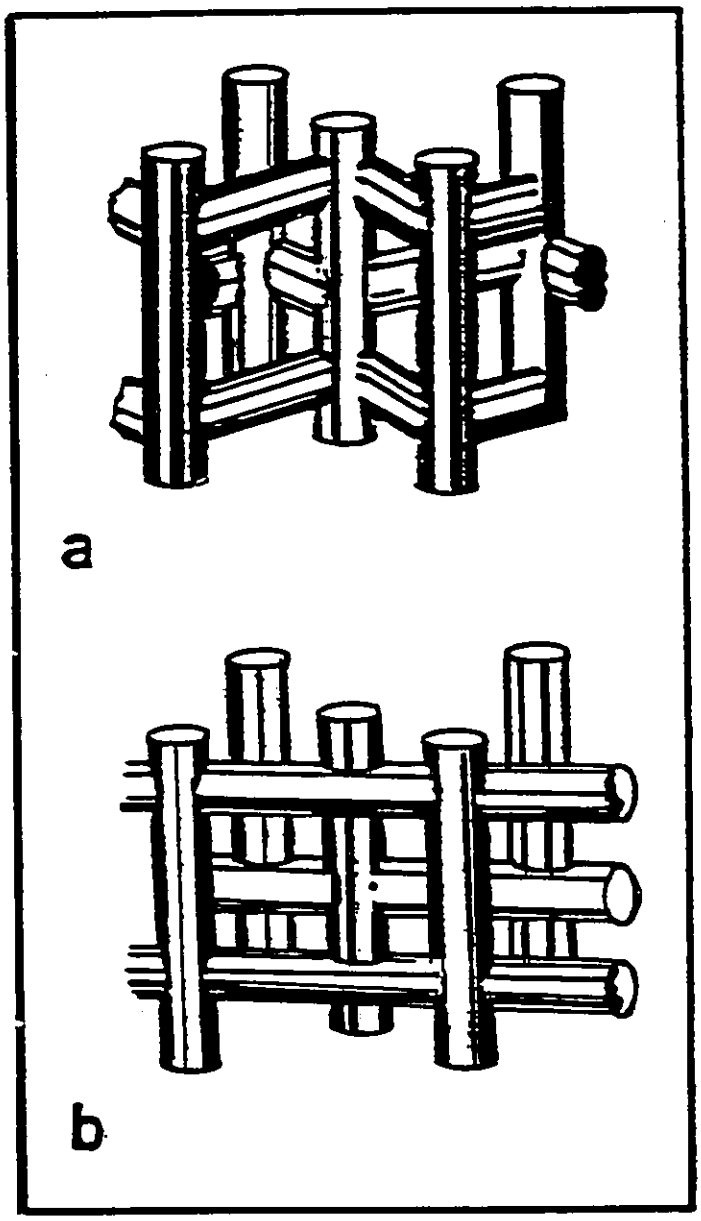

Figure 2.2: Channel structure of molecular sieve zeolites (a) ZSM-5 (b) ZSM-11

2.2 Mordenite

Mordenite is a high silica, orthorhombic zeolite with a SiO_2/Al_2O_3 ratio of approximately 5.0. The basic building unit of mordenite consists of five linked tetrahedra. As determined by Meier [35], whose studies were conducted on natural mordenite samples, the unit cell of Na-Mordenite has dimensions of a=18.13 Å, b=20.49 Å and c=7.52 Å.and is structurally represented by the empirical formula:

$$Na_8\ Al_8\ Si_{40}\ O_{96}\ -\ 24\ H_2O$$

Natural mordenite has a kinetic diameter of approxiamately 3.9 Å.

The hydrogen form of mordenite is achieved through the partial removal of sodium cations from the mordenite framework. Hydrogen atoms then act as the cations.

Extensive studies on Mordenite were first performed by Barrer in the 1940's [2], [4] who reported on the ion exchange properties of the zeolite as well as the adsorption properties of natural mordenite containing sodium, calcium and potassium. By 1954 Barrer had studied the channel structure of natural mordenite and had concluded that due to the fact that there is only one diffusion path available, molecules having a critical diameter greater than 4 Å are not adsorbed by mordenite. He drew his conclusions on the basis that molecules having cross-sections smaller than 3.0 Å, like oxygen and nitrogen were quickly adsorbed by dehydrated mordenite whereas, larger molecules such as ethane and methane were slowly occluded [1]. Union Carbide began manufacturing mordenite under the trade name Zeolon in the 1950's. Synthetic mordenite is also referred to as large-port mordenite because it has a kinetic diameter in the range of 5.0 - 7.0 Å [42]. Mordenite is a unidimensional zeolite and its structure is illustrated in Figure 2.3 [8].

Synthetic hydrogen mordenite (Zeolon-H) was one of the zeolites used in this study.

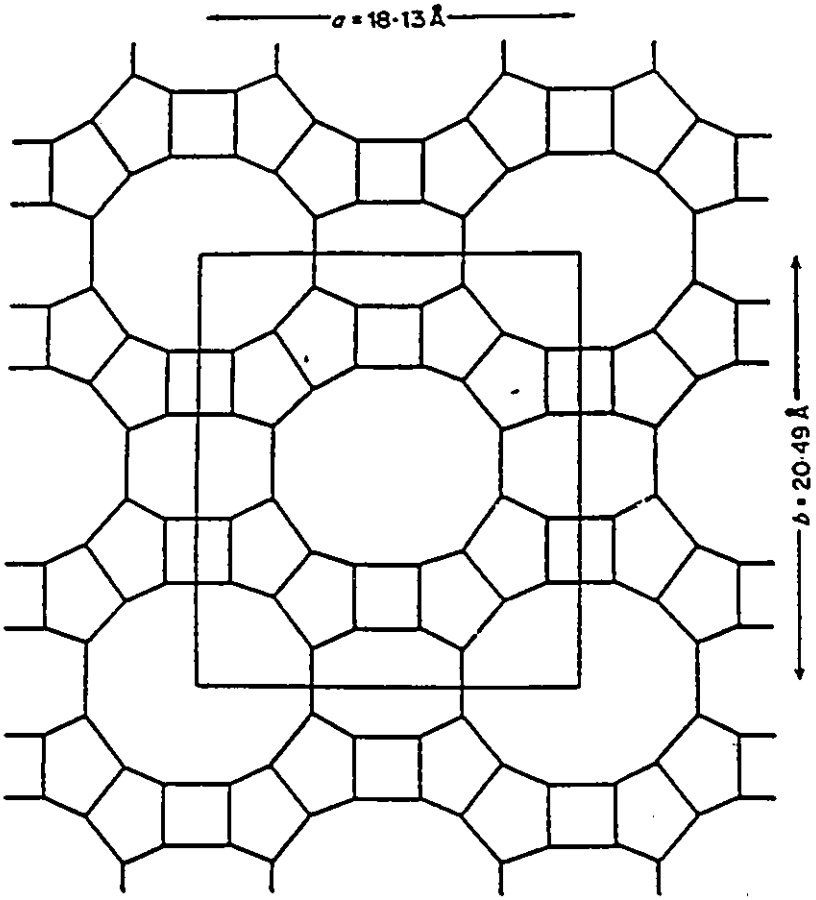

Figure 2.3: Schematic representation of Mordenite Structure

2.3 Type A

The type A zeolites are unique in that they do not have a naturally occurring counterpart. They are the invention of Union Carbide. Type A synthetic zeolites have been available commercially since 1954 and have found extensive practical use in separation, drying and purification of gases [39].

The structural unit in type A zeolite is the truncated octahedron or sodalite cage. The unit cell as shown in Figure 2.4 [8], consists of eight sodalite cages located at the corners of a cube, joined through four membered oxygen rings. The unit cell contains 24 tetrahedra, 12 AlO_4 and 12 SiO_4. When fully hydrated 27 water molecules are contained in the central cavity of the unit cell and the smaller sodalite cages. The free diameter in the central cavity is 11.4 Å, and is entered through six eight membered oxygen rings with a minimum diameter of 4.4 Å. The SiO_2/Al_2O_3 ratio of zeolite A is 1.0 and therefore 12 univalent exchangeable cations are present per unit cell. It is represented by the empirical formula [43]:

$$Na_{12}(AlO_2)_{12}(SiO_2)_{12} \text{ - } 27\ H_2O$$

In the sodium form of type A zeolite (zeolite 4A) there are twelve sodium cations per cage. These twelve cations are located near the 'entering' of the windows thus causing the channels to be partially obstructed. The effective diameter is thus reduced from 4.4 Å to approximately 3.8 Å (= 4 Å, hence the labelling).

As reported by Breck [6], the calcium form of type A zeolite (zeolite 5A) has pore openings of 5.0 - 5.6 Å that lead into cavities of about 11.4 Å in diameter. Zeolite 5A is achieved by exchanging forty percent or more of the univalent sodium cations with divalent calcium ions. This decreases the number of cations present per unit cell thus increasing the effective apperture from 4.4 Å to approximately 5.0 Å [34]. The type A zeolites have three-dimensional channels of equal dimensions.

Many papers have described the behavior of type A zeolites in seperation processes, but detailed adsorption studies of single permanent gases C_1- and C_2- hydrocarbons have been less cumbersome [10] [13] [19] [18] [21] [41] [43] [44] [48] [50] [58].

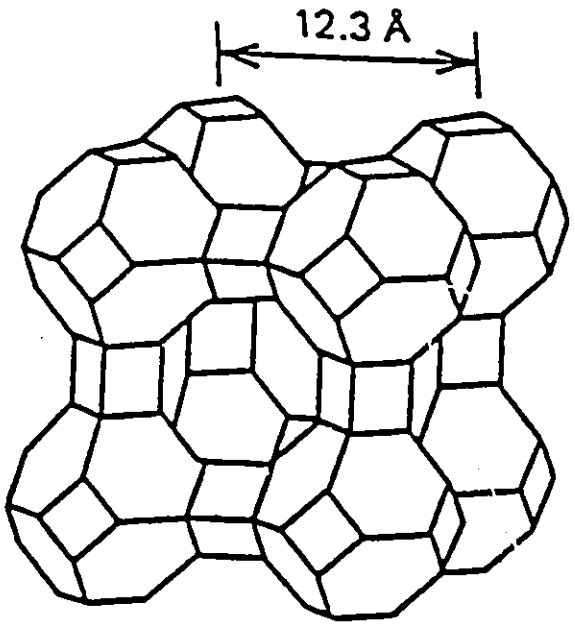

Figure 2.4: Schematic representation of Type A Zeolite Structure

2.4 Chabazite

Chabazite is a naturally occuring zeolite with a rhombohedral crystal form. It was first studied by Lamb in 1936 [29] who with no knowledge of the exact crystal structure, made a careful study of the adsorption capacity of chabazite for H_2, O_2 and CO_2 as it is progressively dehydrated. They found that slightly dehydrated chabazite exhibits a pronounced specificity of adsorption toward all three gases. Their results can be explained in that pre-treatment of the zeolite causes not only the removal of water molecules but also the removal of extraneous material found in the chabazite structure. The removal of impurities results in larger channels more easily accessible to the molecules.

The crystal structure of chabazite was first determined by Dent and Smith in 1958 [11]. The framework can be viewed as parallel six membered rings linked by four membered rings. The structure is illustrated in Figure 2.5 [42]. Chabazite has a kinetic diameter of approximately 4.3 Å.

The cage forms channels of hexagonal symmetry with inner dimensions of 10.0 x 6.6 Å. These channels are interconnected by six membered and eight membered oxygen rings with approximate open diameters of 2.7 Å and 3.7 x 4.2 Å respectively. The unit cell of chabazite has a total of twelve aluminum and silicon atoms and when fully hydrated holds thirteen water molecules. It is represented by the formula,

$$Ca_2\ Al_4\ Si_8\ O_{24}\ -\ 13\ H_2O$$

The unit cell dimensions are, a=13.78 Å and c=15.06 Å.

Though the most frequent cation is calcium, samples have been found containing three sodium cations per unit cell. Potassium, barium and serium cations have also been reported though less frequent [36]. The SiO_2/Al_2O_3 ratio in chabazite varies between 1.0 - 3.0. It has an almost total disorder in the tetrahedral sites. Natural chabazites show considerable variation in cation content and SiO_2/Al_2O_3

ratio. They also exhibit framework distortion upon dehydration. Though chabazite has an inherent rigid framework which does not collapse upon continuous dehydration the calcium ions tend to move within the cavities [57]. Chabazite has a three-dimensional channel network of equal diameters. A sodium chabazite under the trade name Chabsorb was used in this study.

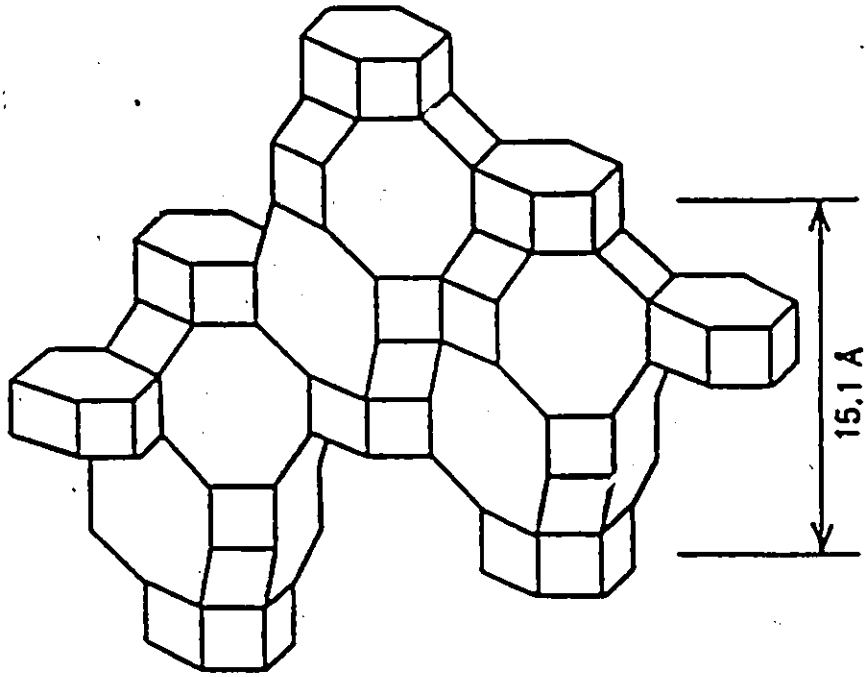

Figure 2.5: Schematic representation of Chabazite Structure

Chapter 3

Study of Adsorption

3.1 Theoretical Approach

The study of adsorption on solids may be approached in one of three manners:

1. the study of the gas (parameters such as pressure, concentration or composition are measured) thus permitting the determination of the amount of substance in the adsorbed layer and its composition.

2. the study of the solid phase, determining the influence of adsorption on the mechanical, thermal, electrical and magnetic properties of the solid phase.

3. the study of the adsorbed layer in terms of the interaction of protons, electrons, ions or atoms with the adsorbed layer.

In this study approach number one was deemed the simplest and most efficient method by which to understand the physical adsorption that is occurring in the solid-gas systems.

3.2 Adsorption Techniques

Three methods are available when conducting adsorption studies on zeolites. These are:

1. Gravimetric Method

2. Volumetric Method

3. Chromatographic Method

3.2.1 Gravimetric Method

In this technique the weight of the adsorbate together with the weight of the adsorbent is determined by using either a spring-type or beam-type balance as illustrated in Figure 3.1 [40]. The principle of the gravimetric determination of the amount of gas adsorbed is identical for all gravimetric methods.

A given weight of adsorbent is placed on a balance and adsorbate is injected into the apparatus. As adsorption occurs the deviation of the balance from the 'zero' position (the initial position of the spring or beam before the introduction of adsorbate) and the force which causes the deviation is measured. The deviation from the 'zero' position is expressed in units of length or angle and related to the unit weight that causes the deviation.

The accuracy of this method depends on the sensitivity of the balance at a given load and the precision by which length or angle can be measured. Since the balances must be very sensitive to provide accurate measurements even very slight external forces can cause interference. Special care must be taken to eliminate these interferences (mounting of the balance, accounting for unwanted oscillations of the

balance during operation, buoyancy etc...) in order that they do not effect the accuracy of the experimental measurements.

Gravimetric methods have a number of advantages for adsorption studies. The main advantage being that the amount of gas adsorbed or desorbed is measured directly. The main disadvantage of the gravimetric techniques is the complicated and precise design of the balances and the complicated mode of operation, especially with high-sensitivity balances. Another disadvantage is the susceptibility to external forces.

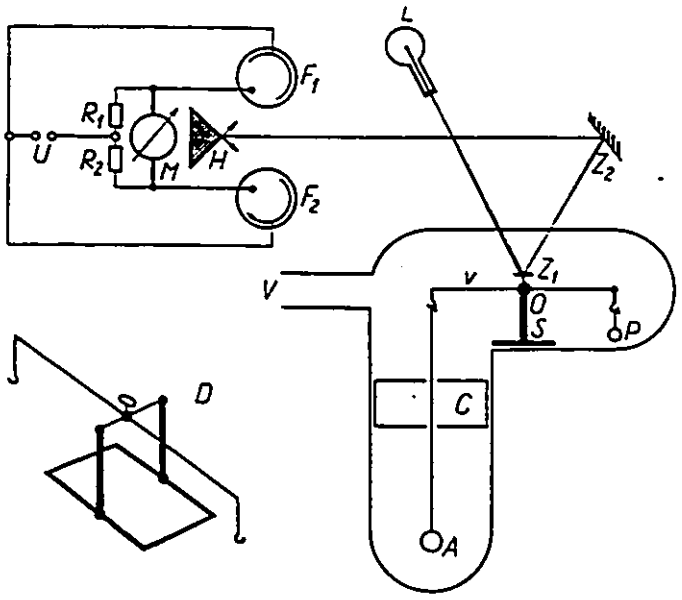

S, support; *O*, axis in which the beam
is pivoted (also the projection of the torsion filament); Z_1 and Z_2, mirrors; *P*, counterweight; *A*, vessel containing the adsorbent; *C*, thermal shield; *V*, connection to the rest of the apparatus; F_1 and F_2, photocells; *H*, reflecting prism; *M*, measuring instrument (or amplifier with recorder); R_1 and R_2, Ohmic resistors; *U*, d.c. voltage source; *L*, light source; *D*, an example of a beam mounting

Figure 3.1: Conventional gravimetric apparatus for studying adsorption (Beam-type torsion balances)

3.2.2 Volumetric Method

With volumetric methods the amount of gas adsorbed is determined from the variation of the gas pressure in a known volume. Two basic conditions must be satisfied when undertaking these methods. Firstly, the gas being studied should only be adsorbed on the surface of the adsorbent being tested and secondly, there should be no source of gas in the apparatus prior to injection.

The amount of gas adsorbed or desorbed is determined as the difference between the amount of gas in the gas phase and in the total volume of the apparatus before and after adsorption or desorption has occured. As in the case of gravimetric methods the amount of gas adsorbed may be determined by volumetric means in both static and dynamic types of apparatus.

The accuracy of volumetric techniques depends on the accuracy of the gas pressure measurement and the accuracy by which the volume not filled by the mass of the adsorbent is calibrated. The ratio of the amount of gas in the dead space to the amount of gas adsorbed must also be considered if the results are to be accurate. This technique is illustrated in Figure 3.2 [40].

The main advantage of volumetric methods is that there exists the possibility of combining these techniques with other methods of studying adsorption. The main disadvantage is that one has to wait a sufficient time before any equilibrium pressure can be read and once again a high degree of accuracy is required for the experimetnal data to be representative of the system.

The conventional gravimetric and volumetric methods work best for relatively slow diffusion and at moderate temperatures and pressures. Most early diffusion studies on zeolites were done by either a constant pressure or a constant volume technique as briefly summarized by Barrer [3].

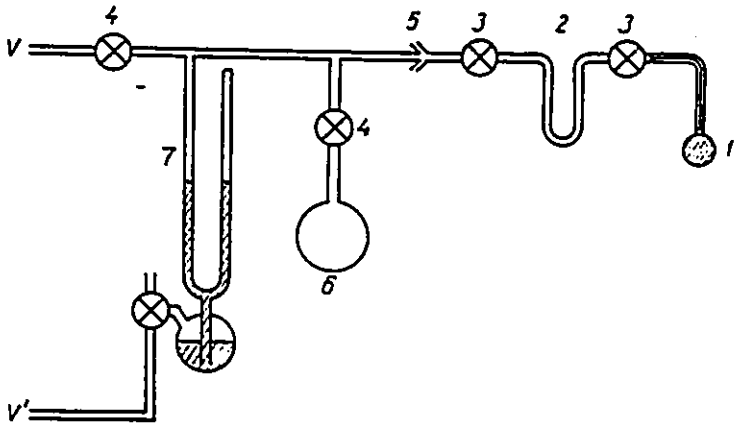

V, connection to high-vacuum pump; *V'*, connection to auxiliary vacuum pump; *1*, adsorption vessel; *2*, cold trap; *3*, high-pressure valves; *4*, ordinary valves (for example, greased valves); *5*, ground glass joint; *6*, gas reservoir; *7*, U-shaped manometer. (Only the part of the apparatus to the right of the ground glass joint must be capable of high-pressure operation)

Figure 3.2: Conventional volumetric apparatus of studying adsorption (Apparatus for studying high-pressure adsorption)

3.2.3 Gas Chromatography

Gas chromatography offers an alternative approach to the gravimetric and volumetric methods for the experimental studies of the kinetics and equilibria of adsorption. It is less cumbersome than other unsteady state adsorption techniques and is applicable to a wider range of diffusivities. It is also more easily extended to extreme conditions of temperature and pressure such as those encountered in commercial processes and can be easily extended to multicomponent systems. The technique is especially suitable for low sorbate concentration measurements of diffusion coefficients and estimation of heat of adsorption. Such information is extremely diffucult to obtain using conventional vacuum techniques of constant volume or constant pressure [24], [16]. In addition, the experimental set-up and the interpretation of the data are relatively simple and a large number of solid particles is normally used, providing a good representative specimen of solids under study.

The method consists of mixing the gas being studied with a stream of nonadsorbable carrier gas and transporting it through a packed bed of solids. The gas being studied is either injected in a single dose (elution chromatography) or continuously mixed in a constant ratio with the carrier gas (frontal chromatography). After being passed through the packed column the dispersion of the emergent peak is measured in the form of a chromatogram as illustrated in Figure 3.3. Where t represents time and d distance on the recorder paper.

Shah and Ruthven [51] have shown that both equilibrium isotherms and the time constants for zeolitic diffusion obtained from the chromatographic peaks agree well with values obtained previously by gravimetric methods. A comparative study performed by Ruthven and Kumar [46] indicated that single-component and binary adsorption equilibria obtained by the chromatographic method agrees well with previously obtained results by both the volumetric and gravimetric techniques.

However, certain restrictions exist in the application of this method [22]:

1. the gas concentration in the inlet pulse must be low enough that the reversible adsorption process is first order

2. the micropores of the zeolitic material must be large enough to have diffusivities sufficiently high to eliminate the possibility of a long tail on the response peak in the effluent from the bed

Elution gas chromatography was the experimental technique chosen for this study.

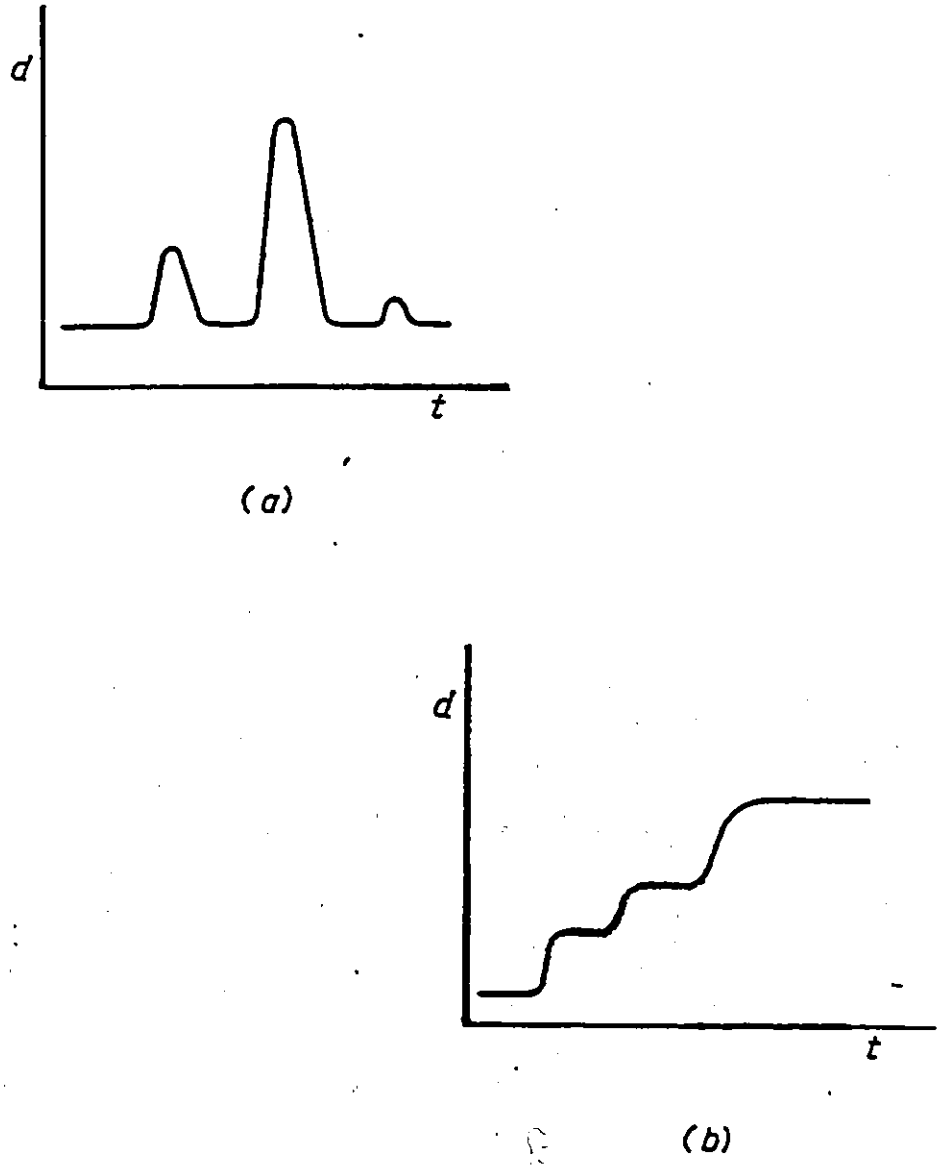

Figure 3.3: Gas chromatograms (a) elution chromatography (b) frontal chromatography

Chapter 4

Mathematical Model for Adsorption

When molecular sieve zeolites are used as adsorbents, a molecule entering a particle will encounter three distinct types of resistances. These are [35]:

1. mass transfer from the moving gas stream to the stationary stream

2. mass transfer within the macropore network of the granules to the external surface of the crystals

3. mass transfer within the micropore system

Haynes and Sarma [29] have discussed a model for the application of gas chromatography to measurements of diffusion in bidispersed structure particles. The model was extended by Shah and Ruthven [51]. Equilibrium and kinetic parameters are derived by matching the response peak to an appropriate mathematical model for the system.

4.1 Theory

The response of a molecular sieve column, subjected to an inlet pulse injection of sorbate at time zero is described by the following set of equations:

Micropore Diffusion

$$D_c\left(\frac{\partial^2 q}{\partial r^2}+\frac{2}{r}\frac{\partial q}{\partial r}\right)=\frac{\partial q}{\partial t} \tag{4.1}$$

$$q(r_c,t)=K_c c(R,t) \tag{4.2}$$

$$\frac{\partial q}{\partial r}(0,t)=0 \tag{4.3}$$

$$\overline{q}=\frac{3}{r_c^3}\int_0^{r_c} r^2 q\,dr \tag{4.4}$$

Macropore Diffusion

$$\theta D_p\left(\frac{\partial^2 c}{\partial R^2}+\frac{2}{R}\frac{\partial c}{\partial R}\right)=w(1-\theta)\frac{\partial \overline{q}}{\partial t}+\theta\frac{\partial c}{\partial t} \tag{4.5}$$

$$\frac{3k}{R_p}\left[C(z,t)-c(R_p,t)\right]=\frac{\partial \overline{Q}}{\partial t} \tag{4.6}$$

$$\frac{\partial c}{\partial t}(0,t)=0 \tag{4.7}$$

$$\overline{Q}=\frac{3w(1-\theta)}{R_p^3}\int_0^{R_p}\overline{q}R^2dr+\frac{3\theta}{R_p^3}\int_0^{R_p} cR^2dR \tag{4.8}$$

Column

$$D_L\frac{\partial^2 C}{\partial z^2}-v\frac{\partial C}{\partial z}-\left(\frac{1-\epsilon}{\epsilon}\right)\frac{\partial \overline{Q}}{\partial t}=\frac{\partial C}{\partial t} \tag{4.9}$$

$$C(z,0) = c(R,0) = q(r,0) = 0 \quad (or\ constant) \tag{4.10}$$

$$C(0,t) = C_0\delta(t) \quad (inlet) \tag{4.11}$$

$$C(\infty,t) = 0 \quad (infinite\ length) \tag{4.12}$$

Implicit to the derivation of these equations are the following assumptions:

1. linear isotherm

   - as concluded by Haynes and Sarma [29] this is a valid assumption for small injection volumes where because of the very low concentration the extent of surface coverage amounts to a few percentage of the monolayer. Schneider and Smith [50] have pointed out that slightly higher inlet pulse concentrations may be tolerated due to the rapid decline in pulse concentration once the pulse enters the column.

2. negligible pressure drop

   (i.e. constant flowrate)

3. diffusivity is independent of concentration

   (Fickian diffusion)

   - this assumption is valid as long as a dilute sample is injected into the bed entrance or in some other manner it is ensured that the system is only slightly perturbed from its steady state concentration [28]. Generally, according to

Shah and Ruthven [51] when the critical molecular diameter is small in comparison to the zeolite pore dimension the Fickian diffusivity is inversely proportional to the concentration whereas, when the molecular diameter and pore size are comparable the Fickian diffusivity is constant.

4. any deviations from plug flow in the column are adequately described by axial dispersion

Obtaining full solutions to these equations is difficult and should a solution be obtained it is rendered too complex to be of any practical use. Solutions are more easily obtained in the Laplace domain and expressions for the first and second moments (mean and variance) of the response peak may be derived directly from these solutions [28], [49]. The method of solution is similar to that employed by Suzuki and Smith [54] for a bed of monodispersed porous particles. The moments (m_n) of the effluent peaks from the bed are evaluated from the equation:

$$m_n = (-1)^n \lim_{p \to 0} \left(\frac{d^n C}{dp^n}(p, z) \right) \tag{4.13}$$

where,

$$m_n = \int_0^\infty C t^n dt \tag{4.14}$$

Thus, experimentally the first moment or mean (μ) is given by:

$$\mu = \frac{\int_0^\infty C t dt}{\int_0^\infty C dt} \tag{4.15}$$

and the second moment or variance (σ^2):

$$\sigma^2 = \frac{\int_0^\infty (t - \mu)^2 C dt}{\int_0^\infty C dt} \tag{4.16}$$

The mean and variance can therefore, be calculated by integration of the experimental chromatogram according to the above equations. In this study the integrations were performed by a computer program using Simpson's Rule.

4.2 Pure Gases

The procedure involves transforming equations 4.1, 4.5 and 4.9 into the ordinary Laplace domain with respect to time and solving the ordinary differential equations with the transformed boundary conditions [29].

Theoretically, for pure gases the first and second moments are given by the expressions [29]:

First Moment:

$$\mu = \frac{L}{v}\left(1 + \left(\frac{1-\epsilon}{\epsilon}\right) \times K_p\right) \tag{4.17}$$

Second Moment:

$$\frac{\sigma^2 L}{2\mu^2 v} = \frac{D_L}{v^2} + \frac{\epsilon}{1-\epsilon}\left(\frac{R_p}{3k} + \frac{R_p^2}{15\theta D_p} + \frac{r_c^2}{15 D_c K_p}\right) \tag{4.18}$$

where it is assumed that $K_p \geq 10.0$, and thus μ is large.

For systems in which $K_p \leq 10.0$ an additional term is required in the equation.

$$\frac{\sigma^2 L}{2\mu^2 v} = \frac{D_L}{v^2} + \frac{\epsilon}{1-\epsilon}\left(\frac{\frac{R_p}{3k} + \frac{R_p^2}{150 D_p} + \frac{r_c^2}{15 D_c K_p}}{\left(1 + \frac{1}{v\mu/L - 1}\right)^2}\right) \tag{4.19}$$

The terms on the right-hand side of equation 4.18 represent the respective contributions of axial dispersion, external film resistance, macropore diffusional resistance and micropore (zeolitic) diffusional resistance.

At low Reynolds' numbers the external film coefficient is approximated by the correlation $kR_p/D_M \simeq 1.0$ (as $N_{Sh} \rightarrow 2.0$) [23]. Thus equation 4.18 simplifies to:

$$\frac{\sigma^2 L}{2\mu^2 v} = \frac{D_L}{v^2} + \frac{\epsilon}{1-\epsilon}\left(\frac{R_p^2}{3D_M} + \frac{R_p^2}{15\theta D_p} + \frac{r_c^2}{15D_c K_p}\right) \tag{4.20}$$

The task is then to numerically evaluate the contributions from axial dispersion and each of the three mass transfer resistances.

The axial dispersion contribution may be evaluated in one of three ways. Firstly, it may be calculated by 'blank' runs on non porous particles of approximately the same size as the zeolites [53]. Secondly, dispersion in gaseous systems has been reviewed by Langer, [32]. Ignoring the effects due to nonuniformity of packing, there are two main mechanisms which contribute to the axial dispersion; molecular diffusion and turbulent mixing arising from the splitting and recombination of flows around the adsorbent particles. The correlation suggested is:

$$D_L = 0.7D_M + vR_p \tag{4.21}$$

Molecular diffusion has been found to be dominant at low velocities and convective mixing dominant at high velocities [53].

Lastly, the axial dispersion can also be determined by plotting $(\sigma^2 L/2\mu^2 v)$ versus $1/v^2$ according to equation 4.18. These plots should be linear within the low Reynolds number regime where D_L is not a strong function of velocity. The slopes of these plots give the corresponding value of D_L.

The external mass transfer coefficient and hence the external mass transfer resistance is calculated by using an empirical correlation such as that suggested by Fuller et. al. in reference [41].

The macropore diffusional coefficient (θD_p) is calculated from the y-intercept of the plots, ($\sigma^2 L/2\mu^2 v$) versus $1/v^2$ for a system in which zeolitic diffusional resistance can be assumed to be negligible. Since calculated values of θD_p by this method are considerably smaller than D_M it can be concluded that Knudsen diffusion rather than bulk molecular diffusion is the dominant mechanism of transport through the macropore network. Therefore,

$$\theta D_p \simeq \frac{\theta r}{\tau} \times 10^4 \times \sqrt{T/MW} \tag{4.22}$$

Once the value of θD_p for a gas in a specific adsorbent is calculated, the value of θD_p for another gas in the same adsorbent, at the same temperature can be estimated by using the molecular weight correction. For example, considering carbon monoxide and nitrogen the equation would be:

$$(\theta D_p)_{N_2} = (\theta D_p)_{CO}\sqrt{(MW)_{CO}/(MW)_{N_2}} \tag{4.23}$$

The micropore diffusional resistance and corresponding values of zeolitic diffusion can then be calculated by subtracting the contributions of axial dispersion, external mass transfer and macropore diffusional resistance from the overall dispersion.

4.3 Limitations

Maximum and minimum limits exist for measuring diffusivities by the chromatographic method and adhering to the mathematical model. The upper limit accounts

for the requirement that the micropore diffusivity should be small enough so that micropore resistance ($r_c^2/15D_cK_p$) is large in comparison with the external mass transfer resistance. That is to say the following requirement must be met:

$$15K_p\frac{D_c}{r_c^2} \ll \frac{D_M}{R_p^2}$$

Diffusivity, however, must be large enough to establish equilibrium with the intracrystalline phase in a relatively small amount of time as compared to the retention time in the column. When diffusivity is very small, no significant adsorption takes place. The pulse of gas does not have sufficient time to penetrate into the crystals and thus it is not possible to obtain information regarding the adsorption equilibrium and kinetics of the system.

Habgood and MacDonald (1970) [18] studied the effects of micropores on peak shape and retention volume in gas-solid chromatography, they concluded that the criteria,

$$\frac{\sigma^2}{2\mu^2} \prec 0.125 \qquad \text{and} \qquad \frac{K_pD_c}{r_c^2} \succ \frac{v}{3L}$$

must hold true, so that the observed peaks correspond to diffusivity in the micropores as opposed to only the dead-space volume.

4.1 Mixed Carrier Gas Systems

Determination of adsorption equilibrium constants by the chromatographic method can be extended to the determination of pure and binary equilibrium isotherms. Assumptions and experimental procedure are basically the same as in the pure carrier system with the exception that retention times are determined for the whole range of composition, at constant total pressure and temperature.

The study of mixed carrier gas systems can be divided into two categories. Firstly, the study of pure gas isotherms that refers to a system in which the carrier gas is a mixture of a non-adsorbing component and an adsorbing component. Secondly, the study of binary mixture isotherms in which the carrier gas is composed of a mixture of two adsorbing components.

The ability of zeolites to separate a gas mixture can be the result of either a sieving effect or a selectivity phenomena. Total and partial sieving effects are due to steric influences. For the total sieving effect one component of the mixture is completely excluded from the adsorbent, whereas for the partial sieving effect the separation is achieved by differences in adsorption capacities or rates of the gas components The selectivity phenomena, on the other hand, is due to the inhibition of adsorption of one component in the gas mixture due to the presence of the other.

4.4.1 Pure Gas Isotherms

For the determination of pure gas isotherms, experiments were carried out with a mixed carrier of the inert gas (helium) and the adsorbable gas at known proportions.

Retention times are measured for small pulses of the adsorbable component at a series of different carrier gas compositions. Experimentally, the first and second moments are still given by equations 4.15 and 4.16 respectively. Theoretically, it is the first moment expression that takes into account the changing sorbate concentration in the carrier gas. The first moment is then given by the expression [51]:

$$\mu = \frac{L}{v}\left[1 + \left(\frac{1-\epsilon}{\epsilon}\right) \times K_p'\right] \tag{4.24}$$

The new equilibrium constant, K_p', represents the slope of the isotherm at that particular composition and by definition is represented by the equation:

$$K_p' = (1 - Y) \frac{dq_1}{dp_1} + Y \frac{dq_2}{dp_2} \tag{4.25}$$

where the inert gas is considered to be component 2 and non adsorbing. Therefore, the derivative $\frac{dq_2}{dp_2}$ is given by a constant and the corresponding isotherm of the adsorbable gas can be obtained by direct integration of equation 4.25.

4.4.2 Binary Mixture Isotherms

For binary systems where both components are adsorbed concentration-pulse retention time data can in many cases be used in conjunction with the Van der Vlist-Van der Meidjen method of data reduction to yield reliable gas mixture adsorption isotherms [13].

Theoretically, the apparent equilibrium constant is given by:

$$\mu = \frac{L}{v} \left[1 + \left(\frac{1 - \epsilon}{\epsilon} \right) \times K \right] \tag{4.26}$$

where K is defined as:

$$K = (1 - Y) \frac{dq_1}{dp_1} + Y \frac{dq_2}{dp_2} \tag{4.27}$$

and dq_1/dp_1 and dq_2/dp_2 are the slopes of the individual isotherms. These slopes are represented by the following second degree polynomials with respect to gas phase composition:

$$\frac{dq_1}{dp_1} = B_0 + B_1 Y + B_2 Y^2 \tag{4.28}$$

$$\frac{dq_2}{dp_2} = C_0 + C_1 Y + C_2 Y^2 \tag{4.29}$$

In this case K is determined experimentally for different gas compositions. The data points are then fitted to a third degree polynomial for the determination of the unknown coefficients:

$$K = A_0 + A_1 Y + A_2 Y^2 + A_3 Y^3 \tag{4.30}$$

Hyun and Danner [27] have studied the applicability of this approach for the determination of binary isotherms. They concluded that for binary equilibria where both species are adsorbing, the reliability of the model rests upon the ability to fit the data with a low order polynomial in vapor phase mole fraction (Y).

As an alternative to a polynomial expression, Tezel [55] has suggested the following equation for the determination of the unknown coefficients:

$$K = A_{-1}(Y + \beta) + A_0 + \frac{A_1}{(Y + \beta)} + \frac{A_2}{(Y + \beta)^2} \tag{4.31}$$

This is a 'trial and error' approach in determining the value of β which gives the best fit. Once a β value is chosen as optimum the corresponding A coefficients are taken to be valid.

The slopes of the individual isotherms are then represented by the following equations:

$$\frac{dq_1}{dp_1} = B_0 + \frac{B_1}{(Y + \beta)} + \frac{B_2}{(Y + \beta)^2} \tag{4.32}$$

$$\frac{dq_2}{dp_2} = C_0 + \frac{C_1}{(Y + \beta)} + \frac{C_2}{(Y + \beta)^2} \tag{4.33}$$

Substitution of equations 4.32 and 4.33 into equation 4.27 yields:

$$\begin{aligned} K = \; & (C_0 - B_0)(Y + \beta) + B_0(1 + \beta) - B_1 - C_0\beta + C_1 \\ & + [B_1(1 + \beta) - B_2 - C_1\beta + C_2]\tfrac{1}{(Y+\beta)} \\ & + [B_2(1 + \beta) - C_2\beta]\tfrac{1}{(Y+\beta)^2} \end{aligned} \tag{4.34}$$

Comparison of equations 4.31 and 4.34 shows that four equations can be obtained by comparing the coefficients of similar powers of (Y + β). The additional two equations are those for the limiting values of q_1 and q_2 at Y=1.0 and Y=0.0. Determination of the B and C coefficients requires that the following equations be solved simultaneously:

$$A_{-1} = C_0 - B_0 \tag{4.35}$$

$$A_0 = B_0(1 + \beta) - B_1 - C_0\beta + C_1 \tag{4.36}$$

$$A_1 = B_1(1 + \beta) - B_2 - C_1\beta + C_2 \tag{4.37}$$

$$A_2 = B_2(1 + \beta) - C_2\beta \tag{4.38}$$

$$q_1(binary) = q_1(pure) \qquad at \;\; Y = 1.0 \tag{4.39}$$

$$q_2(binary) = q_2(pure) \qquad at \;\; Y = 0.0 \tag{4.40}$$

The binary isotherms are then obtained by integration of equations 4.32 and 4.33 as follows:

$$q_1 = P[B_0 Y + B_1 ln(\frac{Y + \beta}{\beta}) + \frac{B_2 Y}{\beta(Y + \beta)}] \tag{4.41}$$

$$q_2 = P[C_0(1 - Y) - C_1 ln(\frac{Y + \beta}{1 + \beta}) + \frac{C_2(1 - Y)}{(1 + \beta)(Y + \beta)}] \tag{4.42}$$

Chapter 5

Apparatus and Method

Schematic representations of the experimental apparatus used for studying the pure gases and binary mixtures are given in Figures 5.1 and 5.2 respectively.

The main component of the experimental set-up was a Hewlett Packard Model 5700 Gas Chromatograph that was connected to a 50 litre tank of liquid nitrogen, in order to be able to perform experiments below room temperature. The column used was made of stainless steel tubing with an inside diameter of 0.63 cm and length of 11.5 cm. The column specifications are given in Table 5.1. All the adsorbents, with the exception of Chabazite were obtained as 0.38 cm (1/8 in.) pellets from Union Carbide. The Chabazite was supplied as 0.19 cm (1/16 in.) extrudes by GSA Resources Inc. of Cortaro, Arizona. It was a product of Bowie, Arizona excavated in 1970.

Table 5.1: Column Specifications

Particle mesh size	20-42
Average particle diameter	602.5 μm
Bed density	0.8947 g/ml
Bed porosity	0.3664
Inside diameter	0.6300 cm
Bed Length	11.50 cm

The porosity of the column was determined by the bulk density of the bed (total mass/total volume) and pellet density according to the equations [5]:

$$\rho_p = \frac{\rho_b}{0.3560(log\ 2R_p - 1)} \tag{5.1}$$

$$\epsilon_b = \frac{\rho_p - \rho_b}{\rho_p} \tag{5.2}$$

Experiments performed fell into two groups:

1. Temperature runs,

   - keeping the carrier gas flow rate constant the temperature was varied between a range of 263 K and 333 K

2. Volumetric flow rate runs,

   - keeping temperature constant at T = 263, 273, 293 and 313 K the carrier gas flow rate was varied.

In adsorption studies on zeolites, film and macropore resistance are dependent upon the nature of the carrier gas and to a certain extent so is micropore resistance. Thus the carrier must be a gas that is not significantly if at all adsorbed For this reason, helium, being such a small molecule that it can readily diffuse through the pore network without significant adsorption occuring, was chosen as the carrier gas. It should be noted that work performed by Ruthven and Kumar [46] found that for species such as oxygen and argon at high temperatures the effect of helium adsorption in the system can be appreciable. adsorbed.

5.1 Pre-Treatment Procedure

Before any experiments were performed the adsorption column was regenerated at a temperature of 623 K for 24 hours under a helium atmosphere. This resulted in ensuring that any impurities or moisture adsorbed from the air did not hinder the adsorption capacity of the perspective zeolite. Thomas, Mange and Eyraud [57] have found that diffusion rates decrease in the presence of trace amounts of moisture.

A regeneration temperature of 623 K was chosen on the basis of the work performed by Federova and Aliev [15] who tested various regeneration methods and found that evidently heating at high temperature (623 K) is required for the recovery of the adsorption properties of zeolites with respect to their adsorption of molecular and monoatomic gases. Studies performed by Thomas, Mange and Eyraud [57] also indicate that for zeolites 4A and 5A structural changes begin to occur at approximately 823 K and 723 K respectively. Thus excessively high temperatures are to be avoided.

5.2 Pure Gases

Pure mixtures refers to the studies performed by using a pure carrier stream or one consisting of only the non-adsorbable component (in this case helium). After regeneration, a carrier gas stream of helium flowed continuously through the system to prevent any moisture adsorption that might occur from the atmosphere. The helium stream was divided into two at the entrance of the gas chromatograph, as is shown in Figure 5.1. One stream flowed directly to the reference side of the thermal conductivity (TC) detector while the other passed through the column then to the sample side of the TC detector. The flow rate was adjusted, at the entrance by the rotameters available on this model of gas chromatograph and checked at the exit by a bubblemeter. The detector was a thermal conductivity detector, that was kept constant at a temperature of 373 K and a sensitivity of 3.0. At time zero a pulse of 0.5 cc of sample gas was injected into the system through a double-loop sampling valve. While the gas is passing through the sample side of the detector the dispergent peak was recorded by a Fisher Recordall (Series 5000) recorder that was directly connected to the TC detector.

The apparatus was arranged so that the 'dead' volumes between pulse injection and column and between column and detector were minimized in order to reduce any corrections necessary to obtain moments from the observed peaks. This was accomplished in that all piping directly connected to the column entrance and exit was of negligible volume (stainless steel, i.d= 0.1875 cm tubing).

5.3 Mixed Carrier Gas Systems

Mixed carrier gas systems refers to the experiments performed in which the composition of the carrier gas was varied. For these runs an additional detector

was installed at the entrance of the gas chromatograph to monitor the composition of the carrier gas. The carrier gas composition was recorded on a Fisher Recordall (Series 5000) recorder. The detector consisted of a Gow Mac Model 40-200 power supply control unit attached to a thermal conductivity cell. The composition of the carrier gas stream was adjusted by 601 tube Matheson rotameters and monitored by the Gow Mac detector before it was divided into two at the entrance of the gas chromatograph. Again, one stream flowed to the reference side of the TC detector and the other to the sample side. The flow rate was once again checked at the exit by a bubblemeter. At time zero a pulse of 0.5 cc of the sample gas was injected into the system through the pulse injection valve and a peak recorded by a Fisher Recordall (Series 5000) recorder.

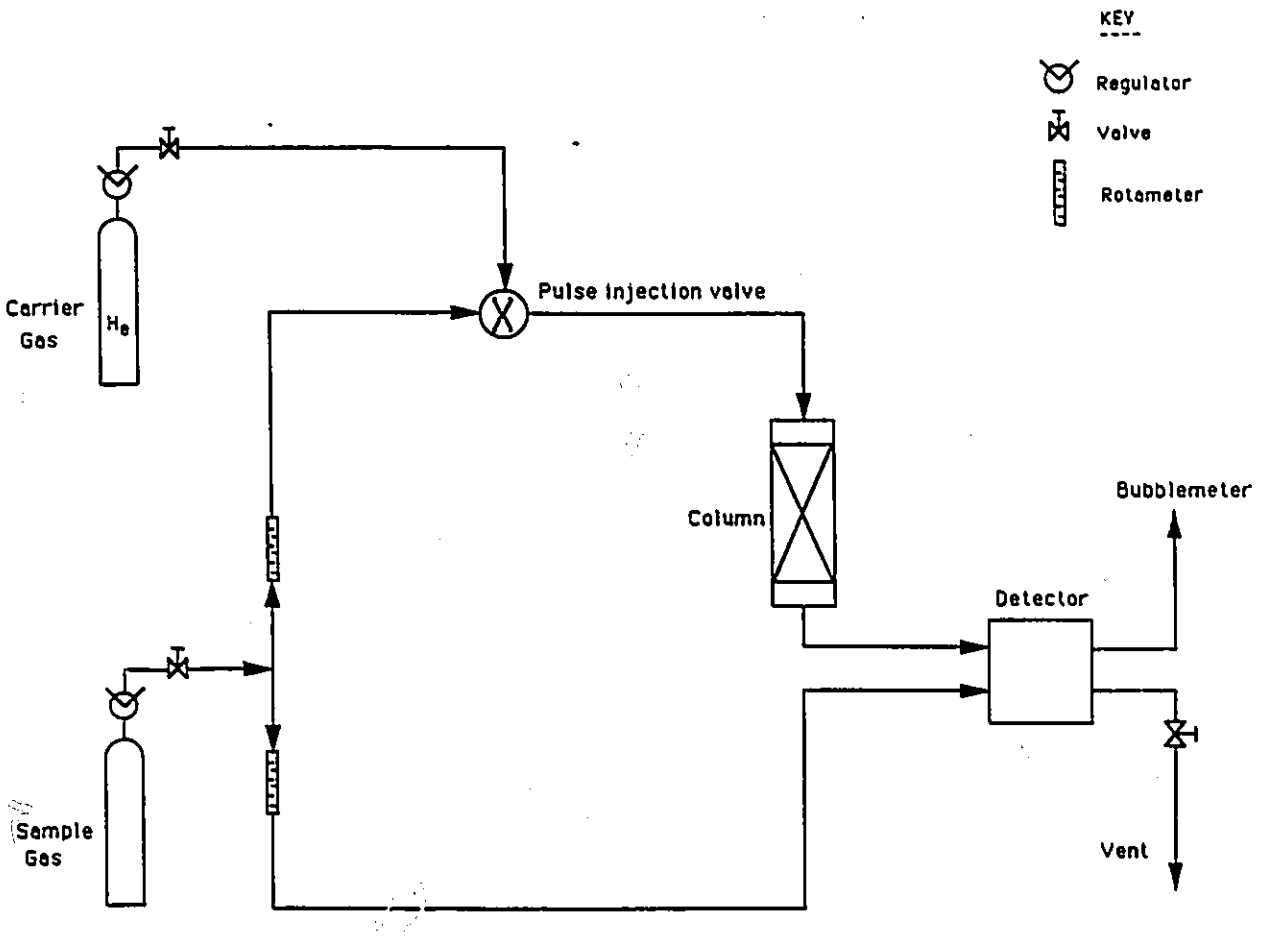

Figure 5.1: Apparatus used in the study of adsorption for Pure Gases

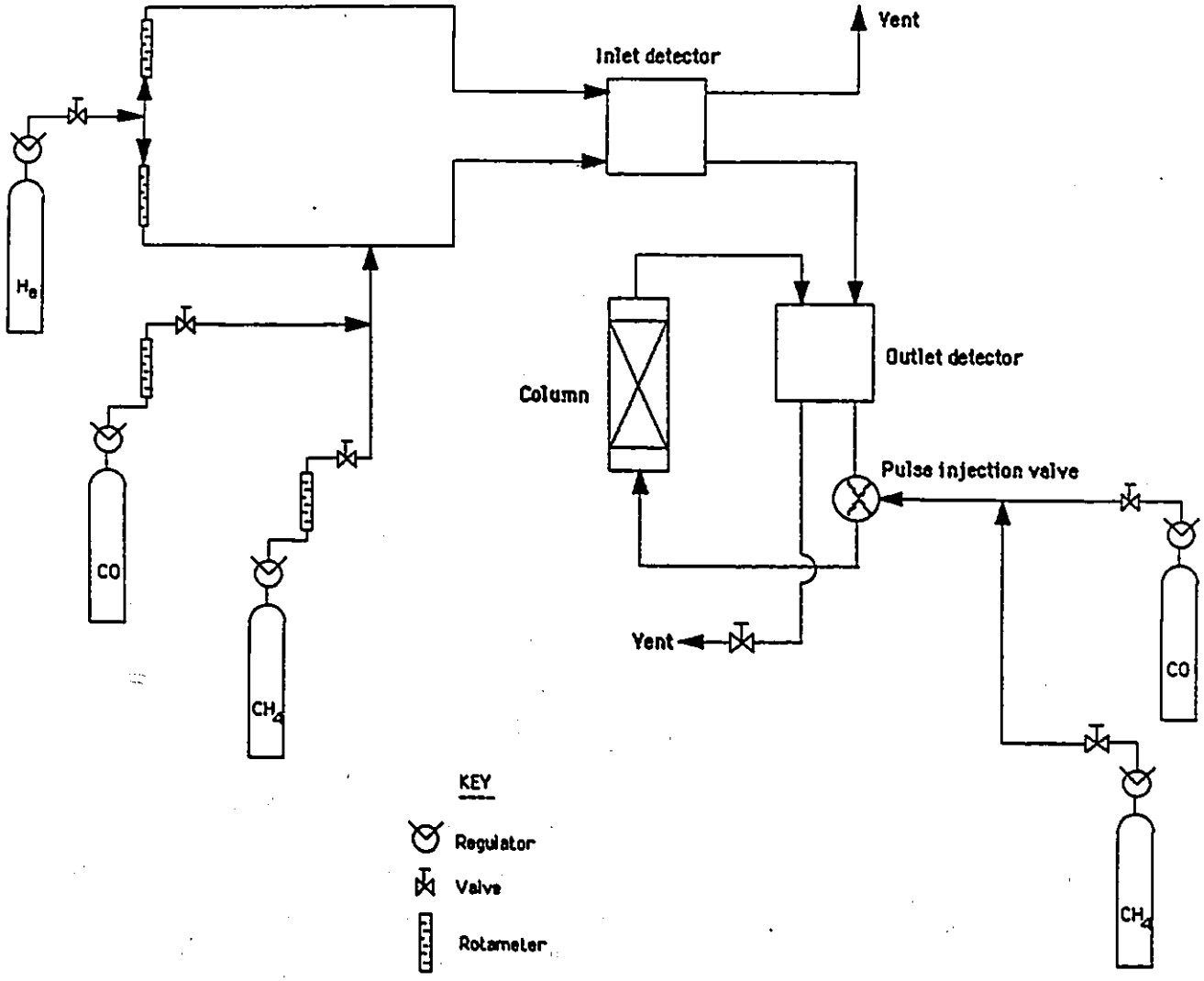

Figure 5.2: Apparatus used in the study of adsorption for Mixed Carrier Gas Systems

Chapter 6

Results and Discussion

In this chapter the experimental results are reported and interpreted. The pertaining computer printouts are given in the Appendices. The volfex program uses the experimental data of concentration versus retention time together with the given experimental conditions to calculate such parameters as interstitial velocity, μ, σ^2, K_p and K'_p. The SAS (Statistical Analysis Software) package was used to fit the experimental data to the corresponding models, in order to determine the parameters ΔU_0, ΔH_0, K_0, E_a and the coefficients of the equations for the binary mixtures. All the integrations for the pure and binary isotherms were performed using the MAPLE package on the IBM mainframes. The IMSL subroutines were used for solving the equations of the binary gas isotherms. Also included in the appendices are the estimates of molecular diffusivity at 1 atm total pressure for each of the three systems (He-N_2, He-CO, He-CH_4) as determined by the empirical correlation suggested by Fuller et. al. in reference [41].

6.1 H-Mordenite

The temperature experiments, in which temperature was varied and volumetric flow rate kept constant, were the first set of experiments to be performed. The purpose of these experiments was to determine if there was a substantial contribution from micropore resistance in the systems being studied. The effective diffusivity measured by gas chromatography would be expected to reflect both pore systems. Diffusion in the macropores would be fast and characterized by low activation energies. In the micropores however, the molecules are always close to the pore walls and the flow would contain properties of both diffusion and adsorption. Thus the diffusivity would be expected to show a stronger dependence on temperature and vary greatly with the nature of the diffusing molecule. This has been verified by Eberly [30] who studied the diffusion of inert gases in a series of zeolites including 3A and 5A Molecular Sieves, Na and H mordenites and Na faujasite. This would result in a decrease in dispersion according to equation 4.18 as temperature is increased. As is evident in Figure 6.1, this trend is exhibited by the N_2-H-Mordenite system. This suggests that, in this system, micropore diffusion is occuring to an extent that can be measured accurately. For the CO-H-Mordenite system, Figure 6.2 indicates that intracrystalline resistance ($r_c^2/15D_cK_p$) is negligible since dispersion does not change with temperature. This is not to say that no micropore diffusion is taking place, it merely suggests that since the value of r_c^2/D_c is very small, D_c/r_c^2 is a large quantity and the chromatographic process may be too rapid to accurately measure diffusion in the micropores. Figure 6.3 shows the results of the CH_4-H-Mordenite system. It appears as though this system behaves as a combination of the other two. At lower temperatures (263 K to approximately 293 K) it behaves like the N_2 system, exhibiting a contribution from intracrystalline resistance, whereas, at the higher temperatures it acts like the CO system in which micropore resistance is negligible.

Volumetric flow rate experiments, however, indicated that the observed decrease in dispersion at the lower temperatures, is due to experimental scatter as opposed to the contribution of micropore diffusional resistance.

For the CO-H-Mordenite system the dispersion is then due mainly to the contributions from axial dispersion, external mass transfer resistance and macropore diffusional resistance. Since contributions from axial dispersion and external mass transfer resistance can be estimated independently, the y-intercept of a plot of $\sigma^2 L/2\mu^2 v$ versus $1/v^2$ (according to equation 4.18) would directly give the macropore diffusional resistance from which the value of $(\theta D_p)_{CO}$ can be obtained. Zeolitic diffusional resistance is a contributing factor in the N_2-H-Mordenite system, thus the value of $(\theta D_p)_{N_2}$ can not be calculated directly from the intercept but must be estimated using molecular weight correction as given by equation 4.23. Table 6.1 gives the slopes and y-intercepts of these plots for the CO system. The plots for the N_2 system showed extreme scatter arising from the difficulty in analyzing the dispersent peak from the gas chromatograph thus for this system the values of axial dispersion and each of the three resistances were calculated individually for each flow rate. Table 6.2 shows the contribution of each of the three mass transfer resistances to the N_2 system. External mass transfer resistance ($R_p^2/3D_M$) is negligible. For this system it appears as though the emergent peak is reflective of the intracrystalline resistance. It is the major conribution to the system and thus the mechanism that controls the overall mass transfer. In comparison the macropores offer little resistance to mass transfer and for all the temperatures the contribution from axial dispersion is small. Table 6.3 lists the intracrystalline diffusivities for the N_2-H-Mordenite system as calculated according to the Arrhenius type equation:

$$D_c/r_c^2 = D_0/r_c^2 exp(-E_a/RT) \qquad (6.1)$$

The parameters of the equation, D_0/r_c^2 and E_a are also given. As can be seen the

intracrystalline diffusivity decreases as temperature decreases indicating that more nitrogen diffusion in the micropores occurs at the higher temperature. The values of intracrystalline diffusivity are plotted in Figure 6.11 for a comparative analysis with D_c/r_c^2 values obtained for the N_2-4A zeolite system.

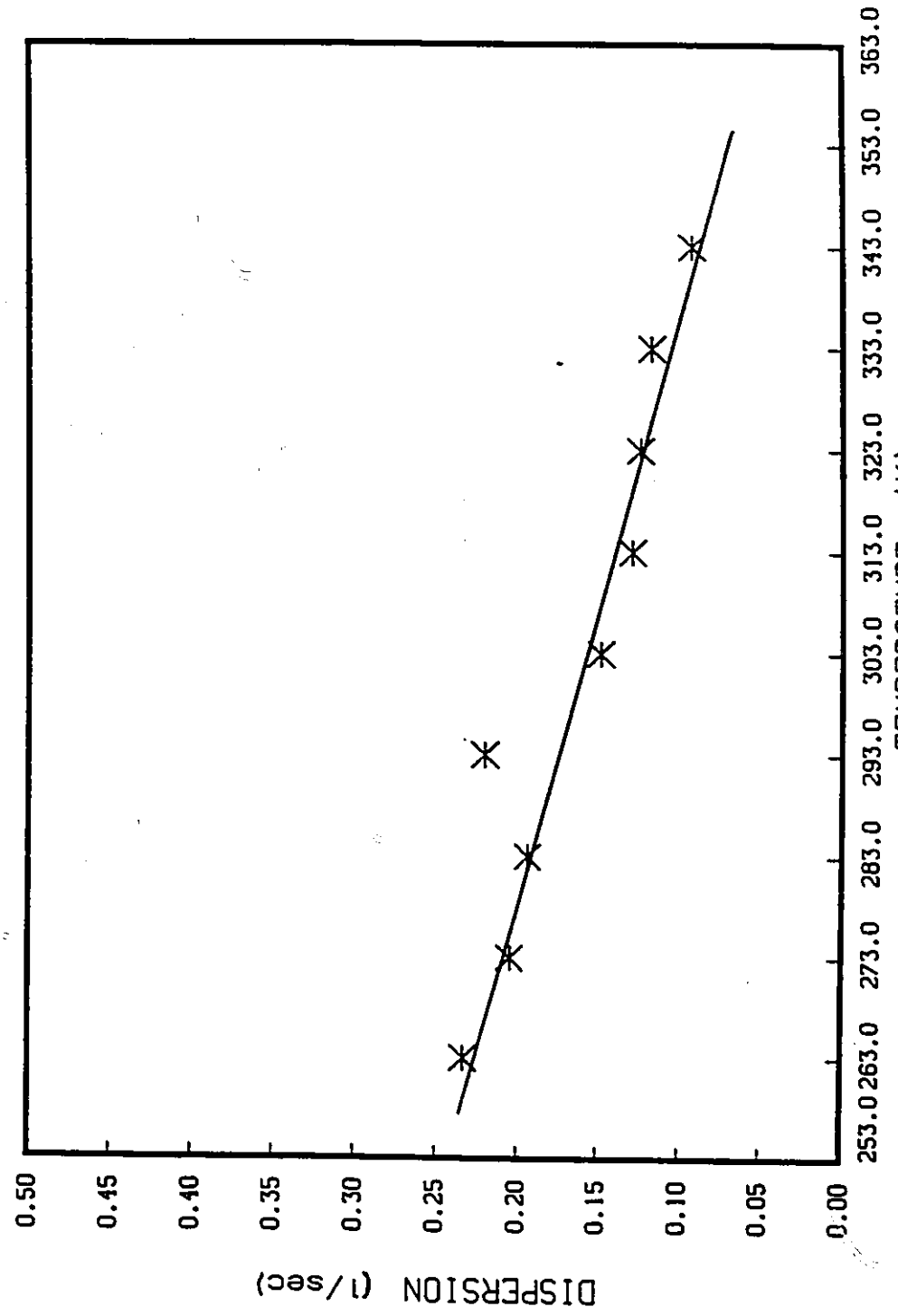

Figure 6.1: Dependence of dispersion ($\sigma^2 L/2\mu^2/v$) on temperature for N_2-H-Mordenite system

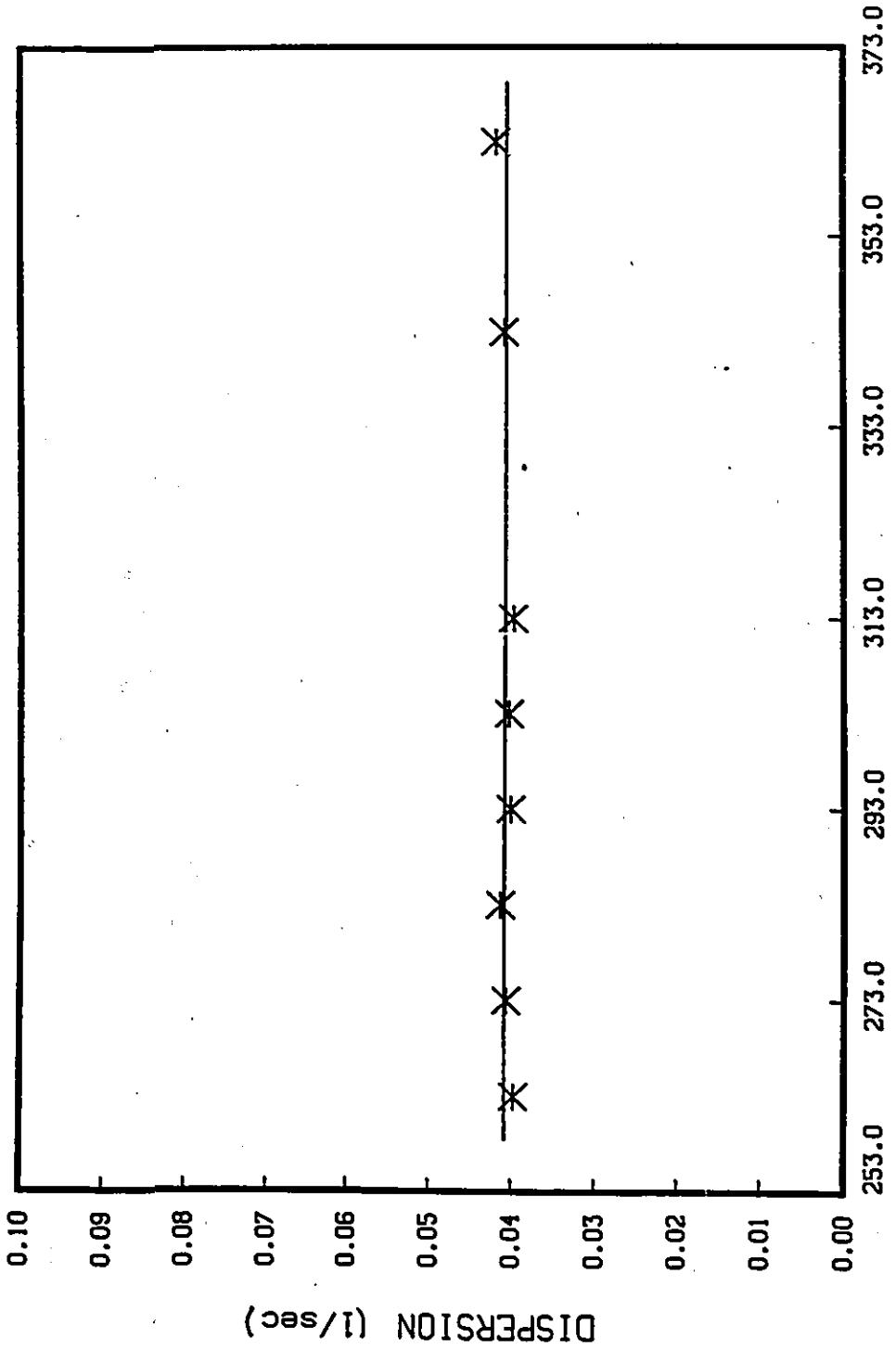

Figure 6.2: Dependence of dispersion ($\sigma^2 L/2\mu^2 v$) on temperature for CO-H-Mordenite system

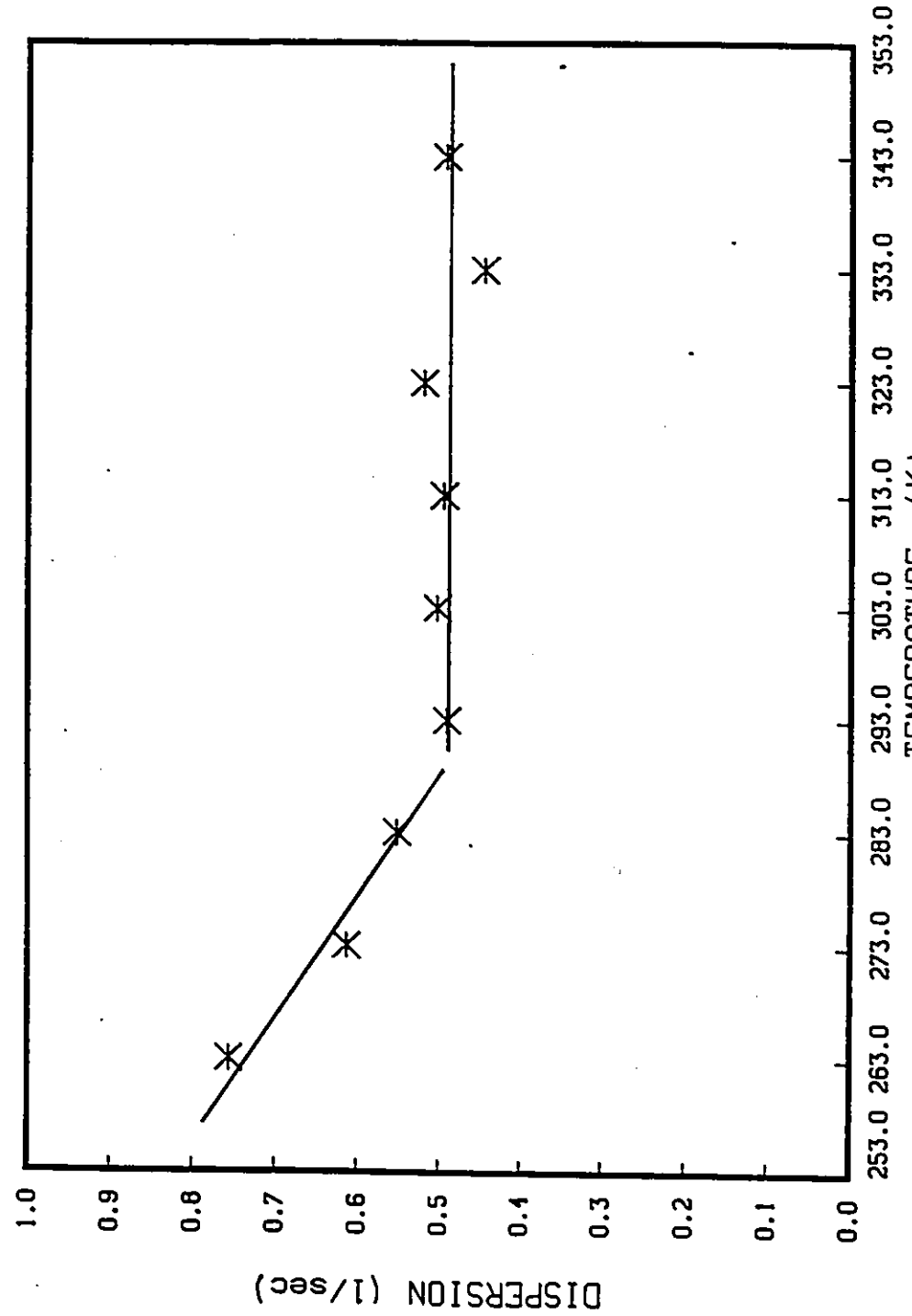

Figure 6.3: Dependence of dispersion ($\sigma^2 L/2\mu^2 v$) on temperature for CH_4-H-Mordenite system

Table 6.1: Linear Regressions for $\sigma^2 L/2\mu^2 v$ versus $1/v^2$ plots (CO-H-Mordenite system).

Temperature (K)	Slope (cm/sec)	Y-intercept (sec)
313	0.7500	0.0313
293	0.6050	0.0360
273	0.4730	0.0379
263	0.3750	0.0390

6.1.1 Effect of Temperature on Adsorption Equilibrium

The effect of temperature on the equilibrium constant of adsorption was studied by considering the temperature experiments as is shown in Figure 6.4. Table 6.4 summarizes the parameters K_0 and ΔU_0, which give the temperature dependence of the dimensionless adosrption equilibrium constant, K_p, according to the vant Hoff expression:

$$K_p = K_0 exp(-\Delta U_0/RT) \tag{6.2}$$

The limiting heat of sorption values, $-\Delta H_0$, are derived from ΔU_0 values using the equation:

$$-\Delta H_0 = -\Delta U_0 + RT \tag{6.3}$$

where T is taken as the mean temperature of the experimental range.

Within the temperature range studied the K_p values for CO in H-Mordenite are much larger than those for either N_2 or CH_4. Adsorption equilibrium selectivities, which are the ratios of the equilibrium constants for each gas are shown graphically in Figure 6.5. The selectivities increase as temperature is decreased, reaching values of approximately 17.0 and 8.0 for CO/CH_4 and CO/N_2 respectively, at a

Table 6.2: Contribution of Mass Transfer Resistances and Axial Dispersion to the N_2 - H-Mordenite System

Temperature (K)	$R_p^2/3D_M$ (sec)	$R_p^2/15\theta D_p$ (sec)	$r_c^2/15D_cK_p$ (sec)	D_L/v^2 (sec)
313	3.906 x 10^{-4}	0.0528	0.1045	0.0684
293	4.384 x 10^{-4}	0.0606	0.2980	0.0390
273	4.926 x 10^{-4}	0.0652	0.3518	0.0315
263	5.296 x 10^{-4}	0.0662	0.4173	0.0481

Table 6.3: Intracrystalline diffusivity for the N_2-H-Mordenite System

Temperature (K)	D_c/r_c^2 (1/sec)	D_0/r_c^2 (1/sec)	E_a (kcal/mol)
313	0.0702	2185.17	5.162
293	0.0181		
273	0.0097		
263	0.0062		

Table 6.4: Parameters K_0 and ΔU_0 giving temperature dependence of K_p according to equation $K_p = K_0 \exp(-\Delta U_0/R\ T)$ for the H-Mordenite system.

Sorbate	K_0 (dimensionless)	ΔU_0 (kcal/mol)	ΔH_0 (kcal/mol)
N_2	0.0384	3.421	3.993
CO	0.0064	5.407	5.979
CH_4	2.889	0.7275	1.300

temperature of 263 K. The selectivities determine the viability of the adsorbent for the separation of any two gases. The higher the value of the selectivity the more feasible the separation is deemed. Thus as can be seen from Figure 6.5 of the three possible separations a N_2-CH_4 separation with H-Mordenite molecular sieve (based on the difference in K_p values) would be the most difficult one, since even at the lower temperature range the equilibrium selectivity only reaches a maximum value of approxiamtely 2.0.

For a comparative study of the N_2-H-Mordenite system, previously reported values of K_p [56] and those obtained in this work are plotted in Figure 6.6. As can be seen the obtained values agree well with those from the literature.

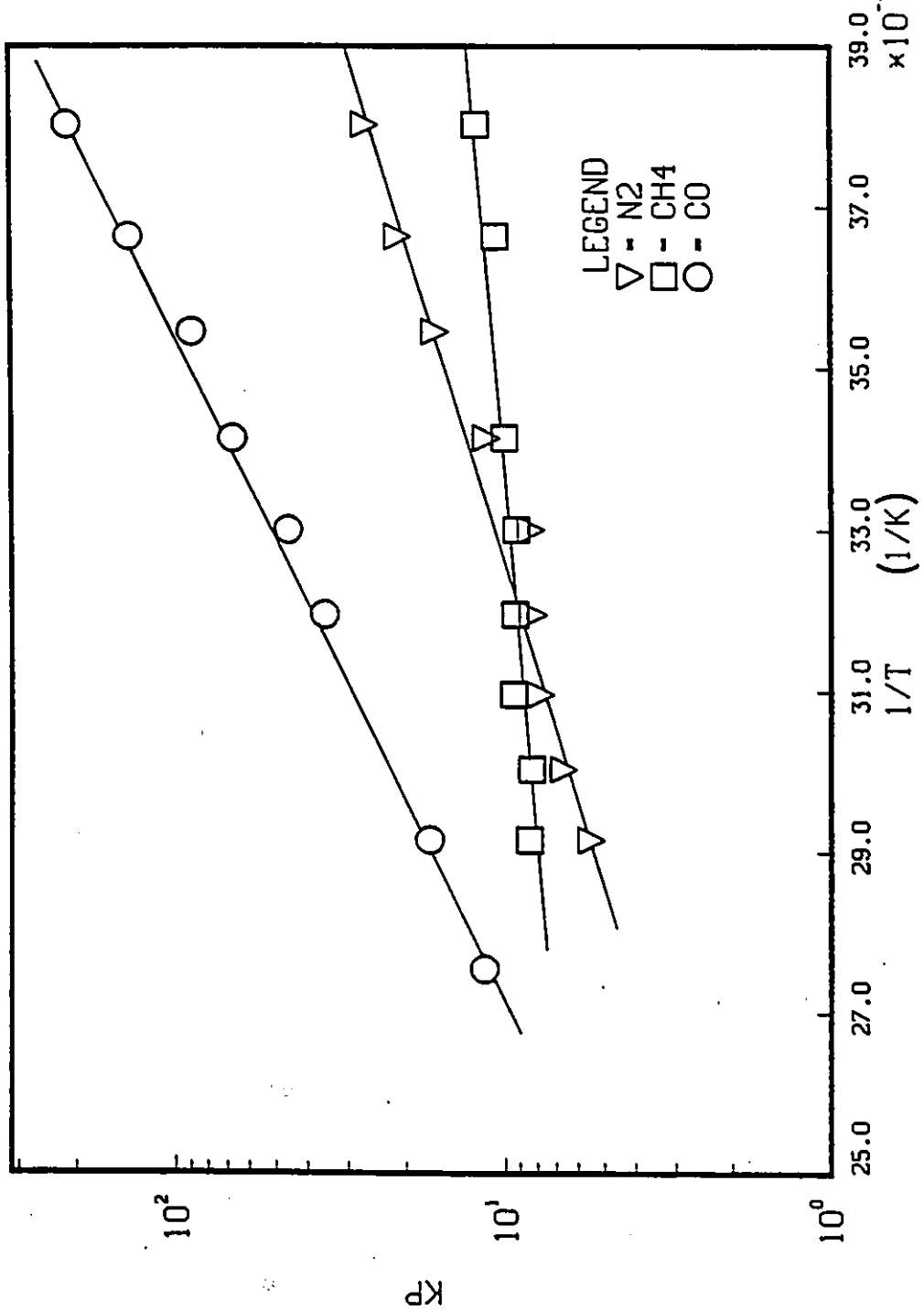

Figure 6.4: Temperature dependence of equilibrium constants according to equation $K_p = K_0 \exp(-\Delta U_0/RT)$ for the adsorption of N_2, CH_4 and CO on H-Mordenite

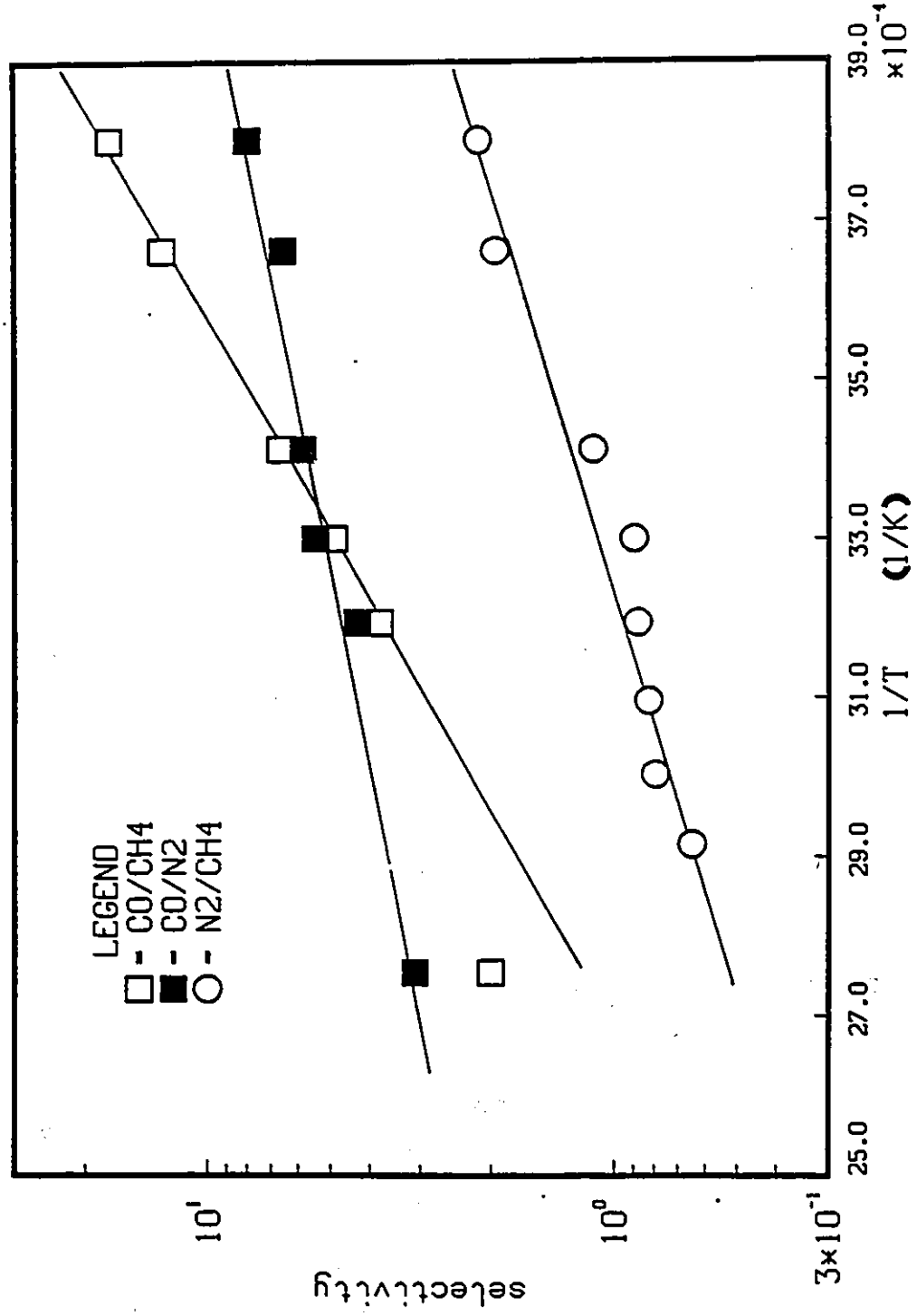

Figure 6.5: Adsorption equilibrium selectivities for the H-Mordenite system

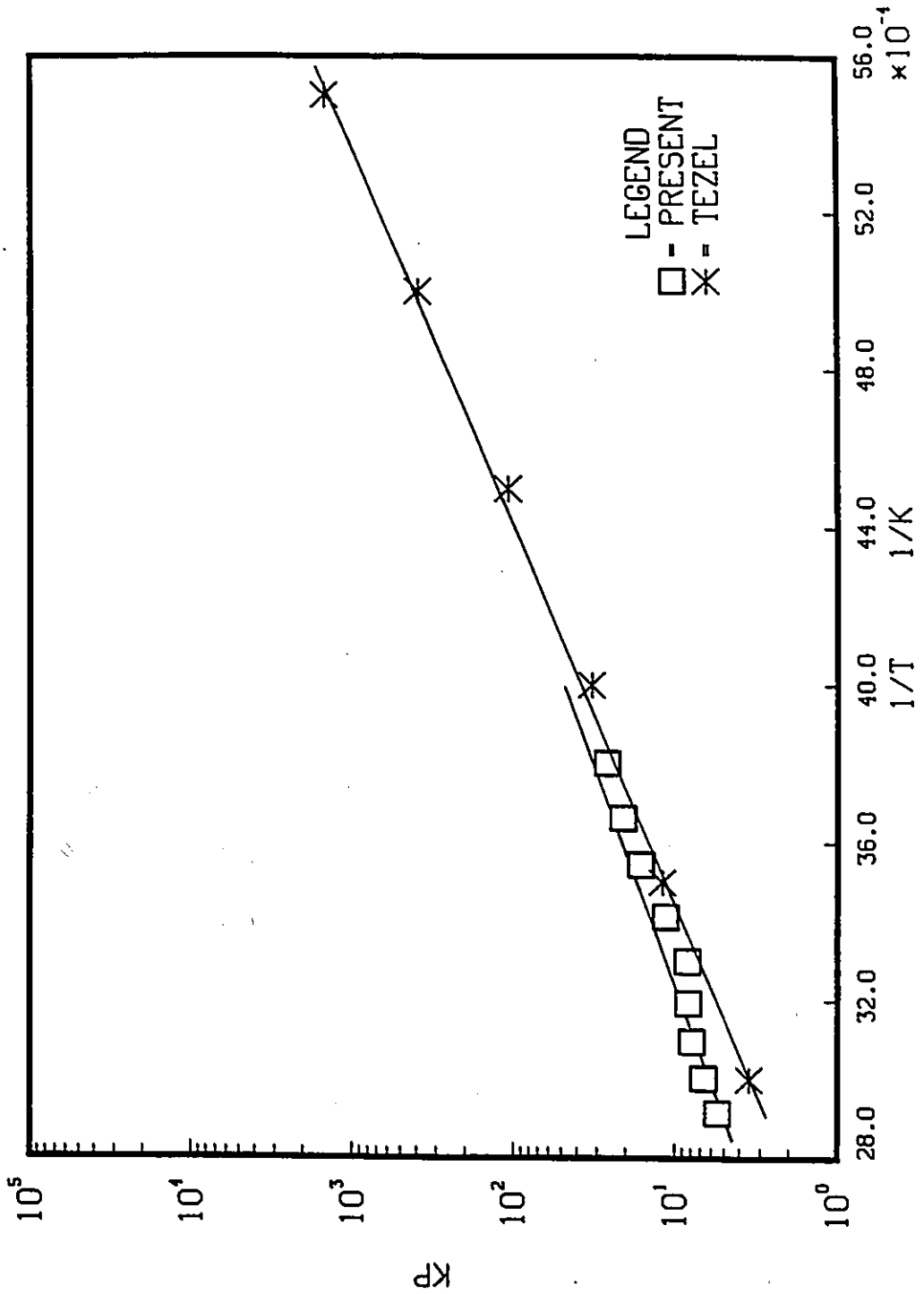

Figure 6.6: Comparative analysis of K_p values for the the adsorption of N_2 on H-Mordenite

6.2 Type 4A Zeolite

Extensive studies were also performed with the Type 4A zeolite and all three gases.

Temperature experiments suggest that of the three systems studied intracrystalline resistance was a contributing factor only in the N_2-4A system, as can be seen in Figure 6.7. As illustrated in Figures 6.8 and 6.9, zeolitic resistance was negligible for both the CO-4A and CH_4-4A systems. Results of the volumetric flow rate experiments are plotted in Figure 6.10. The corresponding contributions of mass transfer resistance and axial dispersion are given in Table 6.5. The intracrystalline resistance is the main contributing factor to the N_2-4A system.

Table 6.6 compares the overall diffusion resistance, which is the summation of the three mass transfer resistances for the N_2-H-Mordenite and N_2-4A systems. The overall diffusion resistance is higher for N_2 in the 4A zeolite. It would be expected that hydrogen mordenite with its unique one-dimensional pore network would yield the higher diffusion resistances. However, though a three-dimensional channel network such as that found in the 4A zeolite, is more accessible to the nitrogen molecules, N_2 with a critical diameter of approxiamately 3.6 Å.encounters greater difficulty when trying to diffuse into the 4 Å.pores as opposed to the much larger mordenite pores. Figure 6.11 plots the intracrystalline diffusivities of N_2 in both the H-Mordenite and 4A zeolites. The diffusivities are plotted according to equation 6.1.

As expected the N_2-H-Mordenite system yields higher intracrystalline diffusivity values. The corresponding parameters of equation 6.1 are given in Table 6.7. The H-Mordenite system yields an activation energy of adsorption (E_a) of 5.162 kcal/mol whereas for the 4A zeolite system the activation energy is higher at a value of 6.703 kcal/mol. This results from the larger barrier to adsorption that the nitrogen

Table 6.5: Contribution of Mass Transfer Resistances and Axial Dispersion to the N_2-4A Zeolite System

Temperature (K)	$R_p^2/3D_M$ (sec)	$R_p^2/15\theta D_p$ (sec)	$r_c^2/15D_cK_p$ (sec)	D_L/v^2 (sec)
313	3.906×10^{-4}	0.0268	0.2209	0.0511
293	4.384×10^{-4}	0.0503	0.3095	0.0353
273	4.926×10^{-4}	0.0613	0.4590	0.0164
263	5.296×10^{-4}	0.0691	0.4696	0.0131

molecules encounter in molecular sieve 4A.

Table 6.8 (as found in reference 18) compares various reported values of E_a for a N_2-4A Zeolite system. The activation energy value of 6.70 kcal/mol obtained in the present study is slightly higher than the range of values previously reported. This discrepancy can be attributed to the different experimental techniques that were used and the conditions under which the various experiments were carried out.

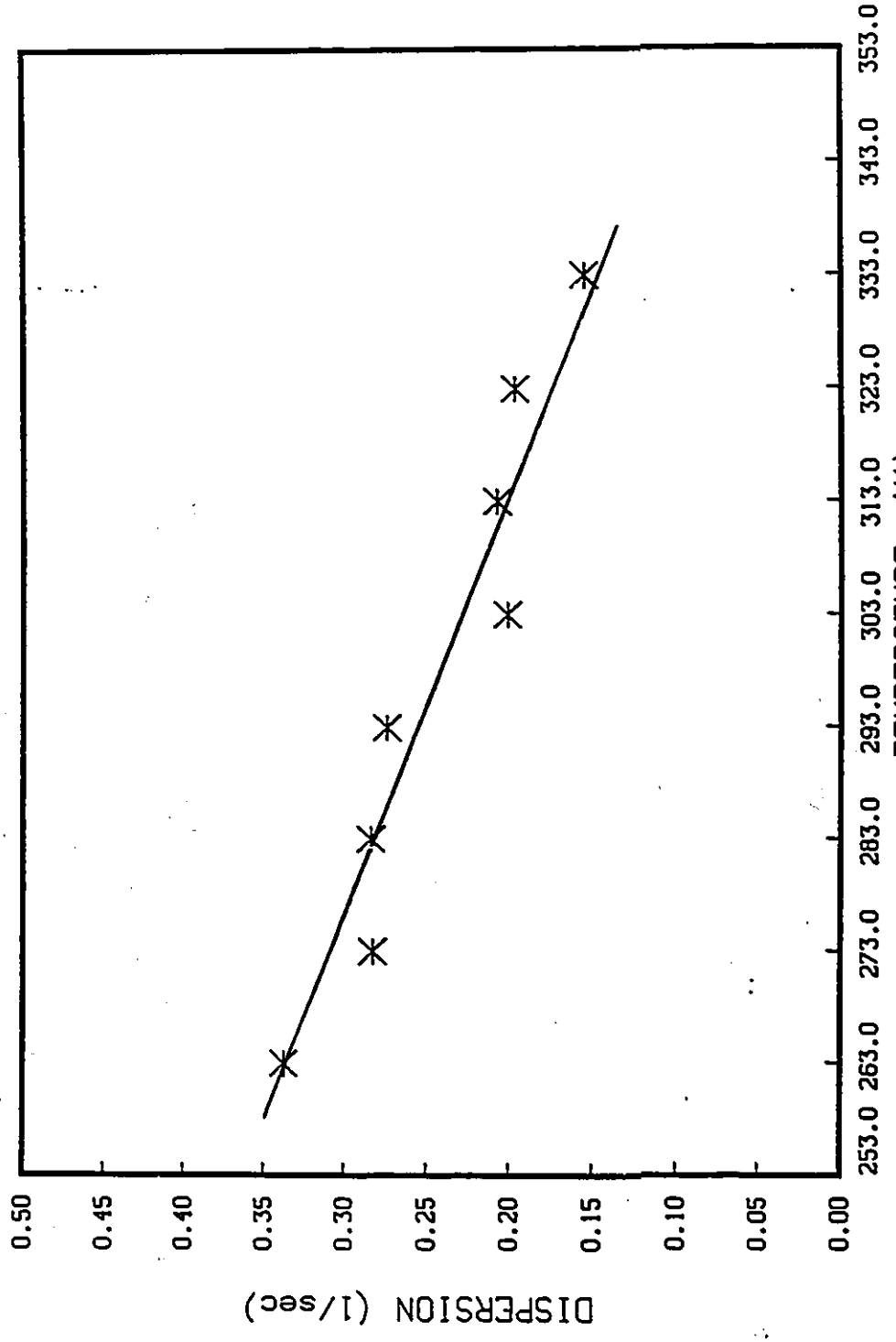

Figure 6.7: Dependence of dispersion ($\sigma^2 L/2\mu^2 v$) on temperature for N_2-4A Zeolite system

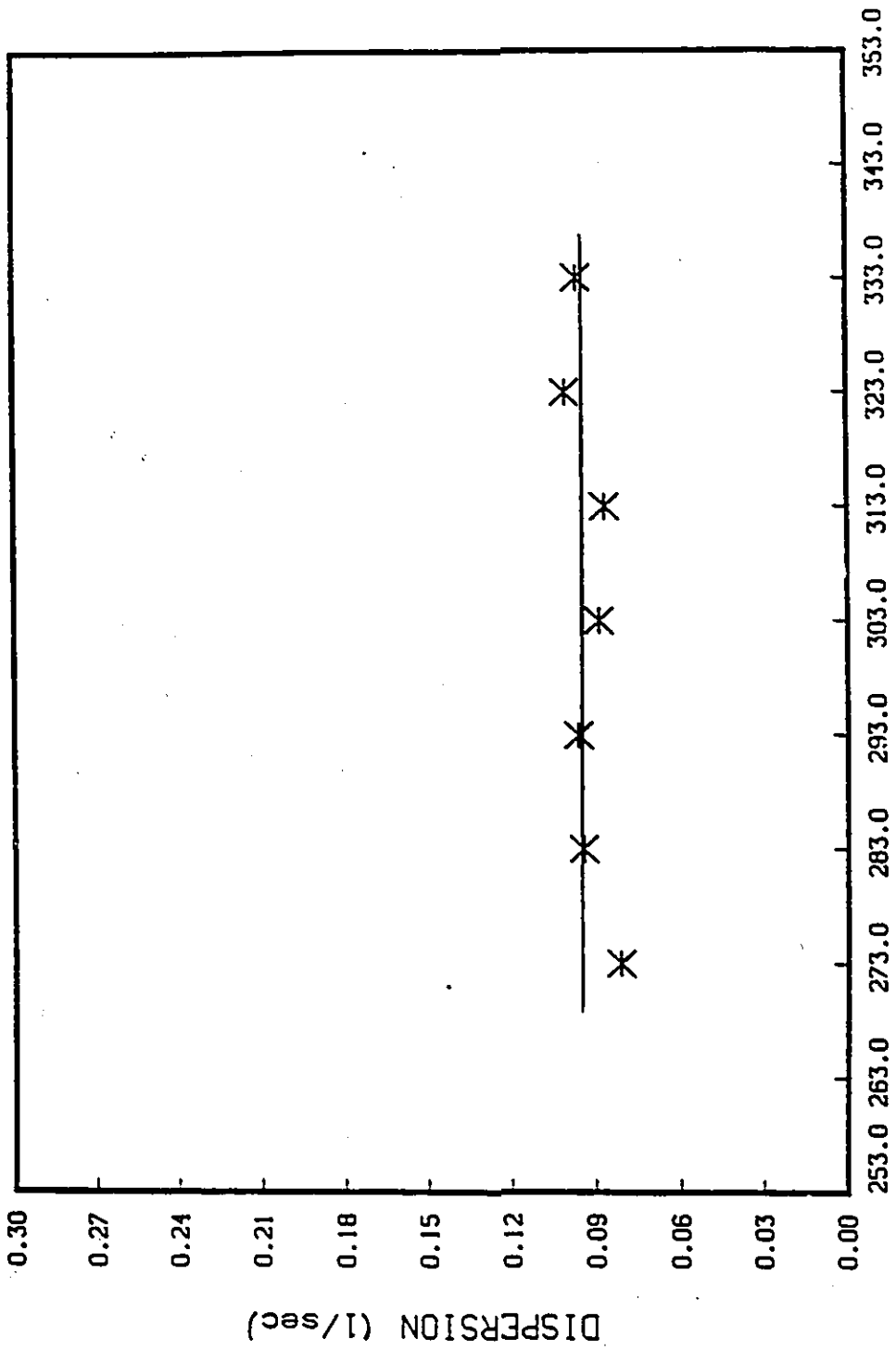

Figure 6.8: Dependence of dispersion ($\sigma^2 L/2\mu^2 v$) on temperature for C(1)-4A Zeolite system

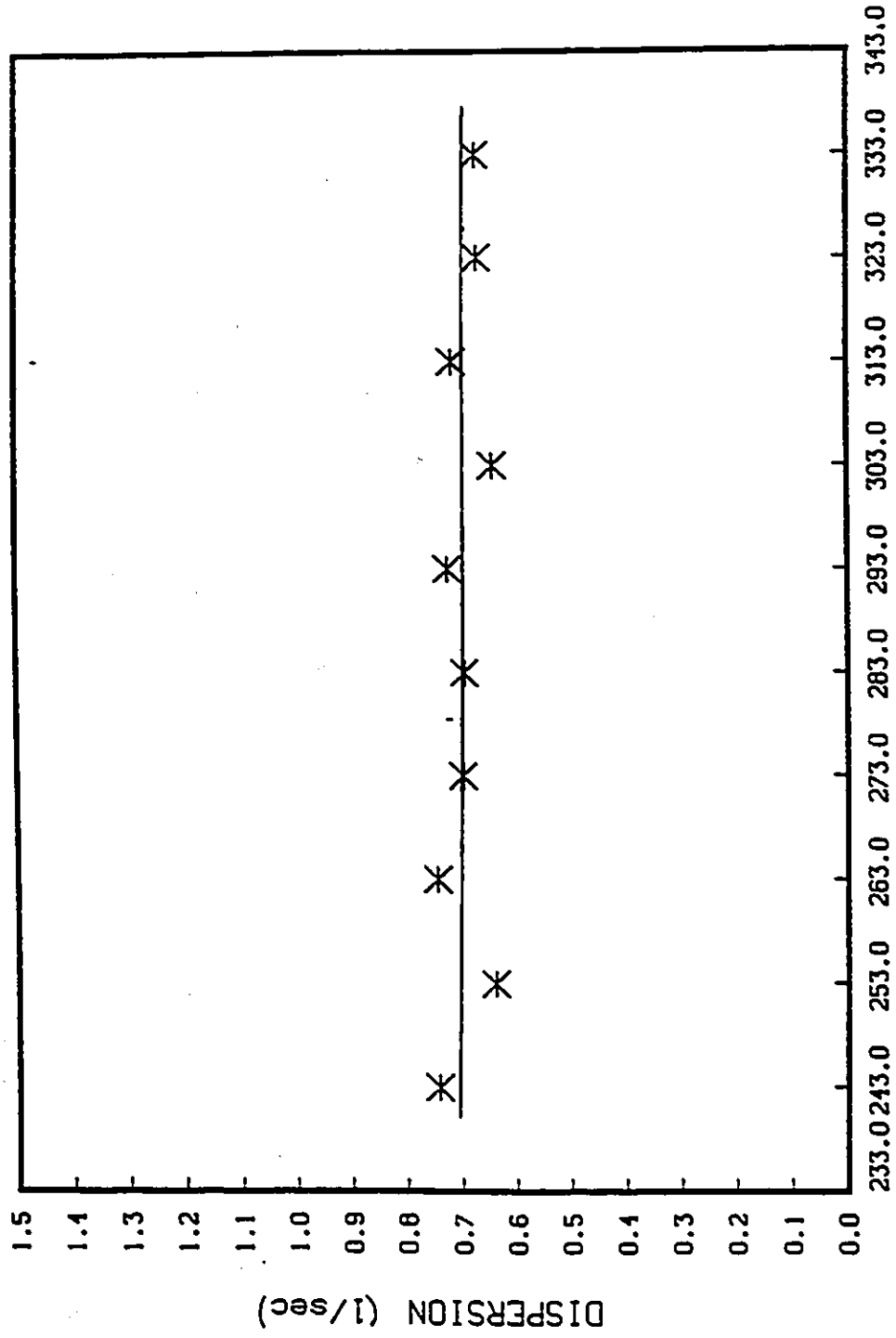

Figure 6.9: Dependence of dispersion ($\sigma^2 L/2\mu^2 v$) on temperature for CH_4-4A Zeolite system

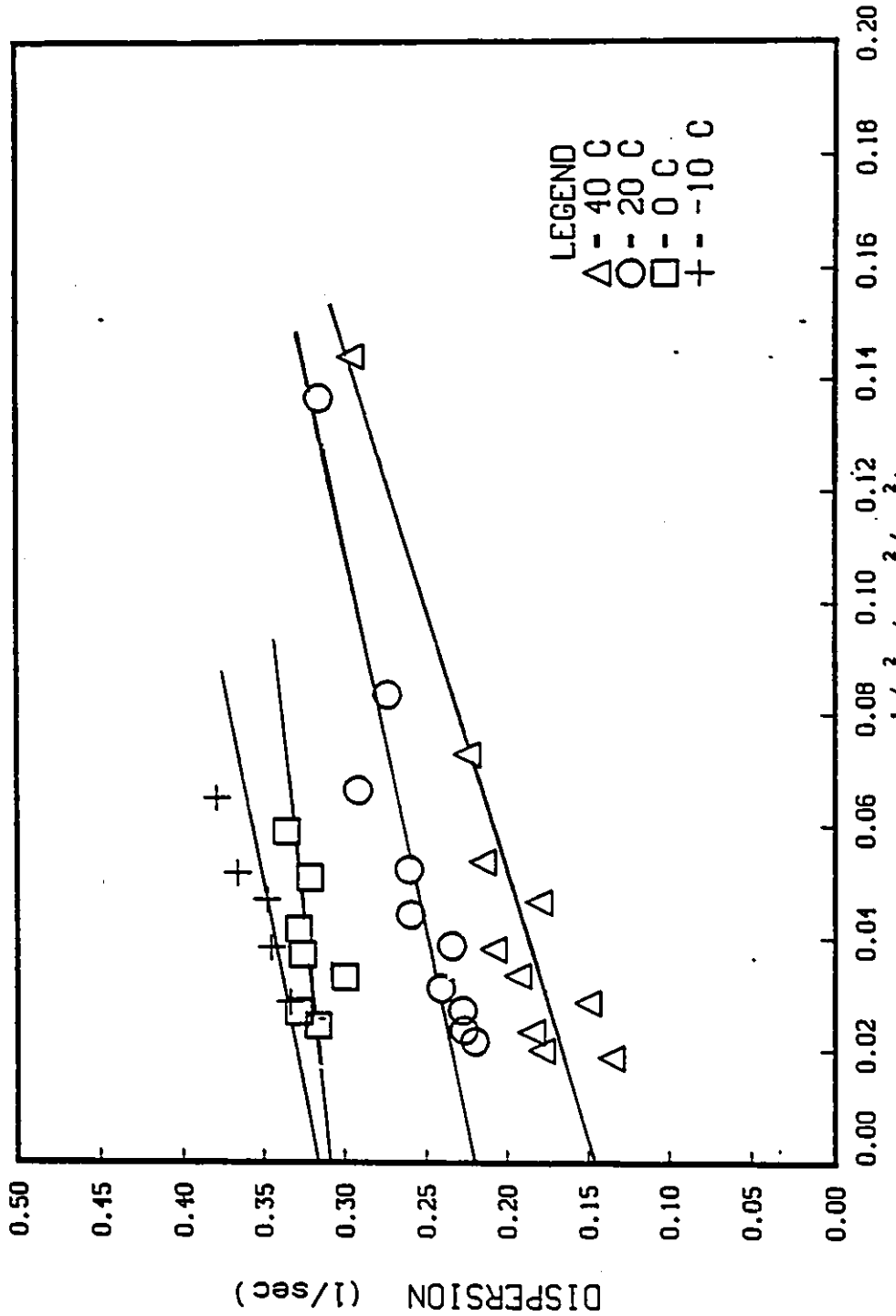

Figure 6.10: Dispersion ($\sigma^2 L/2\mu^2 v$) versus $1/v^2$ for N_2-4A Zeolite system

Table 6.6: Overall Diffusion Resistance for the N_2-H-Mordenite and N_2-4A Zeolite Systems

Temperature	Overall Diffusion Resistance	
	H-Mordenite	4A Zeolite
(K)	(sec)	(sec)
313	0.1577	0.2481
293	0.3590	0.3602
273	0.4175	0.5208
263	0.4840	0.5392

Table 6.7: Parameters D_0/r_c^2 and E_a according to equation 6.1

Adsorbent	D_0/r_c^2 (1/sec)	E_a (kcal/mol)
H-Mordenite	2185.17	5.162
4A Zeolite	93.73	6.703

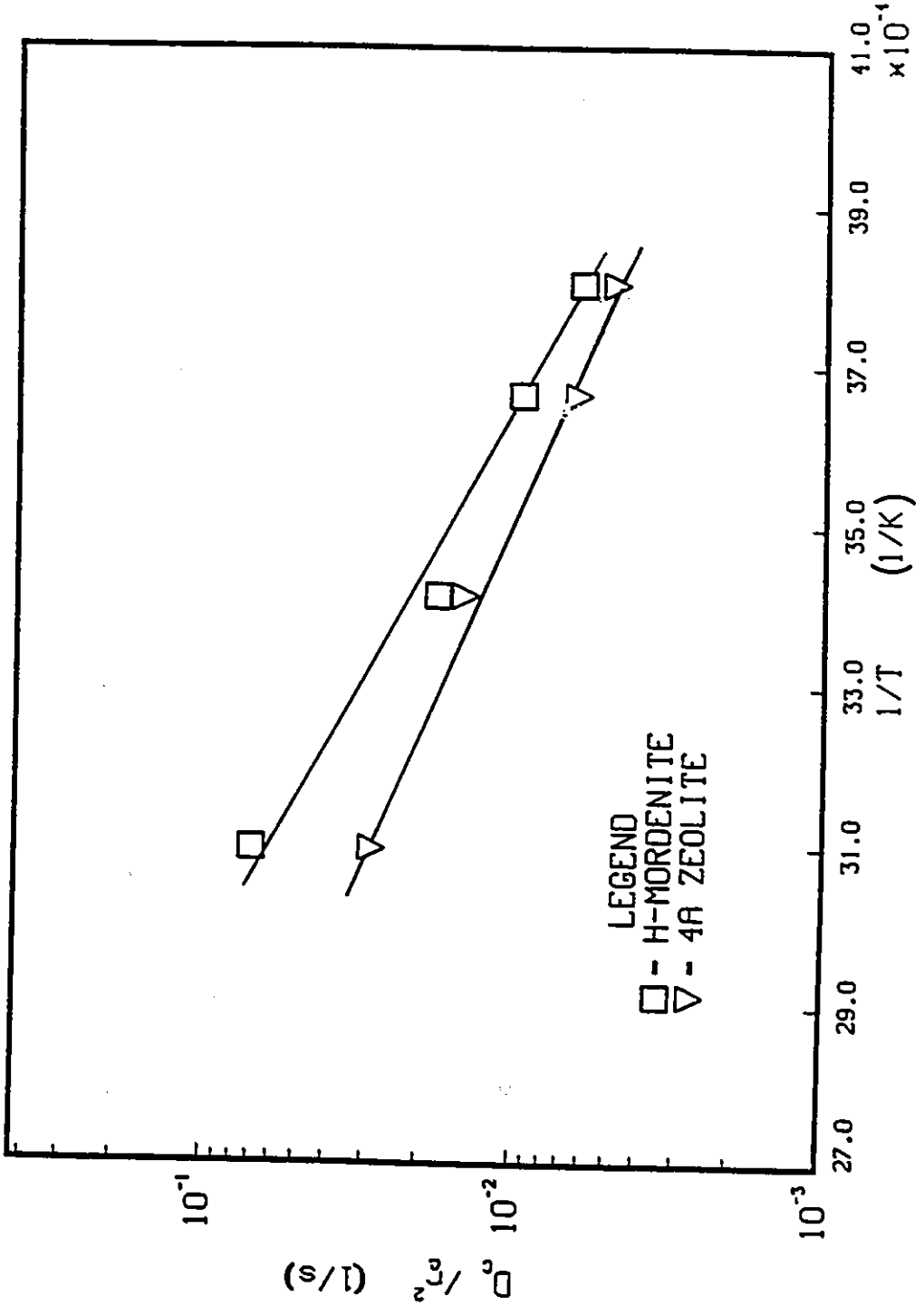

Figure 6.11: Temperature dependence of intracrystalline diffusivity according to equation $D_c/r_c^2 = D_0/r_c^2 exp(-E_a/R\,T)$ for the N_2-H-Mordenite and N_2-4A Zeolite systems

Table 6.8: Comparison of reported values of E_a for the N_2-4A Zeolite system. [19]

Sorbate	Temperature Range (K)	E_a (kcal/mol)
N_2	304 - 363	6.06
	243 - 323	5.58
	194 - 273	4.07
	215 - 279	6.13
	298 - 363	4.46

6.2.1 Effect of Temperature on Adsorption Equilibrium

The equilibrium constants of adsorption for all three gases are shown graphically in Figure 6.12. For the CO-4A system the K_p values are small. The CH_4-4A system exhibits larger values yet they change only slightly with temperature. The parameters of the vant Hoff equation indicating the temperature dependence of K_p are given in Table 6.9. Table 6.10 (as found in reference 18) gives a comparison of reported heats of adsorption for a N_2-4A Zeolite system and a CH_4-4A Zeolite system. For N_2 sorbate the value of ΔH_0 (4.77 kcal/mol) obtained in this study agrees well with the values previously reportrd in literature. For CH_4 sorbate the obtained value of ΔH_0 is somewhat lower than values previously reported.

For a N_2-4A zeolite system Haq and Ruthven [19] have reported values of 3.87 kcal/mol for ΔU_0 and 0.0159 (dimensionless) for K_0. These values are in agreement with those reported in this study (ΔU_0= 4.198 kcal/mol and K_0= 0.0144).

The adsorption selectivities are illustrated in Figure 6.13. All the selectivity values are small in the temperature range that was studied.

Table 6.9: Parameters K_0 and ΔU_0 giving temperature dependence of K_p according to equation $K_p = K_0 \exp(-\Delta U_0 / R\ T)$ for 4A Zeolite

Sorbate	K_0 (dimensionless)	ΔU_0 (kcal/mol)	ΔH_0 (kcal/mol)
N_2	0.0144	4.198	4.770
CO	0.0461	3.044	3.616
CH_4	0.4979	2.068	2.640

Table 6.10: Comparison of reported heats of adsorption (ΔH_0) for the N_2-4A Zeolite system.

[19]

Sorbate	Temperature Range (K)	ΔH_0 (kcal/mol)
N_2	304 - 363	4.20
	243 - 323	4.20
	215 - 277	4.35
	298 - 363	4.53
CH_4	306 - 366	4.90
	243 - 323	4.30
	215 - 277	5.30
	298 - 363	4.60
	323 - 473	4.70

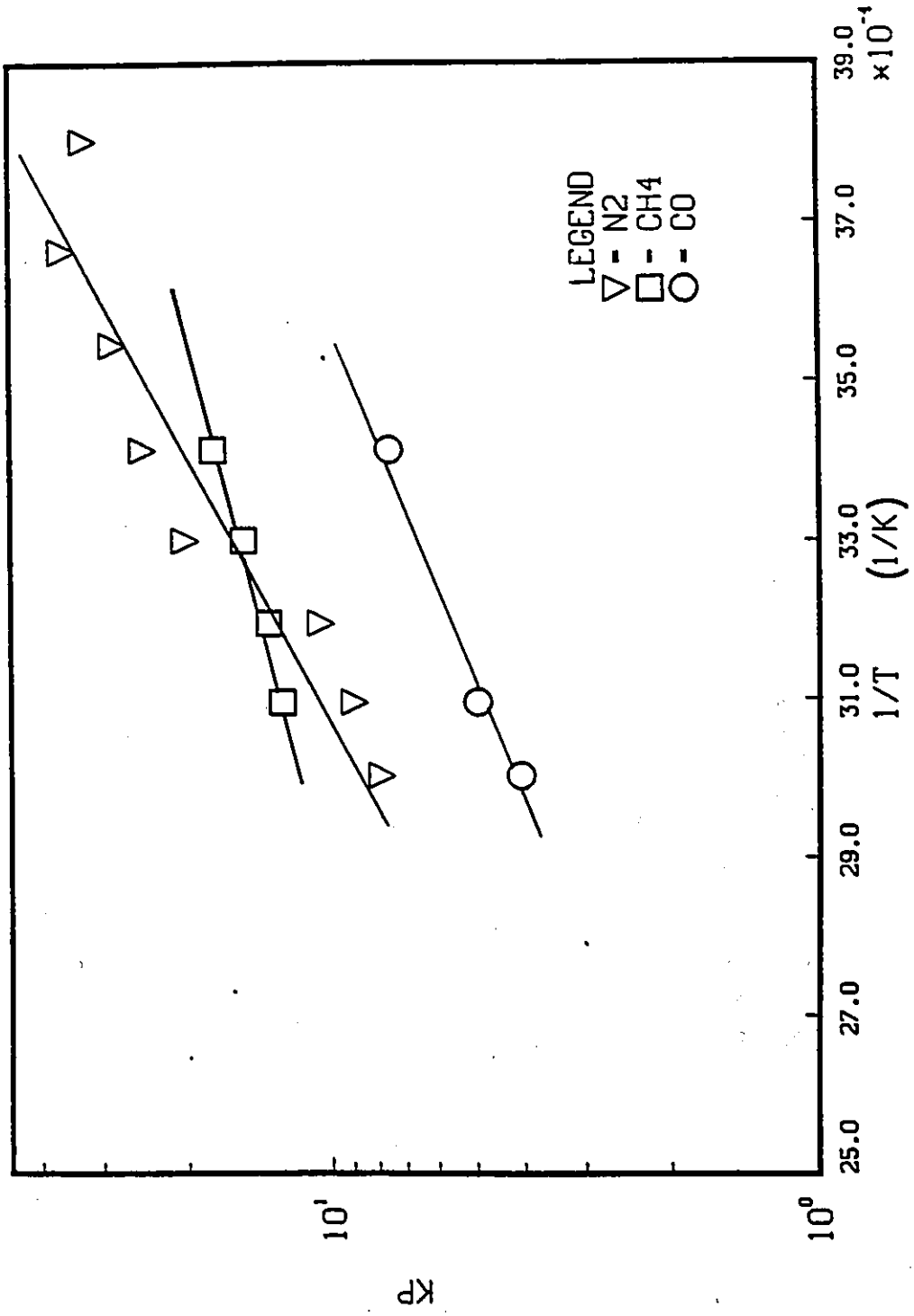

Figure 6.12: Temperature dependence of equilibrium constants according to equation $K_p=K_0 \exp(-\Delta U_0/RT)$ for the adsorption of N_2, CH_4 and CO on 4A Zeolite

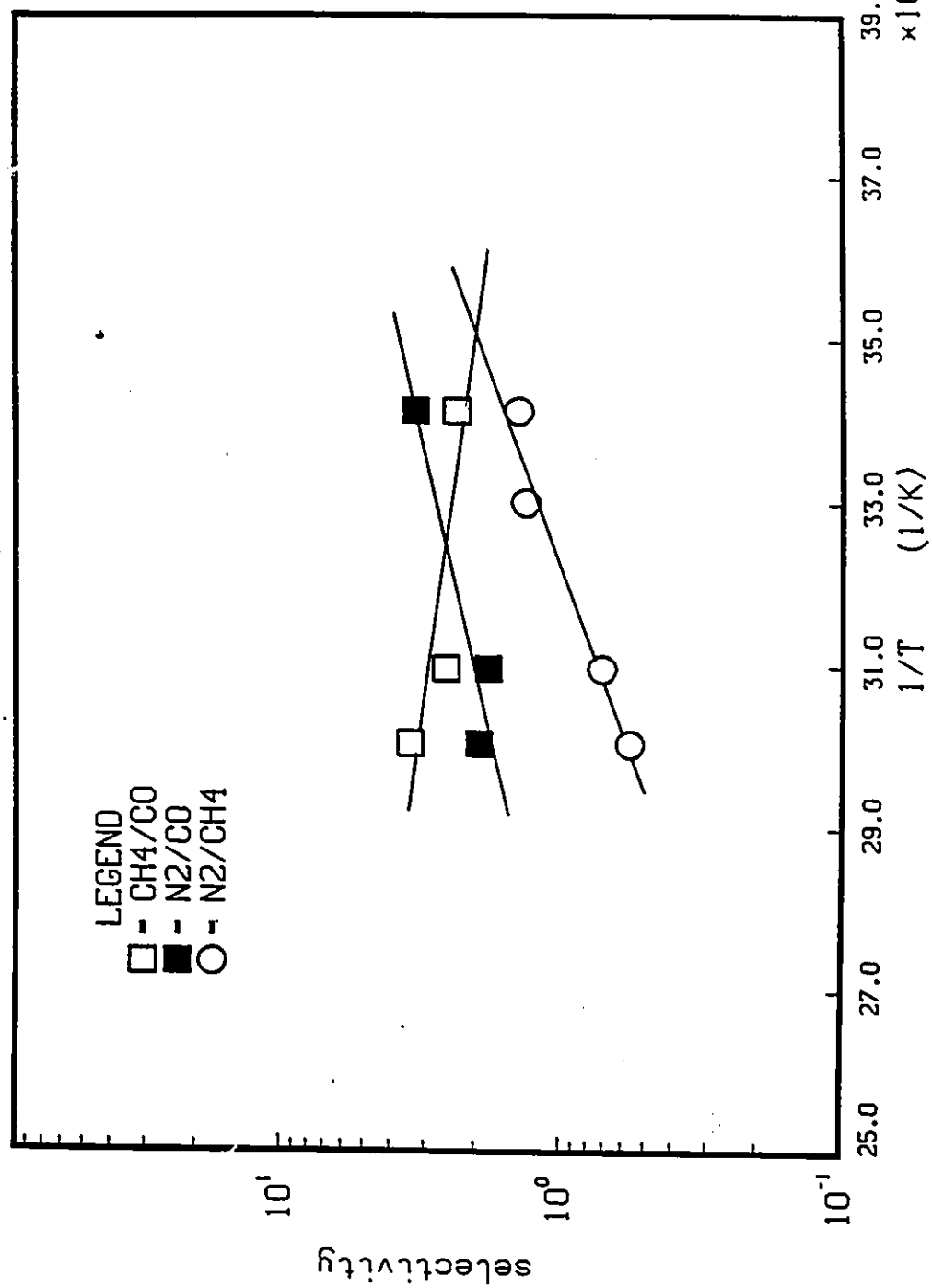

Figure 6.13: Adsorption equilibrium selectivities for the 4A Zeolite system

6.3 Type 5A Zeolite

As illustrated in Figures 6.14 to 6.16, temperature experiments performed with the 5A zeolite suggest that zeolitic diffusional resistance is negligible for all three gases. Due to this observation no volumetric flow rate experiments were performed. In comparison with the 4A molecular sieve, the dispersion of all three gases in the 5A sieve decreases by one decimal place. This can be contributed to the larger pore size of the 5A zeolite in which the molecules more readily diffuse.

The vant Hoff plots showing the temperature dependency of the equilibrium constant for adsorption are given in Figure 6.17 and the corresponding parameters are given in Table 6.11. Table 6.12 compares the obtained parameters of the vant Hoff equation as well as the heats of adosrption for N_2 and CH_4 sorbate with those found in literature [20]. For both sorbates the experimental results of this work agree well with those previously reported.

When equilibrium constants obtained for the three gases with the 4A and 5A zeolites are compared (Table 6.13), it can be seen that the values for the 5A system are substantially larger. These results are explained by considering the available surface area for adsorption in each of the two zeolites. Type 4A and 5A zeolites differ only in the cation present in their frameworks. The 5A zeolite, possessing the calcium cation has a decrease in cation density thus having larger channels. The 4A zeolite contains sodium cations in its framework and has smaller channels. The larger 5A zeolite channels allow for a higher adsorption capacity because they cause an increase in the overall micropore surface area of the zeolite that is accessible. Thus the ratio of the number of moles adsorbed per unit volume of pellet is higher for the 5A system, yielding higher K_p values. Determination of the zeolite surface area through the BET method [8] concurs with this explanation. A BET surface area of 27.1558 m^2/g was obtained for the 4A zeolite whereas the 5A zeolite had a

Table 6.11: Parameters K_0 and ΔU_0 giving temperature dependence of K_p according to equation $K_p = K_0 \exp(-\Delta U_0/R\ T)$ for the 5A Zeolite

Sorbate	K_0 (dimensionless)	ΔU_0 (kcal/mol)	ΔH_0 (kcal/mol)
N_2	0.0156	4.325	4.897
CO	0.6135	3.120	3.692
CH_4	0.0382	3.958	4.530

surface area a magnitude larger, at 390.8316 m^2/g.

This explanation also holds true for the equilibrium constant values obtained with H-Mordenite. The K_p values for H-Mordenite are higher than those obtained for the 4A zeolite and more in accordance with the K_p values observed with the 5A system. Since synthetic hydrogen mordenite was used in this study, the channel radius lies within the range of 5.0 - 6.9 Å.

The equilibrium selectivities for the 5A zeolite are plotted in Figure 6.18. As illustrated both a CO-CH_4 and CO-N_2 separation is quite favorable. The feasibility of the CO-N_2 separation being greater especially at lower temperatures where the selectivity reaches a value of approximately 6.0. A CH_4-N_2 separation would not be recommended since for the whole temperature range the equilibrium selectivity values are not substantially larger than 1.0.

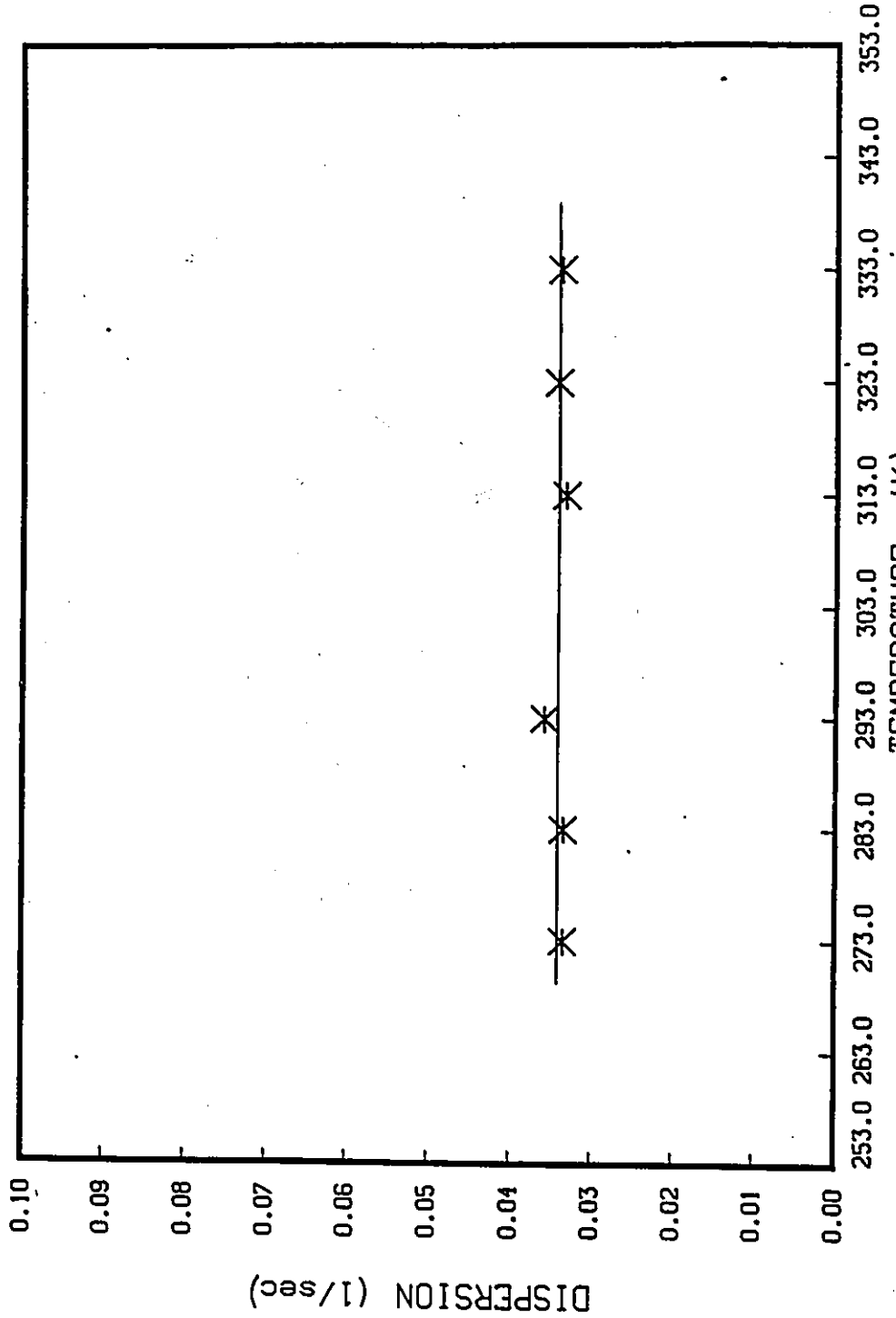

Figure 6.14: Dependence of dispersion ($\sigma^2 L/2\mu^2 v$) on temperature for N_2-5A Zeolite system

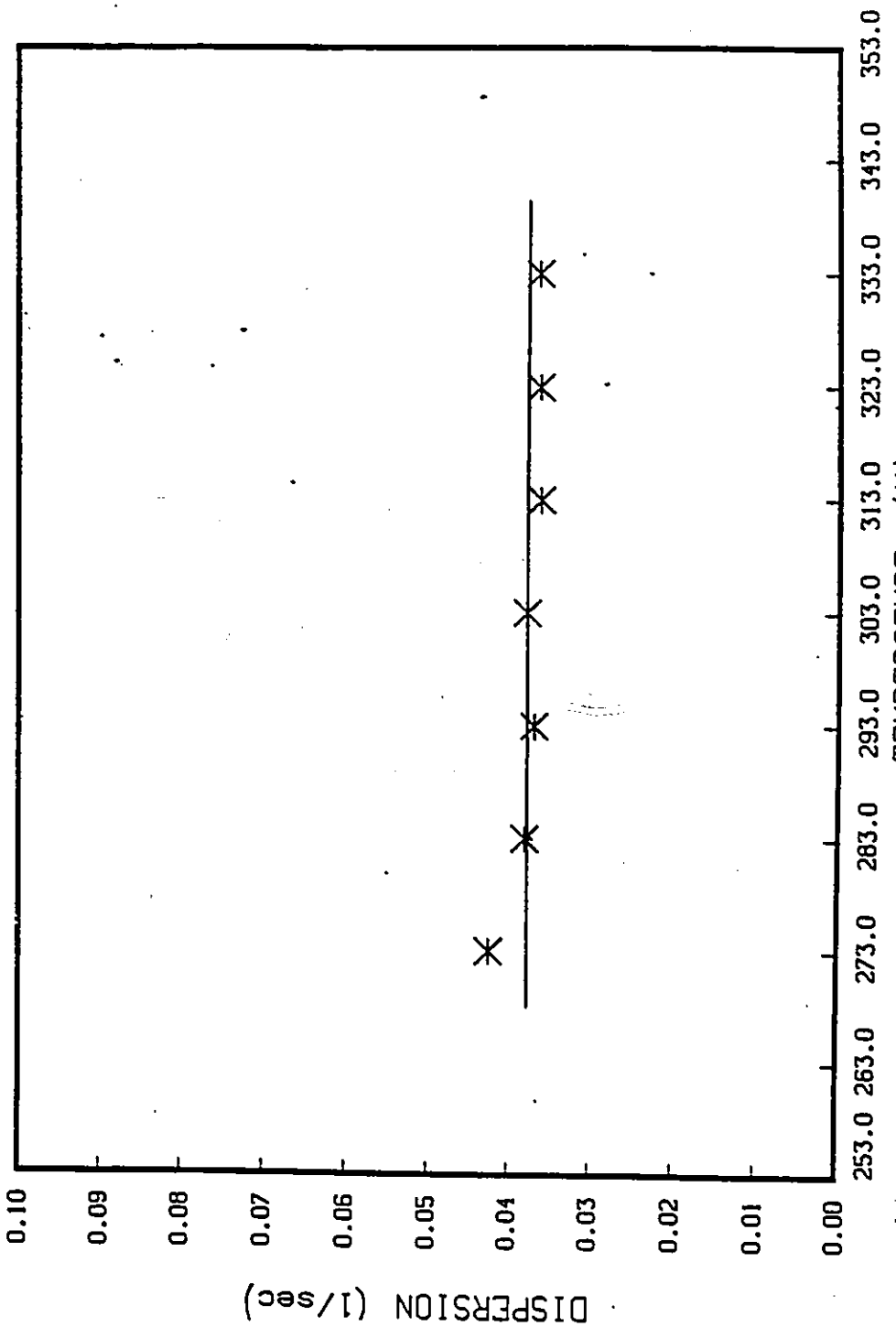

Figure 6.15: Dependence of dispersion ($\sigma^2 L/2\mu^2 v$) on temperature for CO-5A Zeolite system

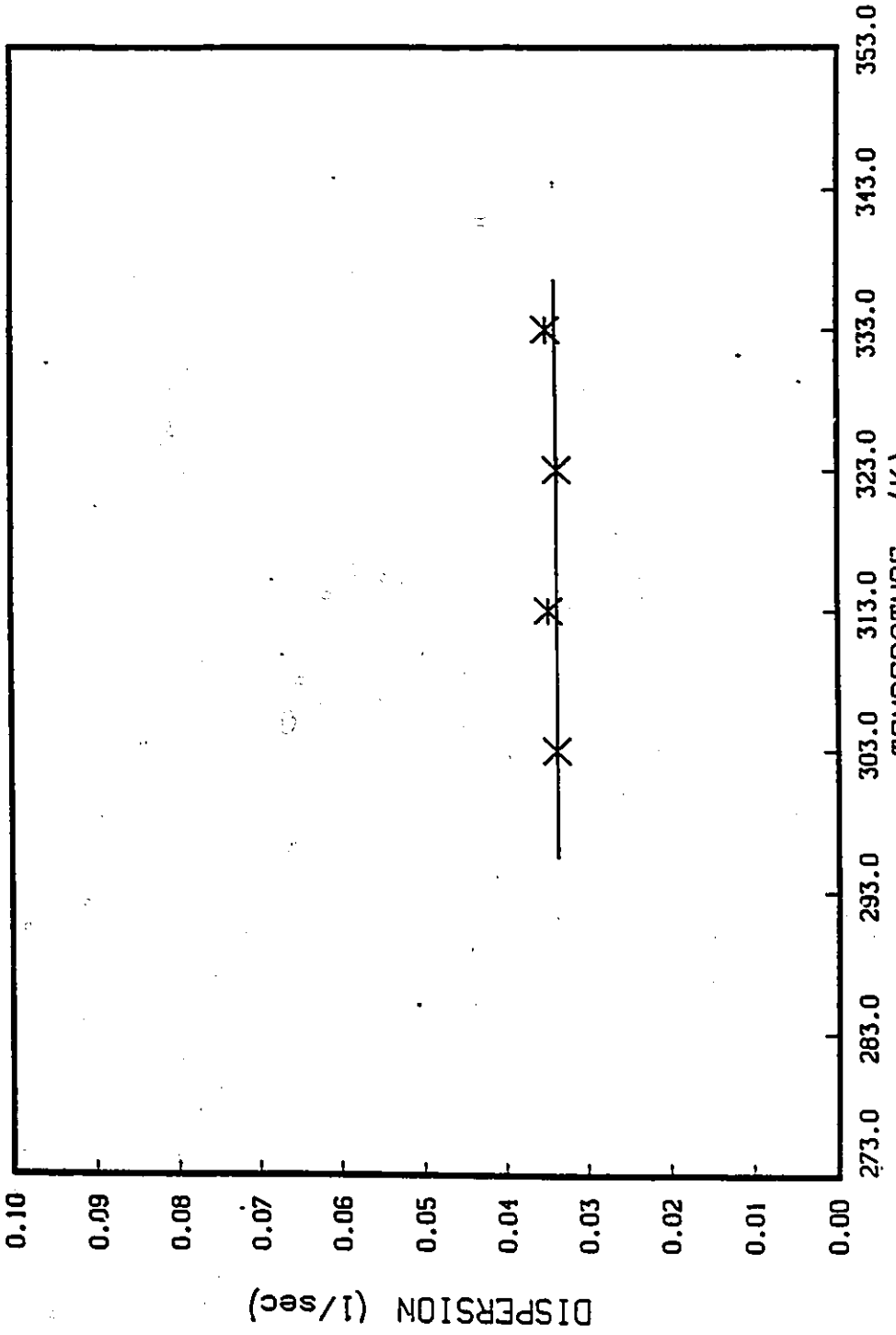

Figure 6.16: Dependence of dispersion ($\sigma^2 L/2\mu^2 v$) on temperature for CH_4-5A Zeolite system

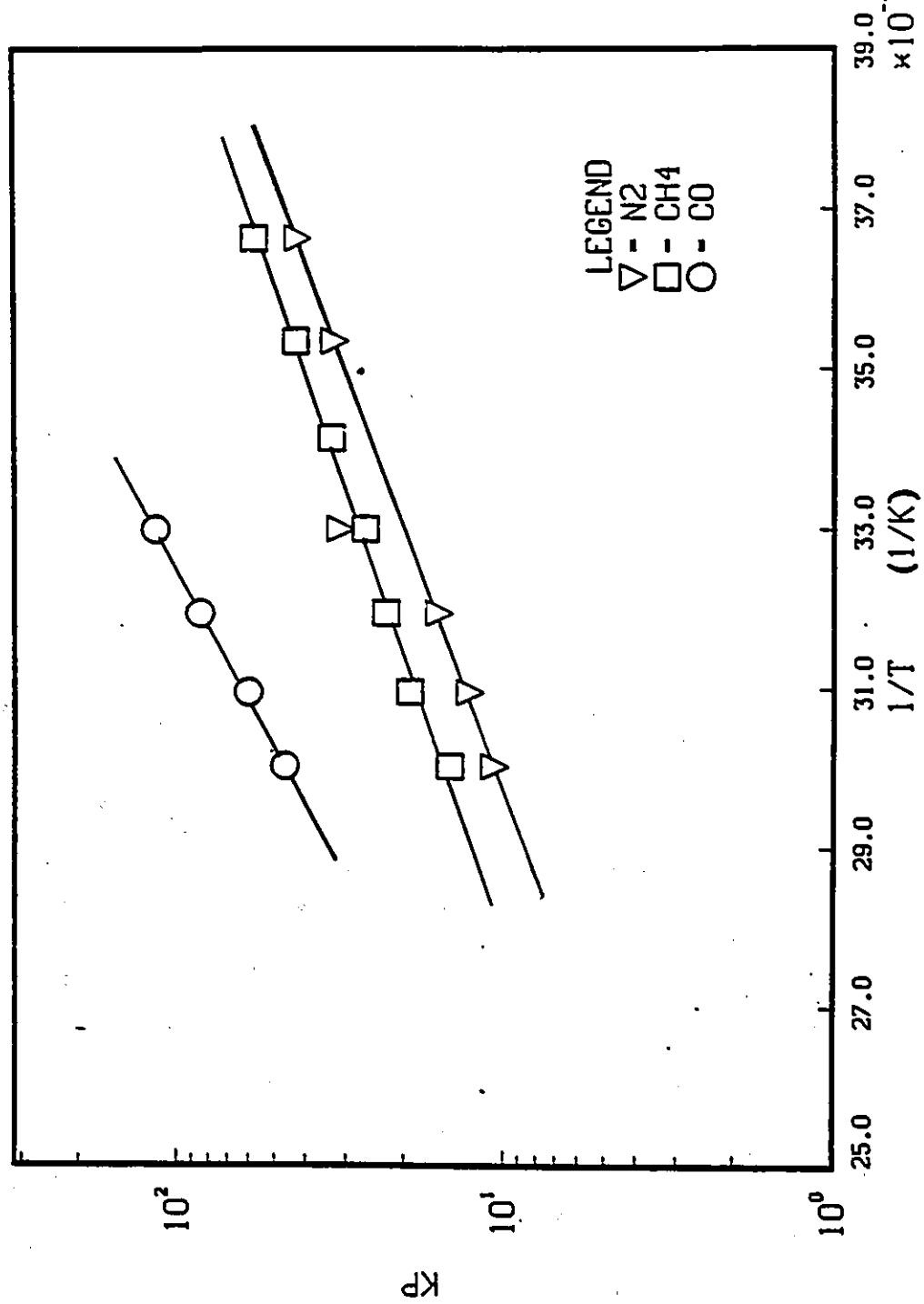

Figure 6.17: Temperature dependence of equilibrium constants according to equation $K_p = K_0 \exp(-\Delta U_0/RT)$ for the adsorption of N_2, CH_4 and CO on 5A Zeolite

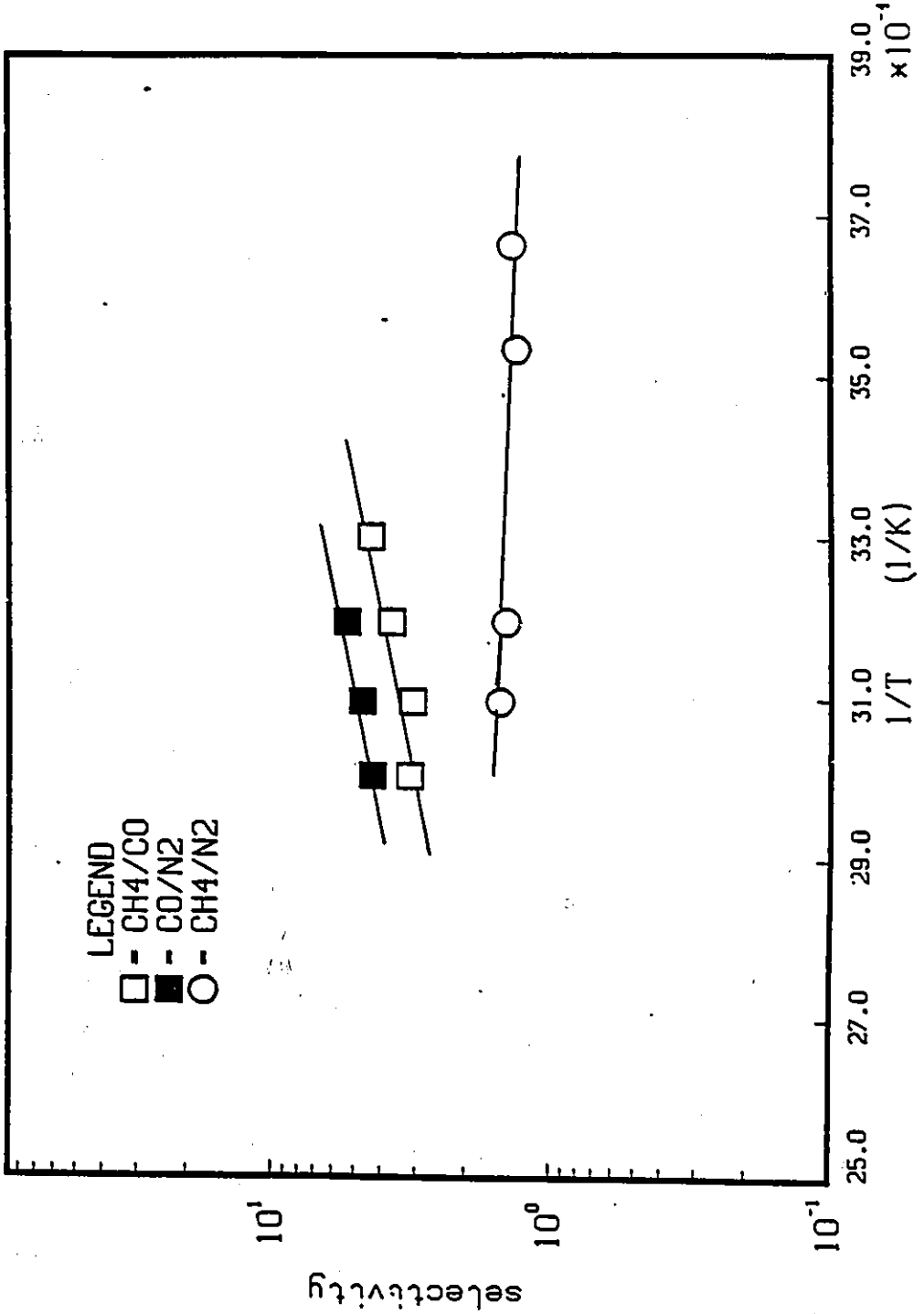

Figure 6.18: Adsorption equilibrium selectivities for the 5A Zeolite system

Table 6.12: Comparison of reported values of parameters K_0 and ΔU_0 of equation $K_p = K_0 \exp(-\Delta U_0/R\,T)$ and heats of adsorption for 5A Zeolite [20]

Sorbate	Reference	K_0 (dimensionless)	ΔU_0 (kcal/mol)	ΔH_0 (kcal/mol)
N_2	(19)	0.00455	4.78	5.44
	(19)			5.00
	present	0.0150	4.33	4.90
CH_4	(19)	0.0363	3.72	4.50
	(19)			5.10
	present	0.0363	3.76	4.53

Table 6.13: Adsorption Equilibrium Constants for the Type A Zeolites

Temp	K_{pN_2}		K_{pCO}		K_{pCH_4}	
	4A	5A	4A	5A	4A	5A
(K)						
263	32.4532	-	-	-	-	
273	36.0260	42.5732	-	-	-	58.0034
283	28.2896	32.7886	-	-	-	43.1432
293	24.6269	31.5198	7.5811	-	17.5937	33.4524
303	20.1902	-	-	116.4302	15.2806	26.4338
313	10.5554	15.8249	-	85.0944	-	22.8687
323	9.0141	12.7369	5.0118	60.5589	12.7157	19.3697
333	7.9181	10.7046	4.0903	46.6988	13.9853	14.6119

6.4 Chabazite

Temperature experiments were performed for all three gases and volumetric flow rate experiments only for N_2 on natural chabazite. From Figure 6.19 it can be seen that zeolitic diffusional resistance is a contributing factor for the N_2-Chabazite system. Dispersion decreases as temperature increases by a wide margin. This trend does not occur in the CO-Chabazite system (Figure 6.20) where dispersion remains constant at a value of approximately 0.30 1/sec. Zeolitic diffusional resistance is also negligible for the CH_4-Chabazite system where as indicated in Figure 6.21, dispersion remains constant at a value of approximately 0.15 1/sec for the whole temperature range.

The temperature dependence of the equilibrium constants for adsorption is shown in Figure 6.22 for the N_2-Chabazite and CO-Chabazite systems. The corresponding parameters of the vant Hoff equation 6.3 are given in Table 6.15.

The K_p values for the CH_4-Chabazite system, are not shown graphically yet are tabulated in Table 6.14. These values are quite small and allowing for experimental error, do not change with temperature.

For the CO-Chabazite system, due to the difficulty in analyzing the experimental peaks that exhibited severe tailing, only three data points are plotted and must be treated with caution.

The unpredictable nature of this molecular sieve with the carbon monoxide and methane gases can also be in part contributed to the impurities that naturally occur in the Chabazite framework. Even with pre-treatment conditioning these impurites can not be completely removed, thus they hinder diffusion and adsorption by obstructing the Chabazite channels. Another factor that might contribute to the observed results is that the calcium cations present in the Chabazite framework,

have been reported to become displaced within the cavities, as a result of dehydration. Thus one might conclude that thermal pretreatment of the Chabazite column at 623 K, might have caused the calcium cations to occupy positions within the framework that would further reduce the apperture of the Chabazite windows.

Even though, zeolitic diffusional resistance was found to contribute to the N_2-Chabazite system, volumetric flow rate experiments to calculate the resistance were not performed due to the results obtained for the other two gases. It was concluded that any (θD_p) values calculated from either the CO-Chabazite system or CH_4-Chabazite system would not be truly representative of the equilibria or kinetics of the adsorption taking place.

In the progress of this study Chabazite was the only naturally occurring zeolite that was tested and it was also the one that posed the most difficulty both from the point of view of obtaining the experimental data and analyzing it.

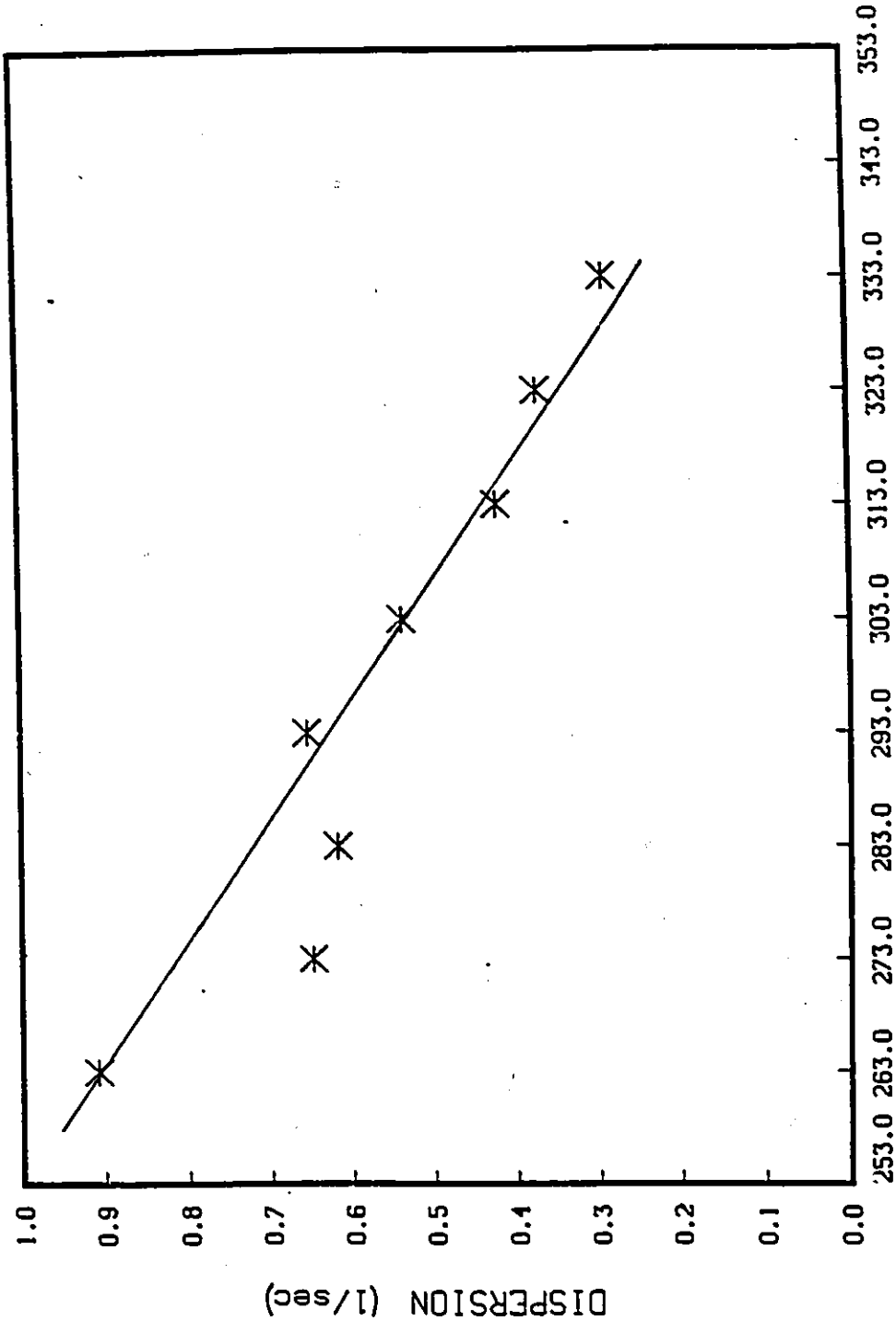

Figure 6.19: Dependence of dispersion ($\sigma^2 L/2\mu^2 v$) on temperature for N_2-Chabazite system

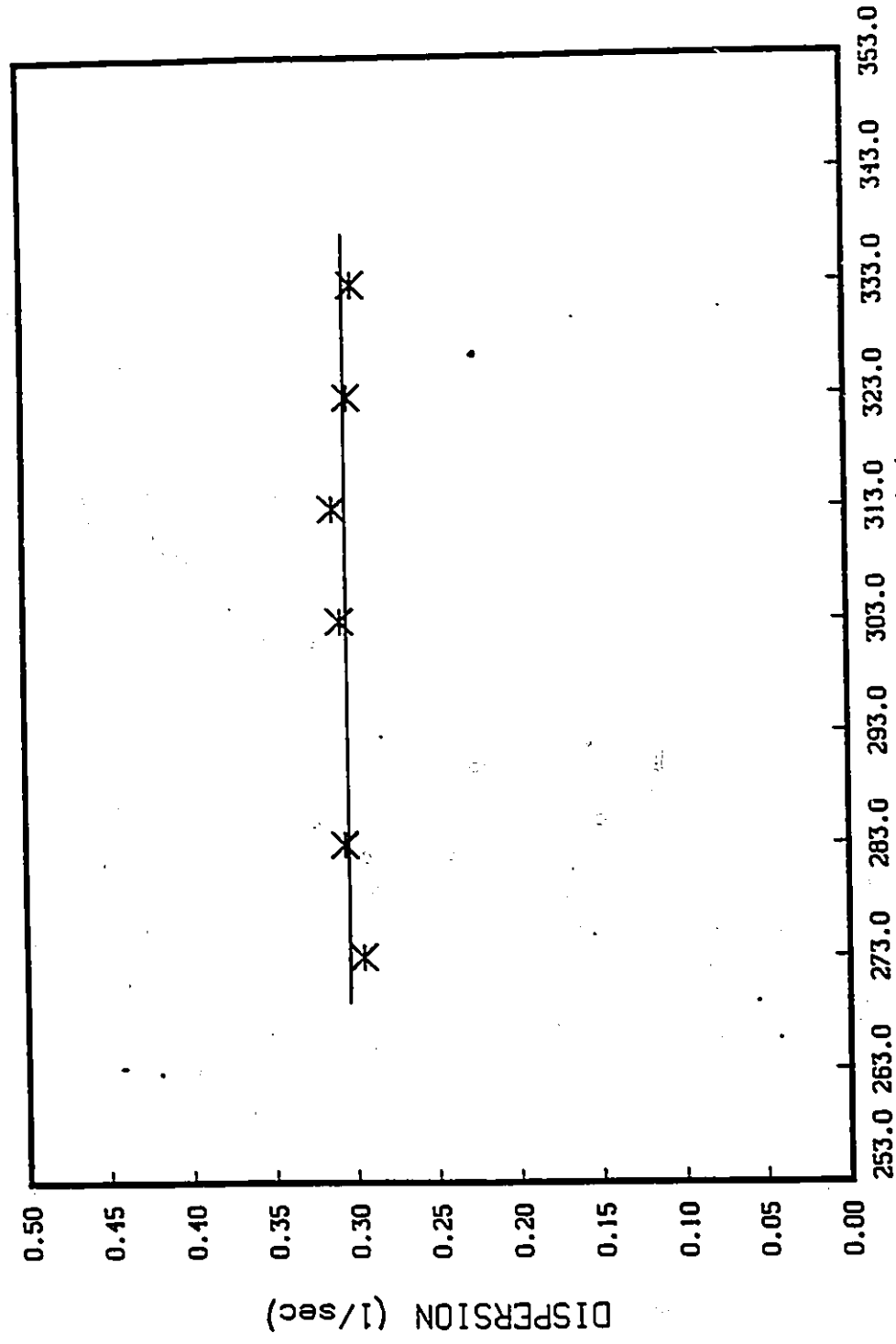

Figure 6.20: Dependence of dispersion ($\sigma^2 L/2\mu^2 v$) on temperature for CO-Chabazite system

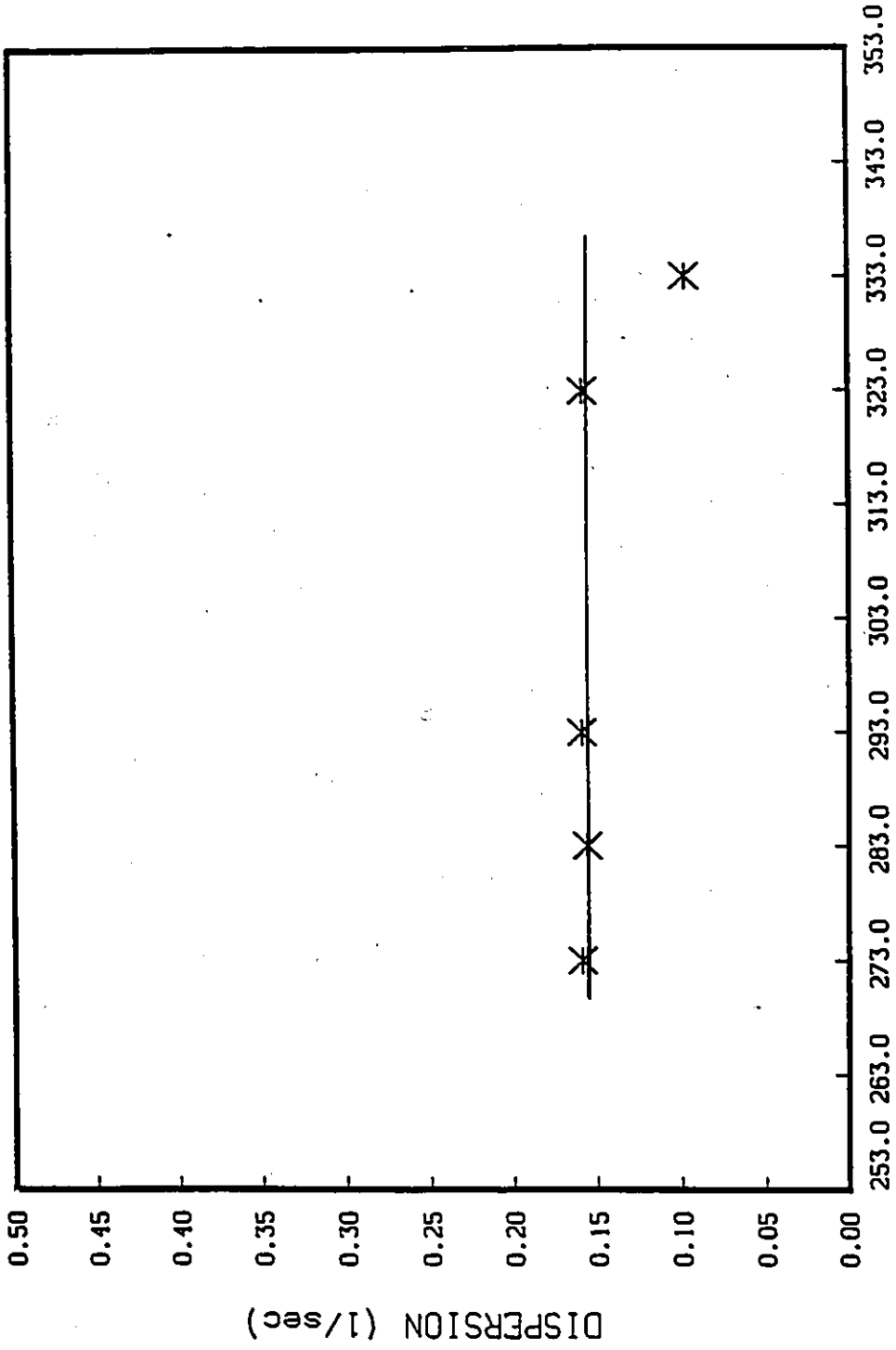

Figure 6.21: Dependence of dispersion ($\sigma^2 L/2\mu^2 v$) on temperature for CH_4-Chabazite system

Table 6.14: Adsorption Equilibrium Constants for Chabazite

Temp (K)	$K_{p_{N_2}}$ (dimensionless)	K_{pCO} (dimensionless)	K_{pCH_4} (dimensionless)
263	16.2686	-	5.7261
273	11.7636	-	2.5109
283	11.0101	-	2.5044
293	11.8703	-	2.4443
303	12.0317	-	2.8176
313	9.9244	9.5640	3.0638
323	9.0792	7.8468	2.4592
333	8.5290	5.7568	2.3622

Table 6.15: Parameters K_0 and ΔU_0 giving temperature dependence of K_p according to equation $K_p = K_0 \exp(-\Delta U_0/R\ T)$ for Chabazite

Sorbate	K_0 (dimensionless)	ΔU_0 (kcal/mol)	ΔH_0 (kcal/mol)
N_2	1.275	1.274	1.846
CO	0.0021	5.239	5.812

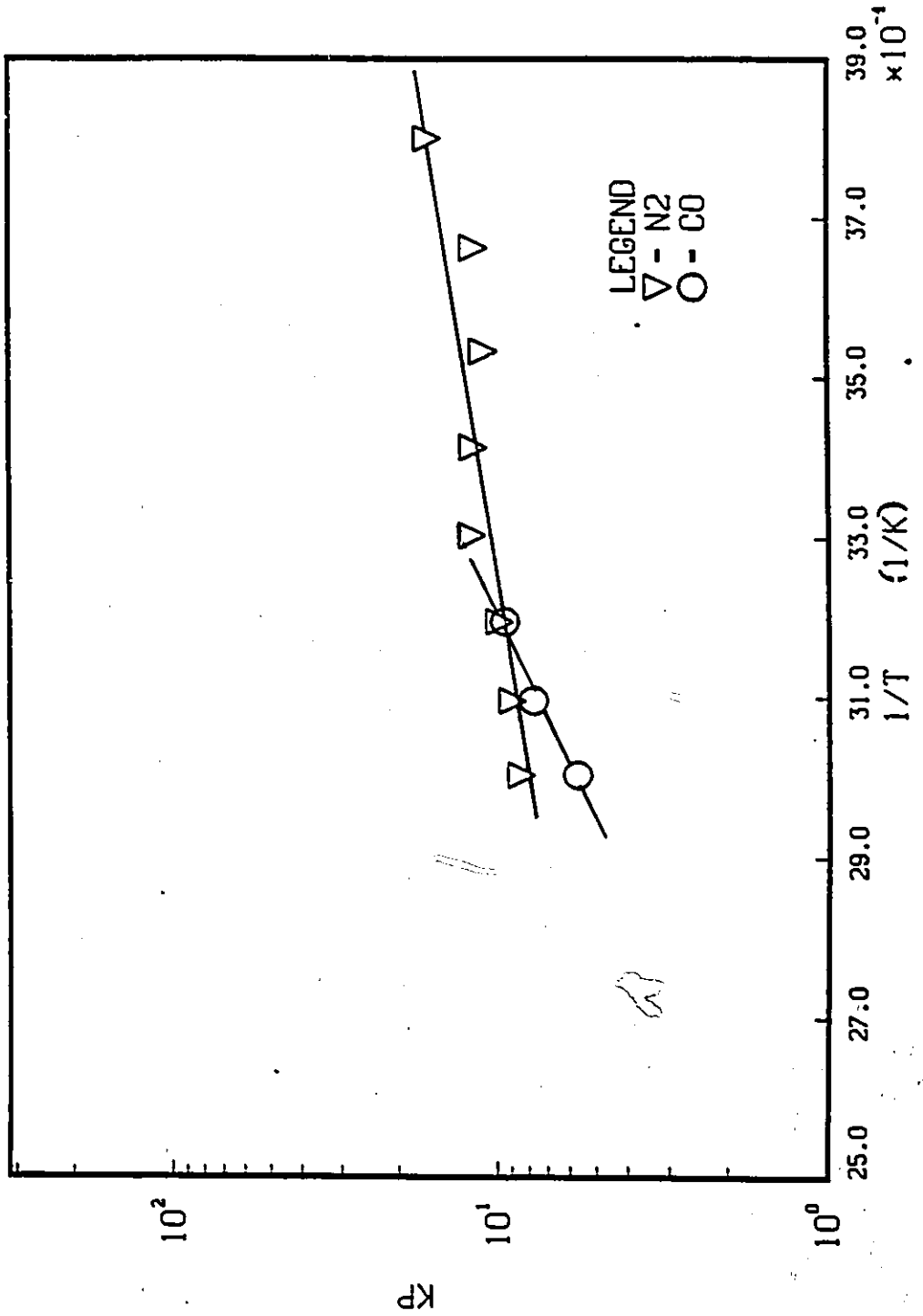

Figure 6.22: Temperature dependence of equilibrium constants according to equation $K_p = K_0 \exp(-\Delta U_0/RT)$ for the adsorption of N_2, CH_4 and CO on Chabazite

6.5 Ethylene

The adsorption of ethylene on H-Mordenite and 4A molecular sieves was also studied. However, no quantitative results are presented because through electron-paramagnetic resonance tests it was found that activity takes place between the solid and the gas phases. Figure 6.23 shows the chromatograms obtained for ethylene and H-Mordenite at a temperature of 313 K. For this system, at 273 K no dispergent peak was obtained. The chromatogram observed for the CH_2=CH_2-4A system is shown in Figure 6.24. For both systems the carrier gas flow rate is sufficiently high (1.0 ml/s), to allow the pulsed gas to pass-thru the bed in a relatively short period of time. However, for the H-Mordenite system the recorder is operating at a paper rate of 10.0 cm/min thus the emergent peak was observed after nearly 4 minutes. For the 4A zeolite system the paper rate is one tenth that of the H-Mordenite system and the chromatogram is obtained after approximately 40 minutes. It is evident therefore, that for both cases ethylene is strongly yet anomalously adsorbed. An explanation to this occurence might be found in the work performed by Harper et. al. [21] who concluded that the surface of type A zeolites is polar and postulated that large electrical fields might exist near the exchangeable cations. Thus specific interactions might be expected between these highly charged sites and molecules containing double or triple bonds. The study also found that molecules with double or triple bonds are strongly adsorbed on type A molecular sieves. Habgood [17] while studying the adsorptive and gas chromatographic properties of various cationic forms of zeolite X, found that the quadropole interactions between the solid and the gas, which depend on the intensity of the electric field gradient, were more intense on zeolite surfaces where the cations occupied positions adjacent to the oxygen anions in the aluminosilicate framework.

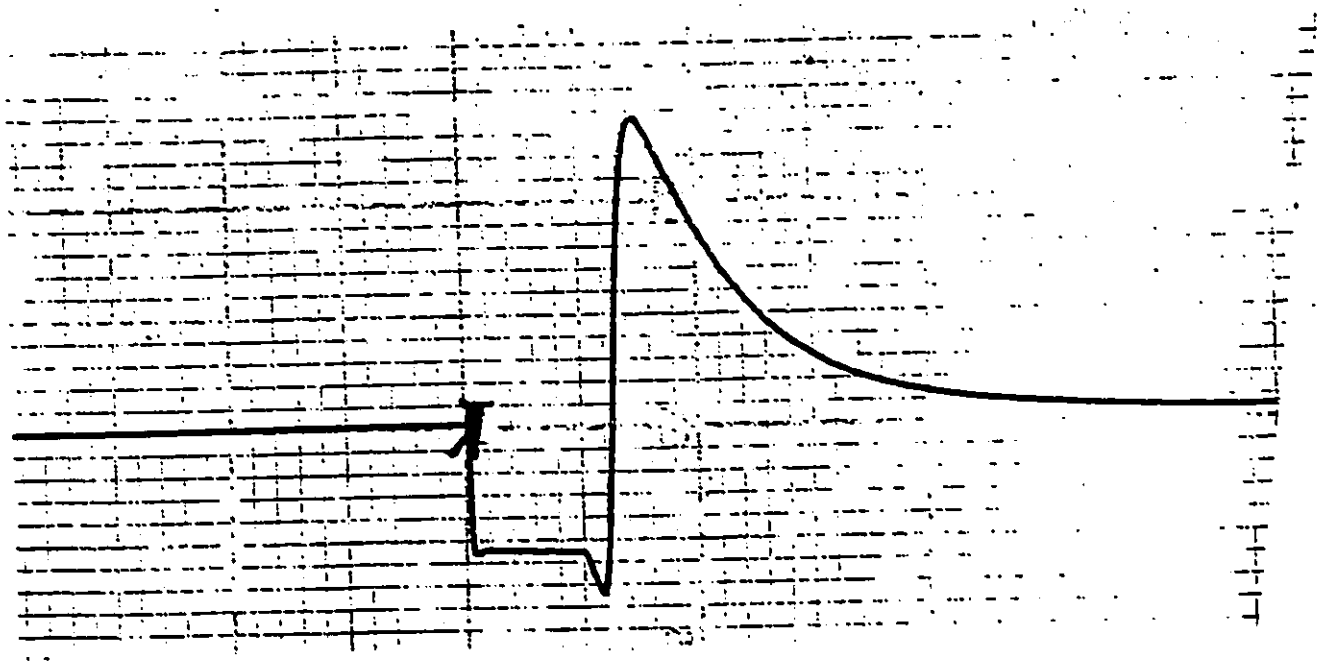

Figure 6.23: Gas chromatogram for CH_2=CH_2-H-Mordenite system at 313 K: attenuation= 1, sensitivity= 1, TC current= 1 recorder voltage= 10 mV, rate= 10 cm/min

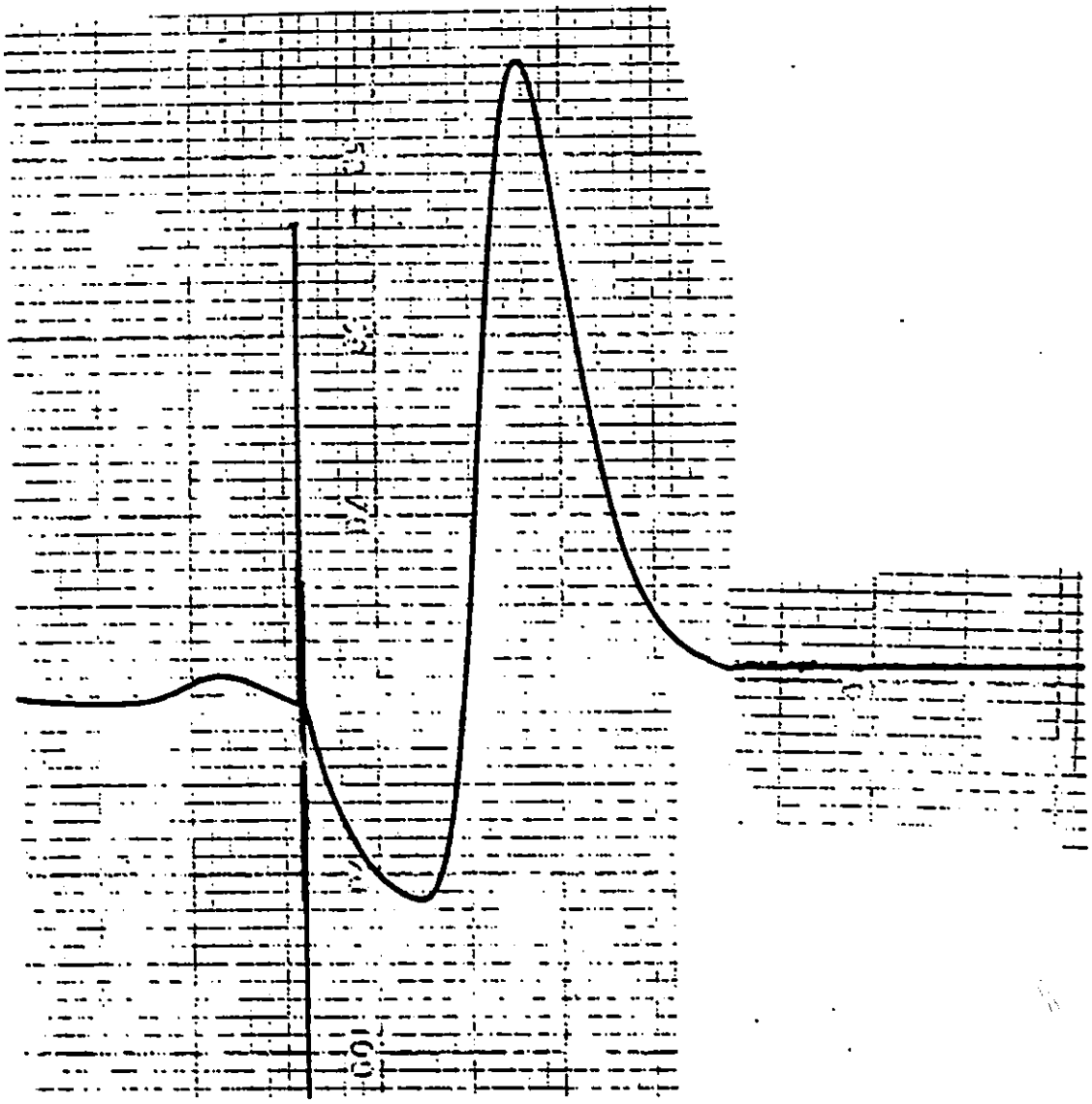

Figure 6.24: Gas chromatogram for CH_2=CH_2-4A Zeolite system at 313 K: attenuation= 1, sensitivity= 1, TC current= 1 recorder voltage= 10 mV, rate= 0.1 cm/min

In studying the results obtained with the four adsorbents it was concluded that, on the basis of equilibrium selectivities a binary separation of either CO-CH_4 or CO-N_2 on 5A zeolite would be the most feasible separation to consider next. A separation of CO-N_2 on H-Mordenite would also seem feasible however, the K_p values of N_2 on H-Mordenite are almost half those for the N_2-4A system and not substantially higher than 10.0. Thus it was felt that the 5A molecular sieve would be the better adsorbent to test for a binary separation.

The binary system chosen was CO-CH_4 on 5A zeolite.

6.6 Mixed Carrier Gas Systems for CO and CH_4 with 5A Zeolite

For the study of the binary carrier gas systems experiments were carried out in which the concentration of the carrier gas was varied between 0% sorbate to approximately 100% sorbate. Experiments were performed at 313 K and 293 K. The column specifications remain the same as those previously given. The study of the binary carrier gas systems can be divided into two sections:

1. the study of the pure gas isotherms

2. the study of the binary mixture isotherms

6.6.1 Pure Gas Isotherms

Pure gas isotherms were determined for carbon monoxide and methane at 313 K and 293 K by using mixtures of carbon monoxide and helium, and methane and helium, pulsing the equilibrated system with the adsorbing gas, and measuring the

retention time.

Figure 6.25 shows the apparent equilibrium constants of adsorption, for each system at 313 K as a function of mole fraction of adsorbate. At the lower concentration range, the He-CO system exhibits substantially larger K'_p values: with a value of 78.6 at Y_{CO}= 0.0 (or pure helium carrier). Yet with only a 10% increase in the carbon monoxide present in the carrier gas the K'_p value is decreased to almost half of its initial value to 46.3. For this system the K'_p values continue to decrease drastically until the carrier gas is composed of approximately 35% carbon monoxide. Any further changes to the composition of the carrier gas causes only slight decreases in the values of the observed equilibrium constants. For example, for the range of $0.60 \leq Y_{CO} \leq 0.95$ the equilibrium constants decrease from 14.5 to 5.8 (dimensionless).

From the same figure it can be seen that the He-CH_4 system, under the same experimental conditions does not show such a wide margin of K'_p values. For a pure helium carrier (Y_{CH_4}=0.0) methane has a K'_p value of 28.0, substantially lower than the value of K'_p obtained for the CO system. However, both systems exhibit the same trend. Once again, for the CH_4 system a sharp decrease in the K'_p values occurs from 0% methane in the carrier gas to approximately 35% methane in the carrier gas, at which point the apparent equilibrium constant has a value of 12.2. For higher concentrations of adsorbate in the carrier the K'_p values decrease only slightly especially for $Y_{CH_4} \geq 0.75$.

Figure 6.26 plots the equilibrium constants as a function of mole fraction of adsorbate for a temperature of 293 K. The trend exhibited by the carbon monoxide system is similar to that observed at 313 K. The K'_p values for the He-CO system begin at 149.0 for a pure helium carrier and decrease to approximately 18.2 when the carrier gas is composed of 56% carbon monoxide and 44% helium; an added increase in the mole fraction of carbon monoxide in the carrier gas only causes

a gradual decrease in the values of the apparent equilibrium constants. The CH_4 system shows a gradual decrease in K_p values, starting with an equilibrium constant value of 38.1 at Y_{CH_4}=0.0 and reaching a value of 3.3 at Y_{CH_4}=0.98. As can be seen in Figure 6.26 for a methane mole fraction greater than 0.50 in the carrier gas the plot becomes linear. The same is true for $Y_{CO} \geq 0.50$ and for both systems when the carrier gas is composed of approximately 50% of the respective adsorbate the K'_p values for CO and CH_4 differ only slightly. Tables 6.16 and 6.17 tabulate these observed equilibrium constants for the carbon monoxide and methane systems at 313 K and 293 K, respectively. The K'_p values (apparent equilibrium constants) are in fact the slopes of the pure gas isotherms. Since the CO system initially exhibits larger K'_p values it would be expected that this system will yield steeper isotherms at lower concentration of adsorbate in the carrier gas.

The complete isotherms for the single component systems are shown in Figures 6.27 and 6.28 for temperatures of 313 K and 293 K, respectively. At both temperatures carbon monoxide is more substantially adsorbed on the 5A zeolite. However, the difference between the amount of carbon monoxide adsorbed and the amount of methane adsorbed is smaller at 313 K. This would indicate that the amount of carbon monoxide adsorbed increases as temperature decreases and is more preferentially adsorbed under experimental conditions of 293 K and 1 atm total pressure. This observation is in accordance with the selectivity values obtained for both gases on the 5A sieve.

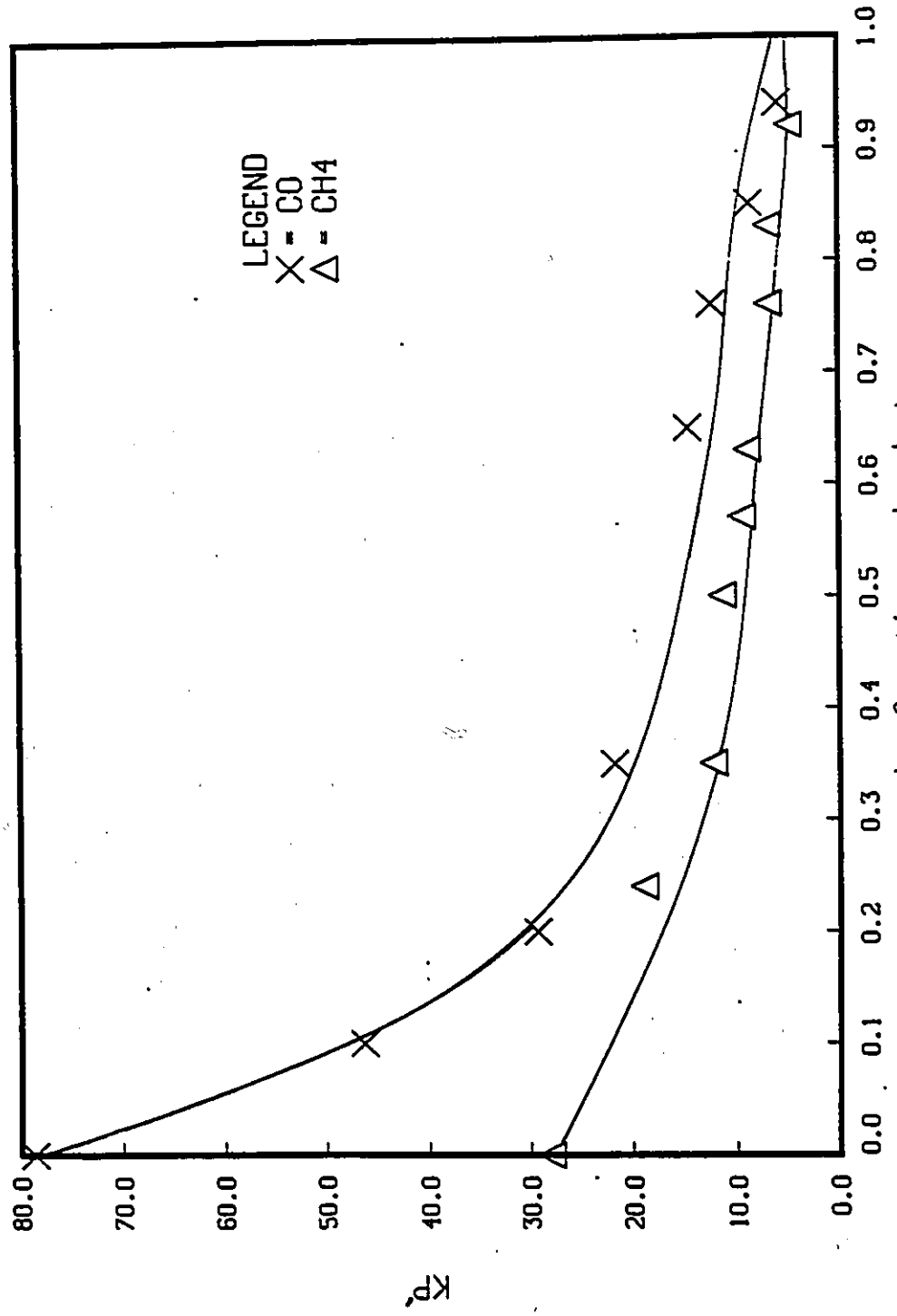

Figure 6.25: K'_p values for the calculation of Pure Gas Isotherms at 313 K for 5A molecular sieve

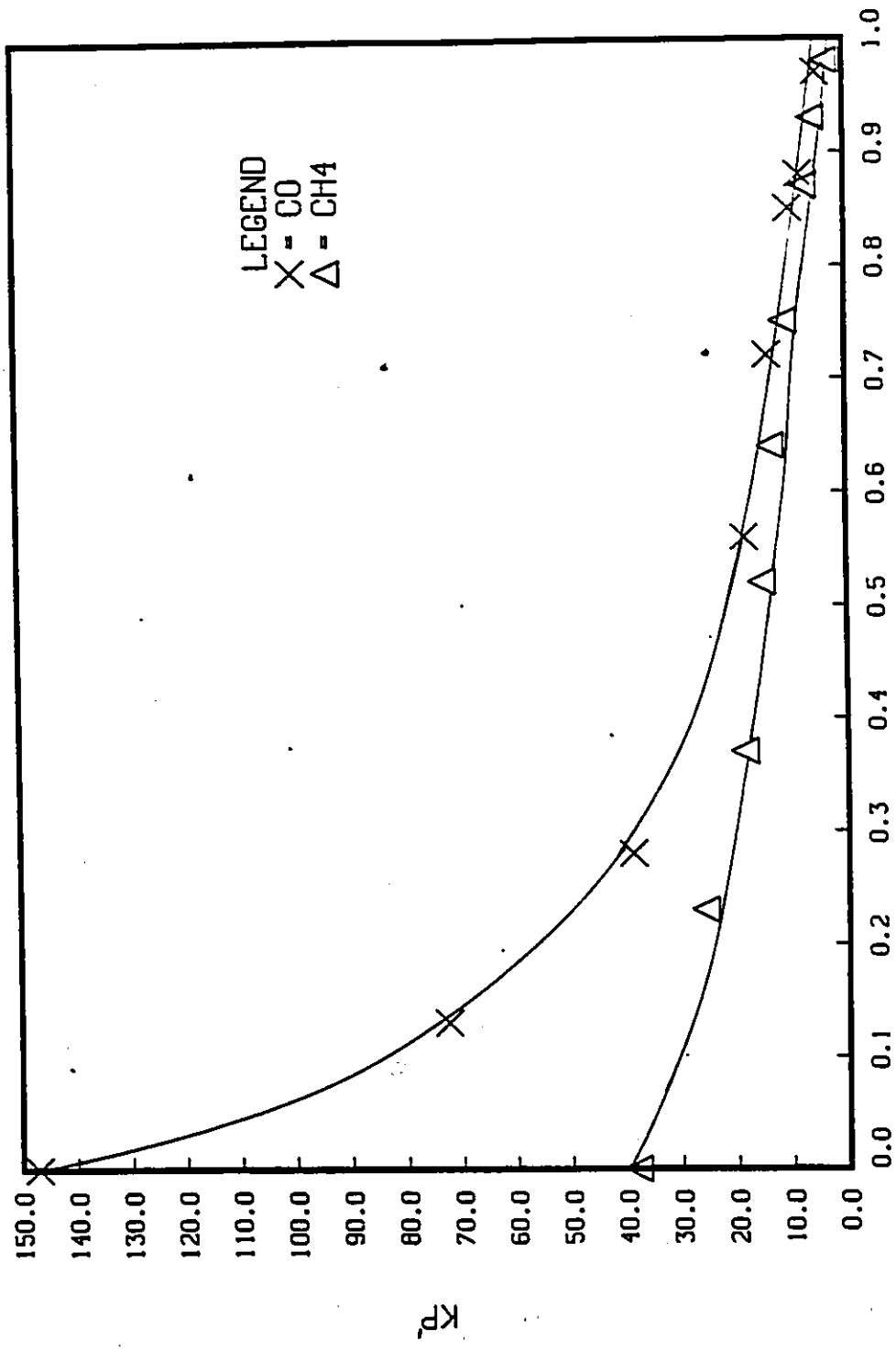

Figure 6.26: K_p' values for the calculation of Pure Gas Isotherms at 293 K for 5A molecular sieve

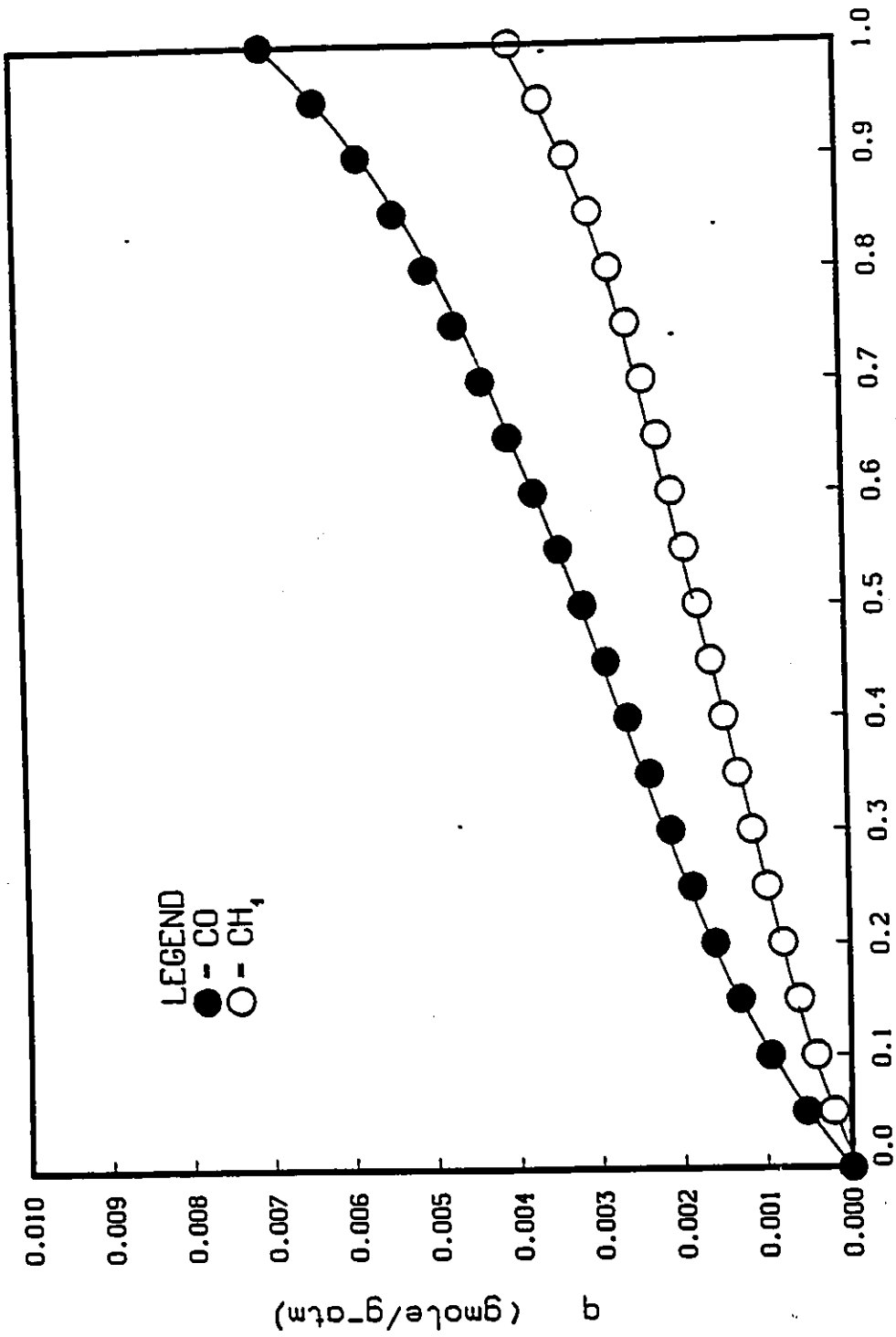

Figure 6.27: Single component isotherms for methane and carbon monoxide at 313 K in 5A molecular sieve

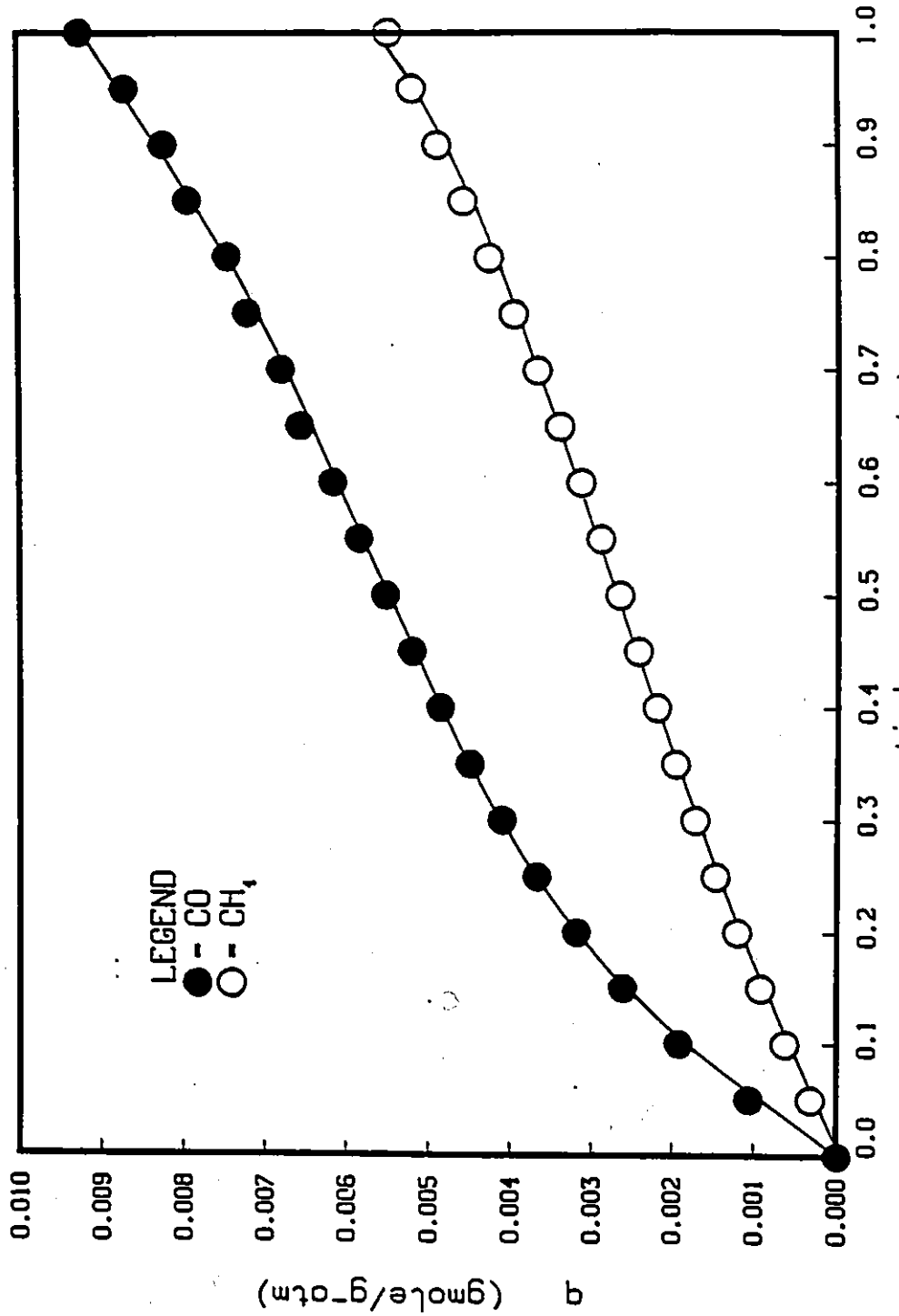

Figure 6.28: Single component isotherms for methane and carbon monoxide at 293 K in 5A molecular sieve

Table 6.16: Apparent Equilibrium Constants for the Pure Gas Isotherms at 313 K

Y_{CO}	K'_{pCO} (dimensionless)	Y_{CH_4}	K'_{pCH_4} (dimensionless)
0.0	78.6423	0.0	27.9970
0.10	46.2791	0.24	18.9301
0.20	29.2720	0.35	12.2371
0.35	21.7663	0.50	11.2767
0.65	14.5140	0.57	9.3684
0.76	12.2495	0.63	8.8510
0.85	8.6270	0.76	6.7697
0.94	5.8399	0.83	6.8324
-	-	0.92	4.7327

6.6.2 Binary Mixture Isotherms

When determining the binary isotherms the experimental data was first fitted to three different expressions. As suggested by Van der Vlist and Van der Meidjen [13] the data was initially fitted to a third degree polynomial. Figure 6.29 shows the pertaining fit at 313 K. The curve fit at 293 K is given in Figure 6.30. As can be seen from these plots a third order polynomial regressed for the entire composition range gives an unsatisfactory representation. By adding a term to equations 4.28-4.30 a completely analogous data reduction method can be obtained which allows for the regression of the data with a fourth order polynomial. A fourth order polynomial fit was attempted and though it showed improvement in representing the data, especially at the lower composition range and 293 K it was still an inadequate representation of the data. A higher order polynomial fit was not attempted

Table 6.17: Apparent Equilibrium Constants for the Pure Gas Isotherms at 293 K

Y_{CO}	K_{pCO} (dimensionless)	Y_{CH_4}	K_{pCH_4} (dimensionless)
0.0	147.010	0.0	38.1317
0.13	72.6103	0.23	25.9614
0.28	38.3773	0.37	18.6554
0.56	18.2298	0.52	15.2439
0.72	13.9126	0.64	13.4605
0.88	8.0524	0.75	11.0270
0.97	4.9348	0.87	7.3080
		0.93	5.8276
		0.98	3.2747

because as concluded by Hyun and Danner [27] the Van der Vlist-Van der Meidjen data reduction procedure will give good binary adsorption values if a low order polynomial can fit the data with the proper slopes between the compositions for which independent adsorption values are available.

The third fit attempted was that suggested by Tezel (according to equation 4.31) [55] . As can be seen in Figure 6.31, at a temperature of 313 K and for a β value of 0.215 the regression of the experimental data according to eqaution 4.31 is quite well. The same is true when analyzing the data at a temperature of 293 K in Figure 6.32. At 293 K the optimum β value was found to be 0.215. In comparison with the polynomial regressions, it was concluded that this model provides the 'best-fit' for the experimental data thus it was the basis from which the binary gas isotherms were calculated. The parameters of this model are tabulated in Table 6.18 (which lists the A coefficients of equation 4.31) and Table 6.19 (which lists the B and C

coefficients of equations 4.32 and 4.33 respectively).

The binary isotherms, as calculated from equations 4.41 and 4.42 for temperatures of 313 K and 293 K and 1 atm total pressure are shown in Figures 6.33 and 6.34. At both temperatures, for a binary mixture of CO-CH_4, carbon monoxide is preferentially adsorbed on the 5A molecular sieve, thus hindering the adsorption of the methane molecules. Therefore, the ability of 5A zeolite to separate the components in a CO-CH_4 mixture is the result of a selective adsorption process. The presence of one component reduces the sorption capacity of the molecular sieve for the other component.

As plotted in Figure 6.33, for a temperature of 313 K the adsorption of CH_4 does not change substantially between a carbon monoxide mole fraction of 0.30 to 0.65. The adsorption of methane decreases from 0.2258×10^{-2} gmole/g-atm when the mixture is composed of 5% CO to 0.5004×10^{-3} gmole/g-atm at a composition of 30% CO, then remains almost constant until $Y_{CO} \geq 0.65$. As the mole fraction of carbon monoxide in the mixture is increased beyond this point the amount of methane adsorbed decreases gradually until the carrier gas is composed purely of carbon monoxide and essentially no methane is adsorbed.

For a temperature of 293 K (Figure 6.34) the same adsorption trends are evident. Due to the lower temperature a larger amount of carbon monoxide and methane are adsorbed. When the mixture is composed of only 5% CO, 0.2989×10^{-2} gmole methane/g-atm are adsorbed. As the amount of carbon monoxide in the carrier gas is increased the amount of methane adsorbed decreases to a value of 0.5167×10^{-3} gmole/g-atm for a mixture consisting of 30% CO and 70% CH_4. A new maximum is reached at Y_{CO}=0.65 (0.6235×10^{-3} gmole/g-atm).

The adsorption of carbon monoxide at 293 K, however, increases gradually from 0.4232×10^{-3} gmole/g-atm to 0.9259×10^{-2} gmole/g-atm as the amount of carbon monoxide in the carrier gas is increased. Table 6.20 lists the binary adsorption

Table 6.18: The A Coefficients for the Binary Isotherms according to equation 4.31 (all dimensionless)

Temp	313 K	293 K
A_{-1}	-43.6638	-46.4121
A_0	97.1271	106.6910
A_1	-41.1081	-45.1646
A_2	7.3344	8.5949

data for a temperature of 313 K. The same information is given in Table 6.21 for a temperature of 293 K.

Table 6.19: The B and C Coefficients for the Binary Isotherms according to equations 4.32 and 4.33 (all dimensionless)

Temp	313 K	293 K
B_0	118.9	147.3
B_1	-68.1	-84.9
B_2	11.7	14.8
C_0	75.4	101.3
C_1	-99.5	-136.0
C_2	32.1	43.8

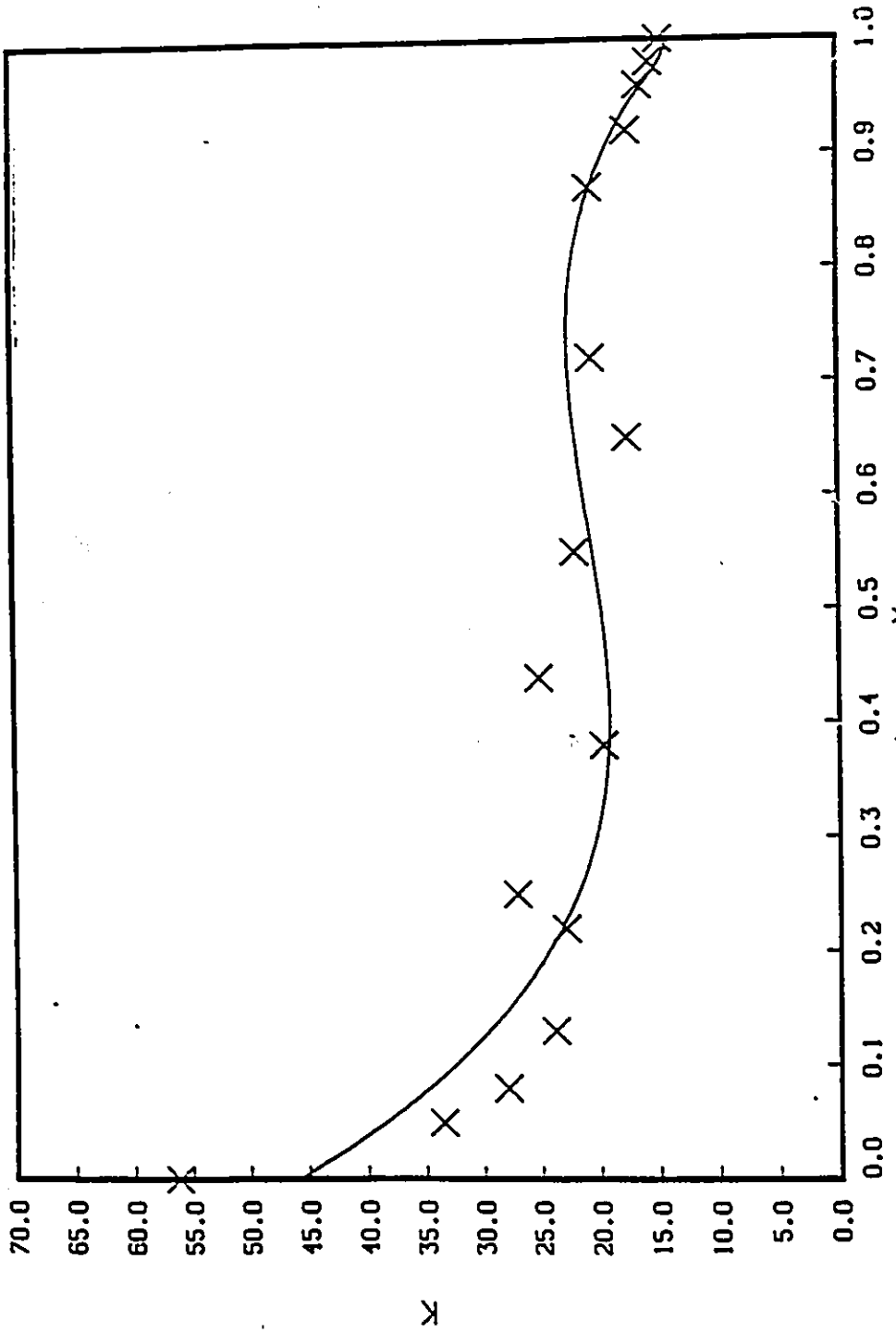

Figure 6.29: Third degree polynomial fit for the data of the CO-CH_4-5A molecular sieve system at 313 K.

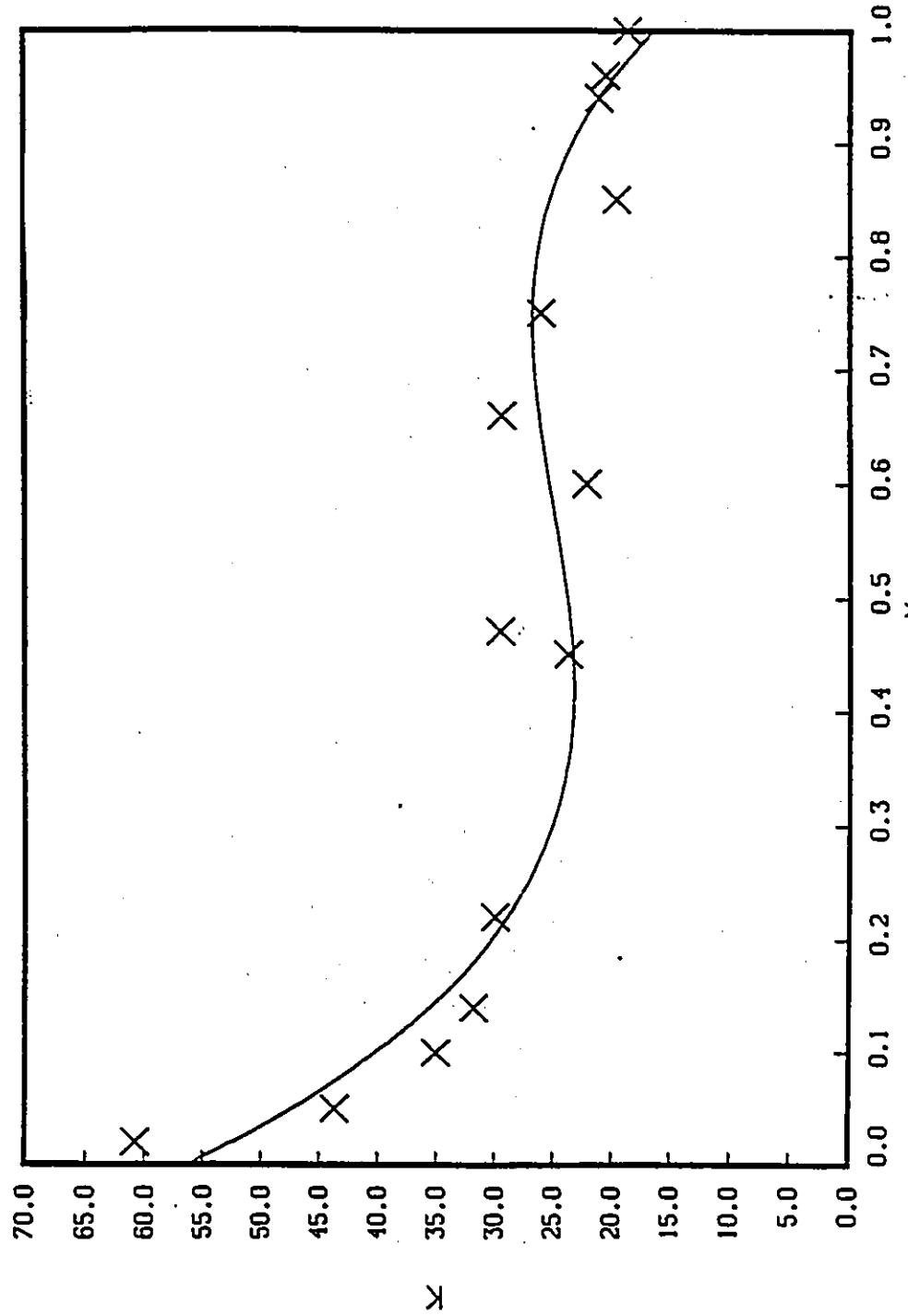

Figure 6.30: Third degree polynomial fit for the data of the CO-CH_4-5A molecular sieve system at 293 K.

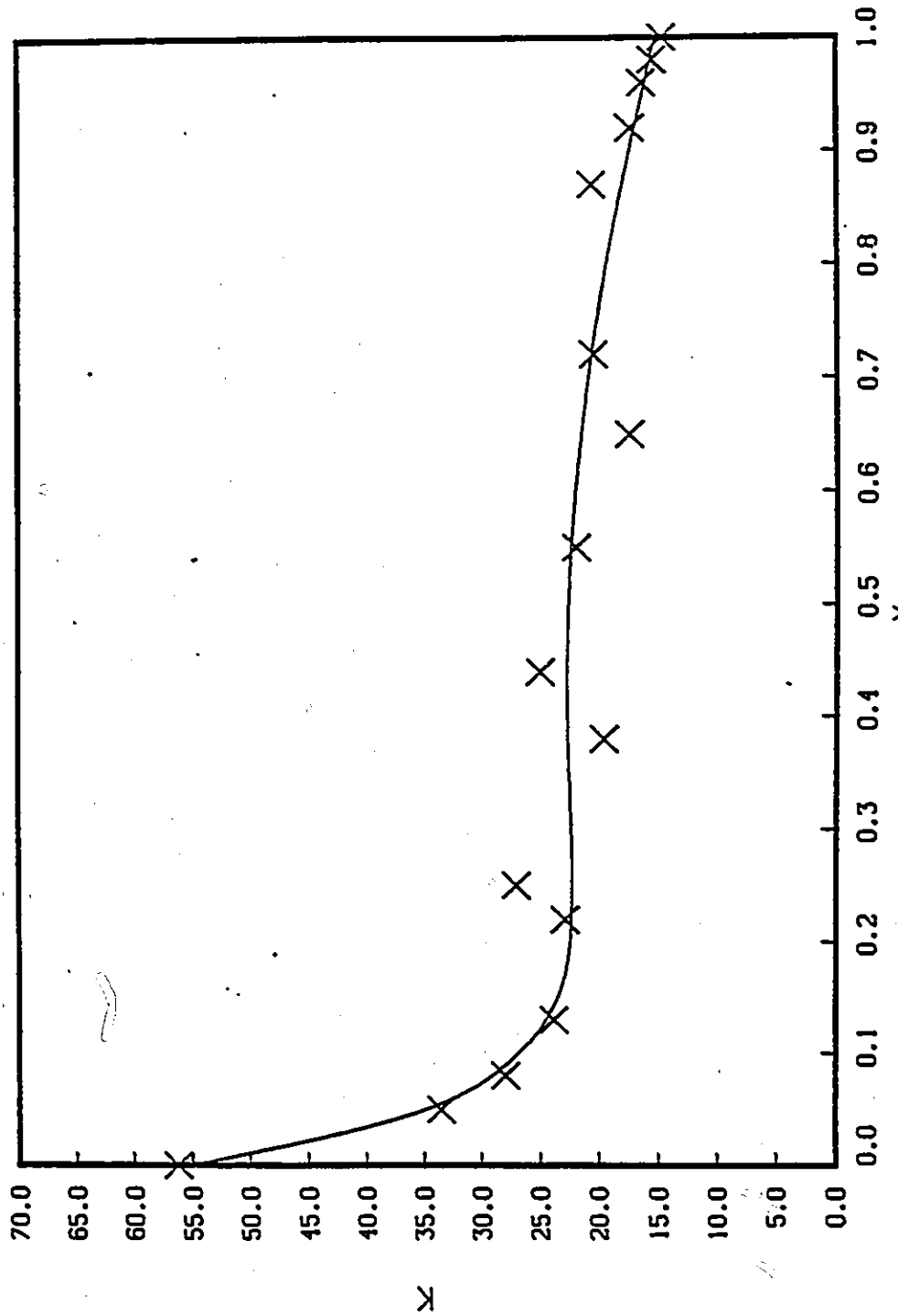

Figure 6.31: Curve fit for the data of the CO-CH_4-5A molecular sieve system at 313 K and β=0.215.

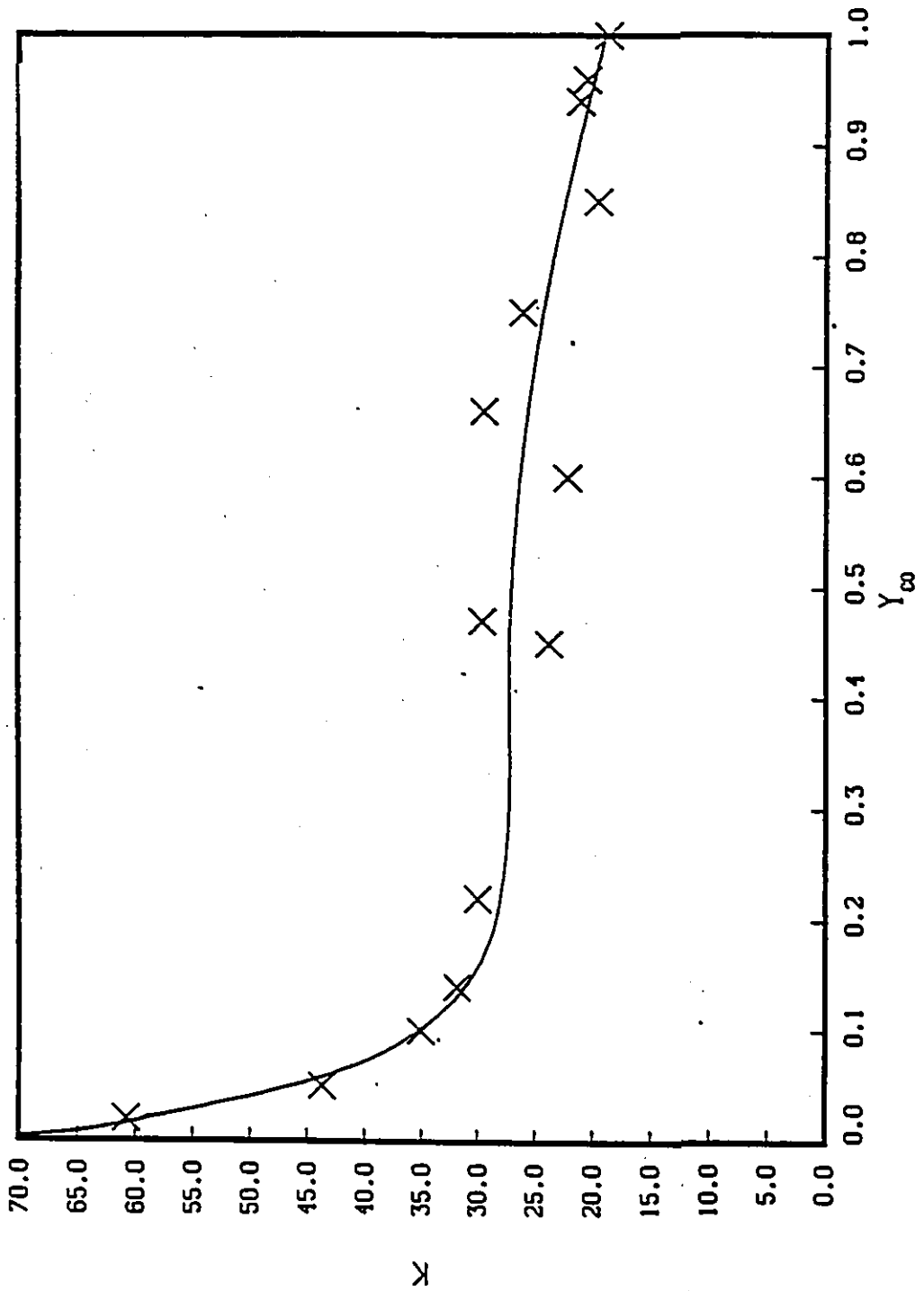

Figure 6.32: Curve fit for the data of the CO-CH_4 -5A molecular sieve system at 293 K and β=0.215.

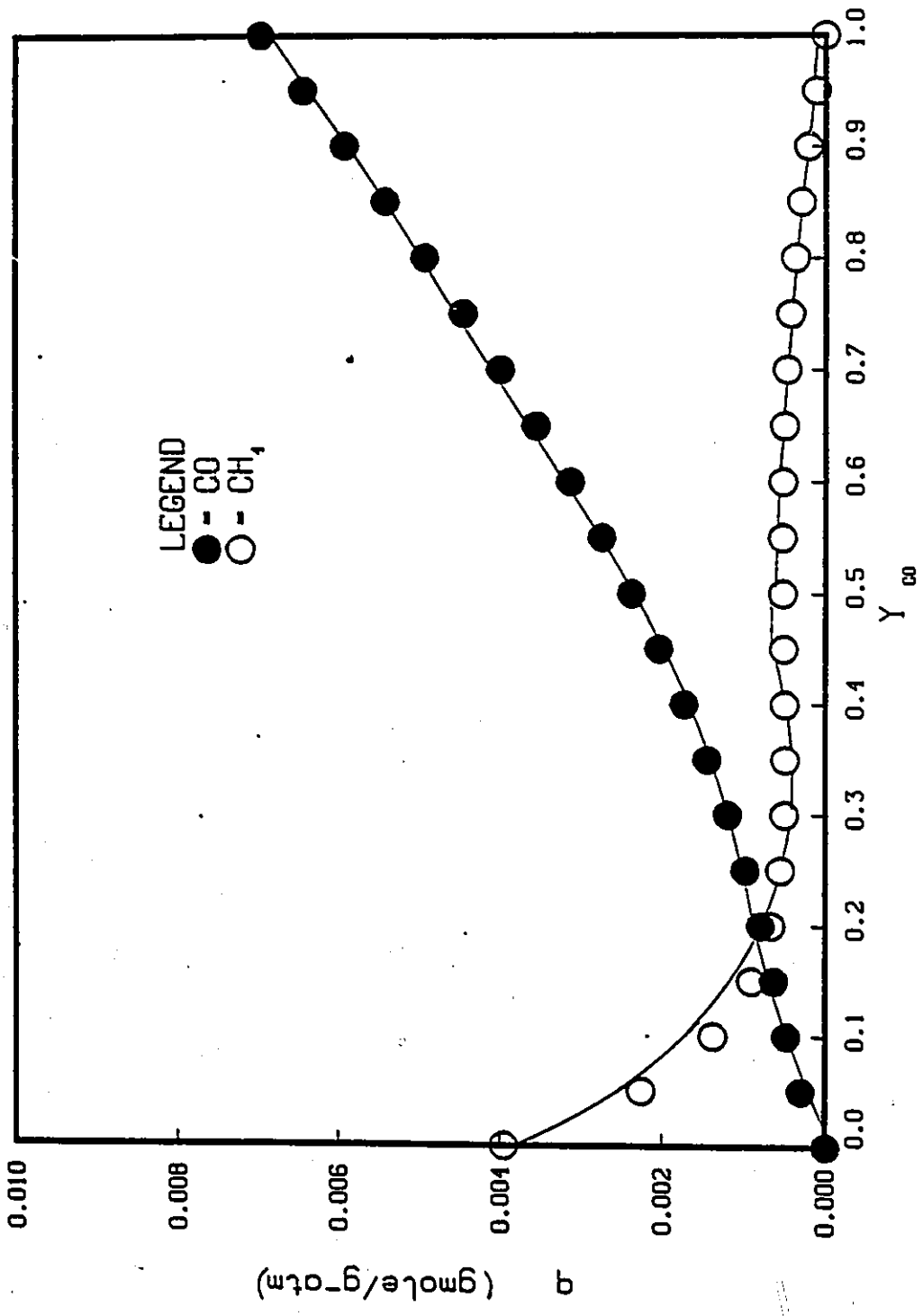

Figure 6.33: Gas-mixture isotherms for the CO-CH_4 -5A molecular sieve system at 313 K.

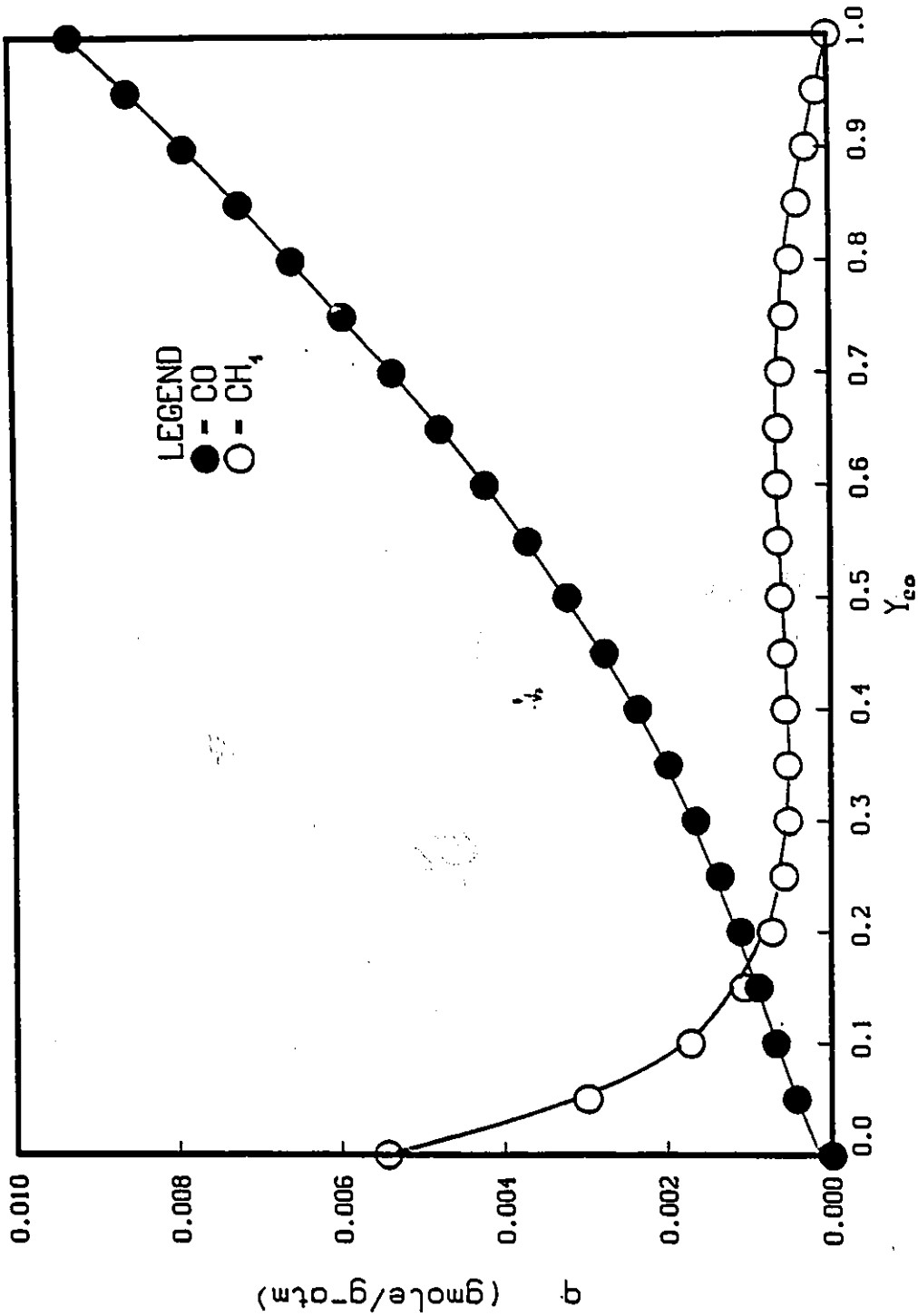

Figure 6.34: Gas-mixture isotherms for the CO-CH_4 -5A molecular sieve system at 293 K.

Table 6.20: Adsorption Data for CO-CH_4 Binary Mixture at 313 K for 5A Zeolite

Y_{CO}	q_{CO}	q_{CH_4}
	(gmole/g-atm)	(gmole/g-atm)
0.00	0.000	3.953×10^{-3}
0.05	3.005×10^{-4}	2.258×10^{-3}
0.10	4.806×10^{-4}	1.375×10^{-3}
0.15	6.329×10^{-4}	9.071×10^{-4}
0.20	7.950×10^{-4}	6.647×10^{-4}
0.25	9.822×10^{-4}	5.477×10^{-4}
0.30	1.200×10^{-3}	5.004×10^{-4}
0.35	1.451×10^{-3}	4.903×10^{-4}
0.40	1.733×10^{-3}	4.977×10^{-4}
0.45	2.046×10^{-3}	5.103×10^{-4}
0.50	2.387×10^{-3}	5.206×10^{-4}
0.55	2.754×10^{-3}	5.238×10^{-4}
0.60	3.145×10^{-3}	5.170×10^{-4}
0.65	3.560×10^{-3}	4.984×10^{-4}
0.70	3.995×10^{-3}	4.670×10^{-4}
0.75	4.449×10^{-3}	4.222×10^{-4}
0.80	4.922×10^{-3}	3.640×10^{-4}
0.85	5.411×10^{-3}	2.924×10^{-4}
0.90	5.915×10^{-3}	2.076×10^{-4}
0.95	6.434×10^{-3}	1.100×10^{-4}
1.00	6.967×10^{-3}	8.817×10^{-10}

Table 6.21: Adsorption Data for CO-CH_4 Binary Mixture at 293 K for 5A Zeolite

Y_{CO}	q_{CO}	q_{CH_4}
	(gmole/g-atm)	(gmole/g-atm)
0.00	0.000	5.440×10^{-3}
0.05	4.232×10^{-4}	2.989×10^{-3}
0.10	6.762×10^{-4}	1.721×10^{-3}
0.15	8.866×10^{-4}	1.058×10^{-3}
0.20	1.106×10^{-3}	7.221×10^{-4}
0.25	1.357×10^{-3}	5.688×10^{-4}
0.30	1.647×10^{-3}	5.167×10^{-4}
0.35	1.979×10^{-3}	5.183×10^{-4}
0.40	2.353×10^{-3}	5.451×10^{-4}
0.45	2.766×10^{-3}	5.794×10^{-4}
0.50	3.216×10^{-3}	6.100×10^{-4}
0.55	3.700×10^{-3}	6.302×10^{-4}
0.60	4.217×10^{-3}	6.355×10^{-4}
0.65	4.764×10^{-3}	6.235×10^{-4}
0.70	5.338×10^{-3}	5.927×10^{-4}
0.75	5.937×10^{-3}	5.423×10^{-4}
0.80	6.561×10^{-3}	4.722×10^{-4}
0.85	7.206×10^{-3}	3.826×10^{-4}
0.90	7.872×10^{-3}	2.736×10^{-4}
0.95	8.557×10^{-3}	1.459×10^{-4}
1.00	9.259×10^{-3}	5.871×10^{-9}

An adsorption phase diagram for the CO-CH_4 mixture on 5A zeolite is given in Figure 6.35. As is evident from the plot the mixture shows decreasing extent of separation with increasing temperature, specifically in the composition range of $0.20 \leq X_{CO} \leq 0.70$. This observation is again consistent with the selectivity values obtained for CO and CH_4 on 5A molecular sieve. At both the lower ($X_{CO} \leq 0.20$) and upper ($X_{CO} \geq 0.70$) limits of the composition range the extent of separation varies only slightly between the two temperatures. Therefore, at these limits, though the lower temperature (293 K) offers a slightly better separation of the components, the process would become a question of economics. The economics of reducing the system to cryogenic temperatures would have to be favorable in comparison to the separation acheived.

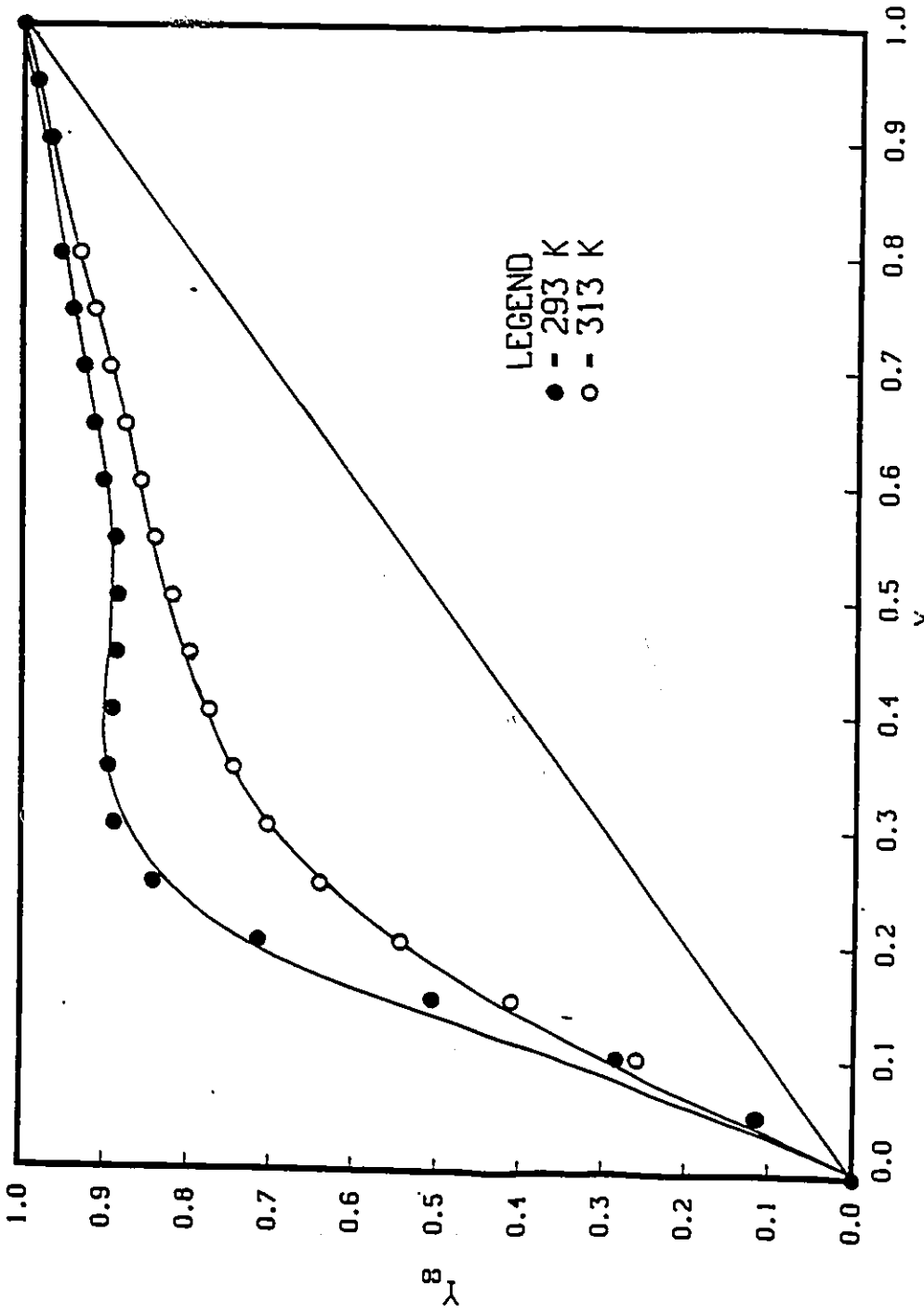

Figure 6.35: Adsorption phase diagram for CO-CH_4 mixture on 5A zeolite at a total pressure of 1 atm.

Conclusions

1. Of the molecular sieves considered in this study, the K_p values obtained for all three gases were higher for the 5A Zeolite and H-Mordenite systems due to the larger surface areas of these sieves.

2. Of the three gases studied micropore diffusion occurs only for N_2 in H-Mordenite, 4A Zeolite and Chabazite.

3. The micropore diffusivity (D_c/r_c^2) of N_2 increases with increasing temperature.

4. A larger energy barrier to adsorption is observed for the N_2-4A Zeolite system as opposed to the N_2-H-Mordenite system and thus the H-Mordenite system yields higher values of micropore diffusivity

5. With temperature pre-treatment as a the method of regeneration Chabazite offers the least promising results for the gases under study.

6. Binary gas isotherms indicate that for a mixture of CO-CH_4 the sorption capacity of 5A zeolite for methane is not as high as that for carbon monoxide. A selective adsorption process occurs for the separation of a CO-CH_4 mixture.

7. A low order polynomial fit is inadequate for analysing the binary gas isotherms of CO and CH_4.

Recommendations

1. Further studies might be conducted with the N_2-H-Mordenite system at temperatures lower than those used in this study in order to get a better understanding of this system.

2. A pressure-swing regeneration of the Chabazite sieve might offer better results than those obtained with thermal pre-treatment since it has been observed that heating at high temperatures might cause the calcium cations to move around in the Chabazite structure.

3. Different regeneration temperatures for all the sieves might be considered to show the effect of thermal pre-treatment on micropore diffusivity.

4. On the basis of equilibrium selectivities other systems to conside would be the binary separation of CO-N_2 on either H-Mordenite or the Type A zeolites.

5. Gas mixture adsorption equilibria can be predicted from single-component adsorption isotherm data by considering models that assume non-ideality of the adsorbed solution. The following two methods can be considered:

- the statistical thermodynamic model
  - as suggested by Ruthven et. al. [48]

- the vacancy solution model
  - as suggested by Suwanayuen and Danner [52]

Bibliography

[1] R. M. Barrer. Channel Structure of Mordenite. *Brennstoff-Chemie*, 35:325, 1954.

[2] R. M. Barrer. Sorption by Gmelinite and Mordenite. *Trans. Faraday Soc.*, 40:555, 1944.

[3] R. M. Barrer. Sorptive and Molcular - Sieve Properties of a New Zeolitic Mineral. *Advan. Chem. Ser.*, 102:133, 1971.

[4] R. M. Barrer. Syntheses and Reactions of Mordenite. *J. Chem. Soc.*, 40:2158, 1948.

[5] R. B. Bird, W. E. Stewart, and E. N. Lightfoot. *Transport Phenomena.* John Wiley and Sons, New York, 1960.

[6] D. W. Breck. *Zeolite Molecular Sieves: Structure, Chemistry and Use.* John Wiley and Sons Inc., New York, 1973.

[7] D. W. Breck. *Zeolite Molecular Sieves: Structure, Chemistry and Use.* John Wiley and Sons Inc., New York, 1973.

[8] S. Brunauer, P. Emmet, and B. Teller. Adsorption of Gases in Multimolecular Layers. *J. Amer. Chem. Soc.*, 60:309, 1938.

[9] L. N. Canjor and D. T. Camp. *Developments In Physical Adsorption.* Chem. Eng. Progress Symp. Ser., New York, 1982.

[10] N. Y. Chen. Hydrophobic Properties of Zeolites. *J. Phys. Chem.*, 80:60, 1976.

[11] W. H. Daly and W. Granville. *The Properties and Applications of Zeolites.* The Chemical Society, Great Britain, 1980.

[12] L. S. Dent and J. V. Smith. Crystal Structure of Chabazite - A Molecular Sieve. *Nature (London)*, 181:1794, 1958.

[13] E. Van der Vlist and J. Van der Meidjen. Determination of Adsorption Isotherms of the Components of Binary Gas Mixtures by Gas Chromatography. *J. Chromatography*, 79:1, 1973.

[14] J. D. Eagan and R. B. Anderson. Kinetics and Equilibrium of Adsorption on 4A Zeolite. *J. Colloid Sci.*, 50:419, 1975.

[15] M. F. Federova and A. N. Aliev. Low Temperature Adsorption of Gases on Zeolites at Low Pressure. *Russian J. Phys. Chem.*, 40:1393, 1966.

[16] H. B. Gilmer and R. Kobayashi. The Study of Multicomponent Gas-Solid Equilibrium at High Pressures by Gas Chomatography. *AIChE J.*, 11:702, 1965.

[17] H. W. Habgood. Adsorptive and Gas Chromatographic Properties of Various Cationic Forms of Zeolite X. *Can. J. Chem.*, 42:2340, 1964.

[18] H. W. Habgood and W. R. MacDonald. Effect of Micropores on Peak Shape and Retention Volume in Gas-Solid Chromatography. *J. Anal. Chem.*, 42:543, 1970.

[19] N. Haq and D. M. Ruthven. A Chromatographic Study of Sorption and Diffusion in 4A Zeolite. *J. Coll. Int. Sci.*, 112:154, 1986.

[20] N. Haq and D. M. Ruthven. A Chromatographic Study of Sorption and Diffusion in 5A Zeolite. *J. Coll. Int. Sci.*, 112:164, 1986.

[21] R. J. Harper, G. R. Stifel, and R. B. Anderson. Adsorption of Gases on 4A Synthetic Zeolite. *Can. J. Chem.*, 47:4661, 1969.

[22] N. Hashimoto and J. M. Smith. Diffusion in Bidispersed Porous Catalyst Pellets. *Ind. Engng. Chem. Fundl.*, 13:115, 1974.

[23] N. Hashimoto and J. M. Smith. Macropore Diffusion in Molecular Sieve Pellets by Gas Chromatography. *Ind. Eng. Chem. Fundl.*, 12:353, 1973.

[24] J. J. Haydel and R. Kobayashi. Adsorption Equilibria in the Methane-Propane-Silica Gel System at High Pressures. *I. E. C. Fundam.*, 6:546, 1967.

[25] C. K. Hersh. *Molecular Sieves.* Reinhold Publishing Co., New York, 1961.

[26] L. K. P. Hsu and H. W. Haynes Jr. Effective Diffusivity by the Gas Chromatography Technique: Analysis and Application to Measurements of Diffusion of Various Hydrocarbons in Zeolite NaY. *AIChE J.*, 27:81, 1981.

[27] S. H. Hyun and R. P. Danner. Determination of Gas Adsorption Equilibria by the Concentration Pulse Technique. *AIChE Sym. Ser.*, 78:19, 1982.

[28] H. W. Haynes Jr. The Determination of Effective Diffusivity by Gas Chromatography. Time Domain Solutions. *Ind. Eng. Sci.*, 30:955, 1975.

[29] H. W. Haynes Jr. and P. N. Sarma. A Model for the Application of Gas Chromatography to Measurements of Diffusion in Bidispersed Structured Catalysts. *AIChE J.*, 19:1045, 1973.

[30] P. E. Eberly Jr. Diffusion Studies in Zeolites and Related Solids by Gas Chromatographic Techniques. *I. E. C. Fundam.*, 1:25, 1969.

[31] A.B. Lamb and J. C. Woodhouse. Adsorption by Dehydrated Chabasite as a Function of the Water Content. *J. Chem. Soc.*, 58:2637, 1936.

[32] S. H. Langer. Determination of Gas Adsorption Equilibria by the Concentration Pulse Technique. *AIChE Sym. Ser.*, 78:19, 1982.

[33] H. Lee. Applied Aspects of Zeolite Adsorbents. *Adv. Chem. Ser.*, 121:311, 1973.

[34] R. A. Llenado. The Use of Sodium Type A Zeolite in Laundry Detergents. *Proc. of the 6th Int. Zeol. Conf.*, 10-15 July:940, 1983.

[35] Y. H. Ma and C. Mancel. Diffusion of Hydrocarbons in Mordenites by Gas Chromatography. *Adv. Che. Ser.*, 121:392, 1974.

[36] Y. H. Ma and C. Mancel. Diffusion Studies of CO2, NO, NO2 and SO2 on Molecular Sieve Zeolites by Gas Chromatography. *AIChE J.*, 18:1148, 1972.

[37] W. M. Meier. The Crystal Structure of Mordenite (Ptilolite. *Zeitschrift fur Kristallographie*, 115:439, 1961.

[38] W. M. Meier. Zeolite Structures. *Proc. of the Conference on Molecular Sieves (London)*, APRIL, 1967.

[39] F. A. Mumpton. Zeolite Exploration: The Early Days. *Proc. of the 6th Int. Zeol. Con.*, 10-15 July:68, 1983.

[40] V. Ponec, Z. Knor, and S. Cerny. *Adsorption on Solids.* Butterworth and Company Ltd., Cleveland, 1974.

[41] R. C. Reid, J. M. Prausnitz, and T. K. Sherwood. *Properties of Gases and Liquids*. McGraw-Hill Book Company Inc., New York, 1977.

[42] D. M. Ruthven. Adsorption in A, X and Y Zeolites: Thirty Years of Science and Technology. *Proc. of the 6th Int. Zeol. Con.*, 10-15 July:31, 1983.

[43] D. M. Ruthven. *Principles of Adsorption and Adsorption Processes*. John Wiley and Sons, New York, 1984.

[44] D. M. Ruthven and R. I Derrah. Diffusion of Monoatomic and Diatomic Gases in 4A and 5A Zeolites. *J. Chem. Soc. Faraday Trans. I*, 71:2031, 1975.

[45] D. M. Ruthven and R. I Derrah. Sorption in Davison 5A Molecular Sieve. *Can. J. Chem. Eng.*, 50:743, 1972.

[46] D. M. Ruthven and R. Kumar. An Experimental Study of Single-Component and Binary Adsorption Equilibria by a Chromatographic Method. *Ind. Eng. Chem. Fundam.*, 19, 1980.

[47] D. M. Ruthven and K. F. Loughlin. The Sorption and Diffusion of n-butane in Linde 5A Molecular Sieve. *Chem. Eng. Sci.*, 26:1145, 1971.

[48] D. M. Ruthven, K. F. Loughlin, and K. A. Holborow. Multicomponent Sorption Equilibrium in Molecular Sieves. *Chem. Eng. Sci.*, 28:701, 1973.

[49] P. N. Sarma and H. W. Haynes Jr. Application of Gas Chromatography to Measurements of Diffusion in Zeolites. *Adv. Chem. Ser.*, 133:205, 1974.

[50] P. Schneider and J. M. Smith. Adsorption Rate Constants from Chromatography. *AIChE J.*, 14:762, 1968.

[51] D. M. Shah and D. M. Ruthven. Measurement of Zeolitic Diffusivities and Equilibrium Isotherms by Chromatography. *AIChE J.*, 23:804, 1977.

BIBLIOGRAPHY

[52] S. Suwanayuen and R. P. Danner. Vacancy Solution Theory of Adsorption From Gas Mixtures. *AIChE. J.*, 26:76, 1980.

[53] M. Suzuki and J. M. Smith. Axial Dispersion in Beds of Small Particles. *J. Chem. Eng.*, 3:256, 1972.

[54] M. Suzuki and J. M. Smith. Determination of Gas Adsorption Equilibria by the Concentration Pulse Technique. *Chem. Eng. Sci.*, 26:221, 1971.

[55] F. H. Tezel. ***Adsorption and Diffusion In Molecular Sieve Zeolites.*** PhD thesis, University of New Brunswick, 1985.

[56] F. H. Tezel. ***Removal of Kr from N2 by Selective Adsorption.*** Master's thesis, University of New Brunswick, 1981.

[57] J. L. Thomas, M. Mange, and C. Eyraud. Evolution of Structure and Texture of a Type 4A Molecular Sieve in the Course of Thermal Treatments between 400 and 800 C. *Adv. Chem. Ser.*, 102:443, 1971.

[58] G. V. Tsitshvilli and T. G. Adronikashvili. Influence of Zeolite Cation Nature on Adsorption and Chromatographic Properties. *Adv. Chem. Ser.*, 101:217, 1970.

[59] G. P. Valueva, I. A. Beltsky, Y. V. Seryotkin, and V. S. Pavlychenko. ***Natural Chabazite: Heats of Rehydration and X-Ray Study in Relation to H2O Contents at Room Temperature.*** Akademiai Kiado, Budapest, 1988.

[60] H. Yucel and D. M. Ruthven. Diffusion in 5A Zeolite - Study of the effect of Crystal Size. *J. C. S. Faraday I*, 76:60, 1980.

Appendix

APPENDIX

Table 6.22: Molecular Diffusivity (D_M) accroding to Fuller et. al. as referenced in (40)

Temperature (K)	D_M He-N_2 (cm^2/sec)	D_M He-CO (cm^2/sec)	D_M He-CH_4 (cm^2/sec)
313	0.7745	0.7567	0.7077
293	0.6950	0.6742	0.6305
273	0.6097	0.5957	0.5571
263	0.5712	0.5580	0.5219

Notation for computer printouts

The various abbreviations found in the computer printouts are summarized below.

Abbreviations

DIAM	diameter of column, cm
DIAMP	diametr of pellet, cm
DISPERSION	the expression $\sigma^2 L/2\mu^2 v$, sec
EPS	bed voidage, dimensionless
I.V	interstitial velocity, cm/sec
$1/(I.V)^2$	$1/v^2$, sec^2/cm^2
LEN	length of chromatographic column, cm
MEAN	mean of the chromatographic peak, sec
MU	viscosity of the carrier gas, poise
PER	percent adsorbate in the carrier gas
RE	Reynolds number, dimensionless

ROE	density of the carrier gas, g/cc
TEMP	experimental temperature, K
VARIANCE	second moment for the chromatographic peak, sec^2

N2 PULSE (I.D=0.63CM) HE CARRIER H-MORDENITE (673 K - 24 H)

LEN	DIAM	EPS	DIAMP	THETA	ROE	MU :
11.50	0.63	0.37	0.0602	0.3300	0.000156	0.000200

TEMP (K)	MEAN	VARIANCE	I.V.	RE.	KP	DISPERSION	1/(I.V)**
	SECS	SEC**2	CM/SEC				
263.0	84.3768	1802.73	6.2530	0.2939	26.3574	0.2328	0.0256
273.0	67.2657	1012.14	6.2868	0.2954	21.0094	0.2046	0.0253
283.0	52.8988	589.39	6.2419	0.2933	16.2753	0.1940	0.0257
293.0	37.6216	340.49	6.2642	0.2944	11.4483	0.2208	0.0255
303.0	28.1248	128.14	6.2499	0.2937	8.3896	0.1490	0.0256
313.0	27.8029	108.93	6.2453	0.2935	8.2803	0.1297	0.0256
323.0	26.2859	94.40	6.3067	0.2964	7.8789	0.1246	0.0251
333.0	22.7511	66.17	6.2523	0.2938	6.6772	0.1176	0.0256
343.0	19.1183	36.85	6.2321	0.2929	5.4975	0.0930	0.0257

N2 PULSE (0.5 CC). HE CARRIER H-MORDENITE (673 K - 24 H)...R1L2

LEN	DIAM	EPS	DIAMP	THETA	ROE	MU :
11.50	0.63	0.37	0.0602	0.3300	0.000156	0.000200

TEMP (K)	MEAN	VARIANCE	I.V.	RE.	KP	DISPERSION	1/(I.V)**2
	SECS	SEC**2	CM/SEC				
313.0	93.2170	953.19	1.8969	0.0891	8.4429	0.3325	0.2779
313.0	85.0638	741.00	2.2416	0.1053	9.1506	0.2627	0.1990
313.0	61.4128	460.34	2.9906	0.1405	8.7923	0.2347	0.1118
313.0	52.8777	323.22	3.7452	0.1760	9.5263	0.1775	0.0713
313.0	41.9373	249.93	4.6161	0.2169	9.2992	0.1770	0.0469
313.0	33.4998	177.92	5.5632	0.2614	8.9304	0.1639	0.0323
313.0	30.3022	161.20	6.4837	0.3047	9.4464	0.1557	0.0238

N2 PULSE (0.5 CC) HE CARRIER H-MORDENITE (673 K - 24 H)...R1L2

LEN	DIAM	EPS	DIAMP	THETA	ROE	MU :
11.50	0.63	0.37	0.0602	0.3300	0.000156	0.000200

TEMP (K)	MEAN	VARIANCE	I.V.	RE.	KP	DISPERSION	1/(I.V)**
	SECS	SEC**2	CM/SEC				
293.0	99.0703	1484.01	2.7995	0.1316	13.5769	0.3105	0.1276
293.0	71.9219	788.00	3.5059	0.1648	12.2898	0.2498	0.0814
293.0	56.5758	521.03	4.3212	0.2031	11.8979	0.2166	0.0536
293.0	45.9469	383.31	5.2077	0.2447	11.6326	0.2005	0.0369
293.0	41.8949	358.75	6.0694	0.2852	12.3985	0.1936	0.0271

N2 PULSE (0.5 CC) HE CARRIER H-MORDENITE (673 K - 24 H)

LEN	DIAM	EPS	DIAMP	THETA	ROE	MU :
11.50	0.63	0.37	0.0602	0.3300	0.000156	0.000200

TEMP (K)	MEAN	VARIANCE	I.V.	RE.	KP	DISPERSION	1/(I.V)**
	SECS	SEC**2	CM/SEC				
273.0	126.1389	2782.76	3.2666	0.1535	20.4554	0.3079	0.0937
273.0	101.0550	1984.89	4.0262	0.1892	20.1914	0.2776	0.0617
273.0	77.1418	1196.35	4.8523	0.2280	18.5287	0.2382	0.0425
273.0	67.6777	1051.51	5.6551	0.2658	18.9583	0.2334	0.0313

N2 PULSE (0.5 CC) HE CARRIER H-MORDENITE (673 K - 24 H)

LEN	DIAM	EPS	DIAMP	THETA	ROE	MU :
11.50	0.63	0.37	0.0602	0.3300	0.000156	0.000200

TEMP (K)	MEAN SECS	VARIANCE SEC**2	I.V. CM/SEC	RE.	KP	DISPERSION	1/(I.V)*
263.0	213.7563	8818.27	2.5129	0.1181	26.8447	0.4416	0.1584
263.0	166.3427	5297.20	3.1469	0.1479	26.1458	0.3498	0.1010
263.0	90.8493	1893.78	5.4480	0.2560	24.6893	0.2422	0.0337
263.0	82.1226	1744.30	6.1929	0.2910	25.3855	0.2401	0.0261

CO PULSE (I.D=0.63CM) HE CARRIER H-MORDENITE (673 K - 24 H)

LEN	DIAM	EPS	DIAMP	THETA	ROE	MU :
11.50	0.63	0.37	0.0602	0.3300	0.000156	0.000200

TEMP (K)	MEAN	VARIANCE	I.V.	RE.	KP	DISPERSION	1/(I.V)**
	SECS	SEC**2	CM/SEC				
263.0	665.5720	19106.24	6.2430	0.2934	211.6144	0.0397	0.0257
273.0	434.2424	8346.25	6.2660	0.2945	138.3721	0.0406	0.0255
283.0	281.1418	3556.49	6.2626	0.2943	89.3304	0.0413	0.0255
293.0	212.6604	1973.71	6.2651	0.2944	67.4545	0.0401	0.0255
303.0	145.8127	934.44	6.2632	0.2943	46.0525	0.0403	0.0255
313.0	113.7147	559.91	6.2627	0.2943	35.7827	0.0398	0.0255
343.0	55.1875	135.74	6.2793	0.2951	17.1103	0.0408	0.0254
363.0	38.4225	66.84	6.2403	0.2933	11.6576	0.0417	0.0257

CO PULSE (I.D=0.63CM) HE CARRIER H-MORDENITE (673 K - 24 H)

LEN	DIAM	EPS	DIAMP	THETA	ROE	MU :
11.50	0.63	0.37	0.0602	0.3300	0.000156	0.000200

TEMP (K)	MEAN	VARIANCE	I.V.	RE.	KP	DISPERSION	1/(I.V)*
	SECS	SEC**2	CM/SEC				
313.0	427.1853	27625.70	0.7543	0.0354	15.5971	1.1541	1.7578
313.0	277.0691	9390.70	1.1776	0.0553	15.8016	0.5973	0.7211
313.0	217.0137	4472.27	1.5350	0.0721	16.1448	0.3557	0.4244
313.0	179.0311	3150.36	1.9111	0.0898	16.5977	0.2957	0.2738
313.0	147.6477	1505.34	2.2657	0.1065	16.2151	0.1752	0.1948
313.0	134.8150	1252.27	2.6958	0.1267	17.6669	0.1470	0.1376
313.0	117.0424	1092.32	3.0122	0.1416	17.1203	0.1522	0.1102
313.0	105.3402	773.54	3.7531	0.1764	19.2688	0.1068	0.0710
313.0	83.2528	559.76	4.6797	0.2199	18.9800	0.0992	0.0457
313.0	63.9085	204.86	6.1074	0.2870	19.0160	0.0472	0.0266
313.0	46.9540	101.14	7.5257	0.3537	17.1611	0.0351	0.0177
313.0	37.8665	72.17	9.5021	0.4466	17.4849	0.0305	0.0111
313.0	29.6499	44.99	11.8415	0.5565	17.0475	0.0249	0.0071
313.0	18.6756	22.01	19.5958	0.9209	17.7936	0.0185	0.0026

CO PULSE (I.D=0.63CM) HE CARRIER H-MORDENITE (673 K - 24 H)

LEN	DIAM	EPS	DIAMP	THETA	RGE	MU :
11.50	0.63	0.37	0.0602	0.3300	0.000156	0.000200

TEMP (K)	MEAN	VARIANCE	I.V.	RE.	KP	DISPERSION	1/(I.V)**
	SECS	SEC**2	CM/SEC				
293.0	249.6225	3433.07	4.3467	0.2043	53.8904	0.0729	0.0529
293.0	224.6597	2916.59	4.8204	0.2265	53.7859	0.0689	0.0430
293.0	217.0901	2500.05	5.1397	0.2415	55.4336	0.0593	0.0379
293.0	201.4973	2001.97	5.5831	0.2624	55.8950	0.0508	0.0321
293.0	180.5720	1682.35	6.1097	0.2871	54.8042	0.0486	0.0268
293.0	167.3222	1521.26	6.5331	0.3070	54.2967	0.0478	0.0234

CO PULSE (1.0=0.63CM) HE CARRIER H-MORDENITE (673 K - 24 H)

LEN	DIAM	EPS	DIAMP	THETA	ROE	MU :
11.50	0.63	0.37	0.0602	0.2800	0.000156	0.000200

TEMP (K)	MEAN	VARIANCE	I.V.	RE.	KP	DISPERSION	1/(I.V)**
	SECS	SEC**2	CM/SEC				
273.0	617.2563	23069.36	1.6272	0.0765	50.7065	0.2140	0.3777
273.0	331.9058	4671.58	3.2592	0.1532	54.6568	0.0748	0.0941
273.0	208.6602	2471.02	4.8141	0.2262	50.7133	0.0678	0.0431
273.0	175.1591	1635.91	6.4293	0.3021	56.9248	0.0477	0.0242

CO PULSE (I.D=0.63CM) HE CARRIER H-MORDENITE (673 K - 24 H)

LEN	DIAM	EPS	DIAMP	THETA	ROE	MU :
11.50	0.63	0.37	0.0602	0.3300	0.000156	0.000200

TEMP (K)	MEAN	VARIANCE	I.V.	RE.	KP	DISPERSION	1/(I.V)**2
	SECS	SEC**2	CM/SEC				
263.0	406.8142	7628.87	3.9492	0.1856	80.0710	0.0671	0.0641
263.0	343.0168	5285.12	4.6913	0.2205	80.2031	0.0551	0.0454
263.0	307.9788	4945.25	5.4686	0.2570	83.9676	0.0548	0.0334
263.0	261.8989	2567.58	6.2310	0.2928	81.3415	0.0345	0.0258
263.0	248.0943	2899.38	7.0526	0.3314	87.2560	0.0384	0.0201

CH4 PULSE (I.D=0.63CM) HE CARRIER H-MORDENITE (673 K - 24 H)...MTL2

LEN	DIAM	EPS	DIAMP	THETA	ROE	MU :
11.50	0.63	0.37	0.0602	0.3300	0.000156	0.000200

TEMP (K)	MEAN	VARIANCE	I.V.	RE.	KP	DISPERSION	1/(I.V)
	SECS	SEC**2	CM/SEC				
263.0	39.7539	1299.14	6.2530	0.2939	12.1076	0.7559	0.025
273.0	36.4526	1132.48	6.0269	0.2832	10.6326	0.8131	0.027
283.0	28.3612	482.23	6.2518	0.2938	8.4679	0.5514	0.025
293.0	33.5899	598.41	6.2187	0.2922	10.0805	0.4904	0.025
303.0	30.8949	523.59	6.2765	0.2950	9.3158	0.5025	0.025
313.0	31.1293	523.39	6.2792	0.2951	9.3952	0.4946	0.025
323.0	31.5208	563.20	6.2736	0.2948	9.5117	0.5195	0.025
333.0	27.9348	380.11	6.2845	0.2953	8.3782	0.4457	0.025
343.0	28.3411	432.05	6.2722	0.2948	8.4910	0.4931	0.025

CH4 PULSE (0.5 CC) HE CARRIER H-MORDENITE (673 K - 24 H)

LEN	DIAM	EPS	DIAMP	THETA	ROE	MU :
11.50	0.63	0.37	0.0602	0.3300	0.000156	0.000200

TEMP (K)	MEAN	VARIANCE	I.V.	RE.	KP	DISPERSION	1/(I.V)**4
	SECS	SEC**2	CM/SEC				
313.0	40.3792	645.18	2.8247	0.1327	5.2377	0.8055	0.1253
313.0	62.4813	2126.33	3.6672	0.1723	11.1145	0.8540	0.0744
313.0	46.2272	932.08	4.4988	0.2114	10.0335	0.5575	0.0494
313.0	46.1765	1569.61	5.5696	0.2617	12.5471	0.7600	0.0322
313.0	27.2950	411.89	6.4204	0.3017	8.3624	0.4951	0.0243
313.0	22.8328	247.19	7.3345	0.3447	7.9652	0.3717	0.0186

CH4 PULSE (0.5 CC) HE CARRIER H-MORDENITE (673 K - 24 H)

LEN	DIAM	EPS	DIAMP	THETA	ROE	MU :
11.50	0.63	0.37	0.0602	0.3300	0.000156	0.000200

TEMP (K)	MEAN SECS	VARIANCE SEC**2	I.V. CM/SEC	RE.	KP	DISPERSION	1/(I.V)**
293.0	99.0703	1484.01	2.7995	0.1316	13.5769	0.3105	0.1276
293.0	71.9220	787.62	3.5059	0.1648	12.2898	0.2497	0.0814
293.0	56.5758	521.03	4.3212	0.2031	11.8979	0.2166	0.0536
293.0	45.9469	383.31	5.2077	0.2447	11.6326	0.2005	0.0369
293.0	41.8949	358.75	6.0694	0.2852	12.3985	0.1936	0.0271

CH4 PULSE (0.5 CC) HE CARRIER H-MORDENITE (673 K - 24 H)

LEN	DIAM	EPS	DIAMP	THETA	ROE	MU :
11.50	0.63	0.37	0.0602	0.3300	0.000156	0.000200

TEMP (K)	MEAN SECS	VARIANCE SEC**2	I.V. CM/SEC	RE.	KP	DISPERSION	1/(I.V)
273.0	136.2013	8165.12	2.4637	0.1158	16.5497	1.0273	0.164
273.0	75.2501	3097.06	3.1986	0.1503	11.7049	0.9832	0.097
273.0	68.4860	3121.65	3.9239	0.1844	13.1367	0.9753	0.064
273.0	32.2957	591.80	5.5999	0.2632	8.6488	0.5826	0.031
273.0	26.1994	393.66	6.3972	0.3006	7.9721	0.5155	0.024

CH4 PULSE (0.5 CC) HE CARRIER H-MORDENITE (673 K - 24 H)

LEN	DIAH	EPS	DIAMP	THETA	ROE	MU :
11.50	0.63	0.37	0.0602	0.3300	0.000156	0.000200

TEMP (K)	MEAN	VARIANCE	I.V.	RE.	KP	DISPERSION	1/(1.V)**
	SECS	SEC**2	CM/SEC				
263.0	74.0141	4430.25	4.2185	0.1982	15.3580	1.1023	0.0562
263.0	85.6020	6450.79	4.6799	0.2199	19.8717	1.0816	0.0457
263.0	42.5124	1304.94	5.0481	0.2372	10.3727	0.8224	0.0392
263.0	44.7819	1762.29	5.3948	0.2535	11.7506	0.9366	0.0344
263.0	31.8364	820.89	5.8093	0.2730	8.8578	0.8017	0.0296

N2 PULSE (0.5 CC) HE CARRIER 4A-ZEOLITE (673 K - 24 H)

LEN	DIAM	EPS	DIAMP	THETA	ROE	MU :
11.50	0.63	0.37	0.0602	0.3300	0.000156	0.000200

TEMP (K)	MEAN	VARIANCE	I.V.	RE.	KP	DISPERSION	1/(I.V)**2
	SECS	SEC**2	CM/SEC				
263.0	103.2943	3917.88	6.2634	0.2943	32.4532	0.3371	0.0255
273.0	114.3641	4028.90	6.2688	0.2946	36.0260	0.2825	0.0254
283.0	89.7337	2505.31	6.3013	0.2961	28.2896	0.2839	0.0252
293.0	78.8957	1859.42	6.2579	0.2941	24.6269	0.2745	0.0255
303.0	65.0611	927.34	6.2533	0.2939	20.1902	0.2014	0.0256
313.0	34.7564	274.01	6.2748	0.2949	10.5504	0.2079	0.0254
323.0	29.6254	191.15	6.3461	0.2982	9.0141	0.1973	0.0248
333.0	27.2971	122.84	6.1012	0.2867	7.9181	0.1554	0.0269

N2 PULSE (0.5 CC) HE CARRIER 4A-ZEOLITE (673 K - 24 H)

LEN	DIAM	EPS	DIAMP	THETA	ROE	MU :
11.50	0.63	0.37	0.0602	0.3300	0.000156	0.000200

TEMP (K)	MEAN	VARIANCE	I.V.	RE.	KP	DISPERSION	1/(I.V)**
	SECS	SEC**2	CM/SEC				
313.0	75.4142	769.78	2.6356	0.1239	9.5633	0.2953	0.1440
313.0	56.4152	460.10	3.7063	0.1742	10.0911	0.2243	0.0728
313.0	50.2552	407.41	4.3190	0.2030	10.4975	0.2148	0.0536
313.0	47.1036	323.84	4.6364	0.2179	10.5658	0.1810	0.0465
313.0	41.5901	321.59	5.1249	0.2408	10.2979	0.2086	0.0381
313.0	37.8736	264.19	5.4689	0.2570	9.9906	0.1936	0.0334
313.0	37.9043	222.42	5.9123	0.2778	10.8577	0.1506	0.0286
313.0	33.6047	237.82	6.5314	0.3069	10.6218	0.1854	0.0234
313.0	29.8082	195.25	7.0549	0.3315	10.1523	0.1791	0.0201
313.0	31.2012	167.98	7.3014	0.3431	11.0470	0.1359	0.0188

N2 PULSE (0.5 CC) HE CARRIER 4A-ZEOLITE (673 K - 24 H)

LEN	DIAM	EPS	DIAMP	THETA	ROE	MU :
11.50	0.63	0.37	0.0602	0.3300	0.000156	0.000200

TEMP (K)	MEAN SECS	VARIANCE SEC**2	I.V. CM/SEC	RE.	KP	DISPERSION	1/(I.V)**2
293.0	107.7830	1722.18	2.7054	0.1271	14.3044	0.3151	0.1366
293.0	82.5115	1120.38	3.4615	0.1627	13.9987	0.2734	0.0835
293.0	77.9060	1195.18	3.8848	0.1826	14.8691	0.2915	0.0663
293.0	68.8722	914.41	4.2564	0.2000	14.3836	0.2604	0.0552
293.0	62.3947	836.01	4.7584	0.2236	14.5753	0.2595	0.0442
293.0	56.6846	698.50	5.3399	0.2510	14.8711	0.2341	0.0351
293.0	52.8067	662.27	5.6700	0.2665	14.7037	0.2408	0.0311
293.0	49.1516	578.23	6.0511	0.2844	14.6018	0.2274	0.0273
293.0	46.8028	560.59	6.4969	0.3053	14.9417	0.2265	0.0237
293.0	42.9261	478.75	6.7933	0.3193	14.3051	0.2199	0.0217

N2 PULSE (0.5 CC) HE CARRIER 4A-ZEOLITE (673 K - 24 H)

LEN	DIAM	EPS	DIAMP	THETA	ROE	MU :
11.50	0.63	0.37	0.0602	0.3300	0.000156	0.000200

TEMP (K)	MEAN	VARIANCE	I.V.	RE.	KP	DISPERSION	1/(I.V)**
	SECS	SEC**2	CM/SEC				
273.0	115.7505	3221.58	4.1204	0.1936	23.7700	0.3355	0.0589
273.0	102.6049	2612.96	4.4425	0.2088	22.6912	0.3212	0.0507
273.0	92.1976	2382.64	4.9094	0.2307	22.5287	0.3283	0.0415
273.0	80.2857	1900.40	5.2009	0.2444	20.7371	0.3260	0.0370
273.0	86.8954	2169.76	5.5068	0.2588	23.8503	0.3000	0.0330
273.0	71.3480	1775.87	6.1082	0.2871	21.6692	0.3284	0.0268
273.0	69.5223	1706.29	6.4101	0.3012	22.1716	0.3167	0.0243

N2 PULSE (0.5 CC) HE CARRIER 4A-ZEOLITE (673 K - 24 H)

LEN	DIAM	EPS	DIAMP	THETA	ROE	MU :
11.50	0.63	0.37	0.0602	0.3300	0.000156	0.000200

TEMP (K)	MEAN	VARIANCE	I.V.	RE.	KP	DISPERSION	1/(I.V)**
	SECS	SEC**2	CM/SEC				
263.0	144.9393	5428.77	3.9253	0.1845	28.4677	0.3786	0.0649
263.0	150.8250	6357.46	4.4015	0.2068	33.3157	0.3651	0.0516
263.0	125.2030	4381.61	4.6218	0.2172	28.9647	0.3477	0.0468
263.0	119.6944	4391.86	5.1096	0.2401	30.6466	0.3450	0.0383
263.0	107.2473	3326.03	5.3935	0.2535	28.9533	0.3083	0.0344
263.0	101.2506	3515.19	5.9116	0.2778	29.9806	0.3335	0.0286
263.0	100.9046	3525.01	6.2552	0.2940	31.6467	0.3182	0.0256

CO PULSE (0.5 CC) HE CARRIER 4A-ZEOLITE (673 K - 24 H)...RIL2

LEN	DIAM	EPS	DIAMP	THETA	ROE	MU :
11.50	0.63	0.37	0.0602	0.3300	0.000156	0.000200

TEMP (K)	MEAN	VARIANCE	I.V.	RE.	KP	DISPERSION	1/(I.V)**2
	SECS	SEC**2	CM/SEC				
273.0	21.9524	42.79	6.2860	0.2954	6.4600	0.0812	0.0253
283.0	14.0355	20.19	6.2510	0.2938	3.8934	0.0943	0.0256
293.0	25.7949	68.95	6.2007	0.2914	7.5811	0.0961	0.0260
303.0	39.0989	147.70	6.2499	0.2937	11.8923	0.0889	0.0256
313.0	27.8191	73.13	6.2453	0.2935	8.2855	0.0870	0.0256
323.0	17.4286	33.55	6.2906	0.2956	5.0118	0.1009	0.0253
333.0	14.9504	23.05	6.1264	0.2879	4.0903	0.0968	0.0266

CO PULSE (0.5 CC) HE CARRIER 4A-ZEOLITE (673 K - 24 HI...SIL?

LEN	DIAM	EPS	DIAMP	THETA	ROT	MU :
11.50	0.63	0.37	0.0602	0.4700	0.000156	0.000200

TEMP (K)	MEAN	VARIANCE	I.V.	RE.	KP	DISPERSION	1/(I.V)**2
	SECS	SEC**2	CM/SEC				
313.0	157.5590	1884.04	4.6789	0.2199	37.0616	0.0908	0.0457
313.0	149.9363	1228.24	5.0565	0.2376	36.1310	0.0621	0.0391
313.0	12[illegible].8211	958.06	5.6149	0.2639	36.3523	0.0591	0.0317
313.0	115.7609	796.48	6.0467	0.2848	36.1720	0.0565	0.0273
313.0	114.4691	805.82	6.4768	0.3042	37.2618	0.0548	0.0239
313.0	103.1134	591.37	6.9607	0.3271	36.0[illegible]7	0.0459	0.0206
313.0	99.7955	552.67	7.2118	0.3339	36.1677	0.0442	0.0192

CO PULSE (0.5 CC) HE CARRIER 4A-ZEOLITE (573 K - 24 H)

LEN	DIAM	EPS	DIAMP	THETA	ROE	MU :
11.50	0.63	0.37	0.0602	0.4700	0.000156	0.000200

TEMP (K)	MEAN SECS	VARIANCE SEC**2	I.V. CM/SEC	RE.	KP	DISPERSION	1/(I.V)**
293.0	276.9492	4237.73	4.4211	0.2078	61.9432	0.0719	0.0512
293.0	261.6285	3939.72	4.7630	0.2238	63.0514	0.0695	0.0441
293.0	262.9521	3733.18	5.0962	0.2395	67.8492	0.0609	0.0385
293.0	224.2195	2873.59	5.6654	0.2662	64.2865	0.0580	0.0312
293.0	215.5429	2658.58	6.1244	0.2878	66.8285	0.0537	0.0267
293.0	207.9531	2328.14	6.4172	0.3016	67.5640	0.0482	0.0243

CO PULSE (0.5 CC) HE CARRIER 4A-ZEOLITE (673 K - 24 H)

LEN	DIAM	EPS	DIAMP	THETA	RCE	MU :
11.50	0.63	0.37	0.0602	0.4700	0.000156	0.000200

TEMP (K)	MEAN SECS	VARIANCE SEC**2	I.V. CM/SEC	RE.	KP	DISPERSION	1/(I.V)**2
273.0	531.1145	14443.13	4.7919	0.2252	129.3867	0.0614	0.0436
273.0	472.9614	12313.75	5.3675	0.2522	129.0595	0.0590	0.0347
273.0	481.9065	12002.45	5.7097	0.2683	139.9225	0.0520	0.0307
273.0	433.4067	10178.19	5.9721	0.2807	131.5995	0.0522	0.0280
273.0	394.4531	8905.68	6.3795	0.2998	127.9253	0.0516	0.0246

CO PULSE (0.5 CC) HE CARRIER 4A-ZEOLITE (673 K - 24 H)

LEN	DIAM	EPS	DIAMP	THETA	ROE	MU :
17.50	0.63	0.37	0.0602	0.4700	0.000156	0.000200

TEMP (K)	MEAN	VARIANCE	I.V.	RE.	KP	DISPERSION	1/(I.V)**2
	SECS	SEC**2	CM/SEC				
263.0	353.0779	35275.96	4.0947	0.2206	203.9483	0.0594	0.0454
263.0	307.0671	33117.98	5.1094	0.2401	210.0144	0.0572	0.0383
263.0	726.3652	27335.70	5.3570	0.2518	198.1334	0.0566	0.0348
263.0	697.2292	26014.99	5.8488	0.2749	207.2715	0.0526	0.0292
263.0	637.4424	22501.22	6.1459	0.2886	199.4336	0.0513	0.0265

CH4 PULSE (0.5 CC) HE CARRIER 4A-ZEOLITE (673 K - 24 H)

LEN	DIAM	EPS	DIAMP	THETA	ROE	MU :
11.50	0.63	0.37	0.0602	0.3300	0.000156	0.000200

TEMP (K)	MEAN SECS	VARIANCE SEC**2	I.V. CM/SEC	RE.	KP	DISPERSION	1/(I.V)**2
243.0	44.5749	1609.12	6.2754	0.2949	13.6982	0.7421	0.0254
253.0	39.9305	1109.55	6.2673	0.2945	12.1932	0.6384	0.0255
263.0	37.9979	1183.16	6.3265	0.2973	11.6896	0.7448	0.0250
273.0	47.5816	1733.31	6.3095	0.2965	14.7446	0.6977	0.0251
283.0	50.1354	1920.51	6.3228	0.2971	15.6015	0.6948	0.0250
293.0	56.8604	2551.15	6.2610	0.2942	17.5937	0.7247	0.0255
303.0	49.6746	1720.60	6.2549	0.2939	15.2806	0.6410	0.0256
313.0	44.0491	1515.49	6.2879	0.2955	13.5576	0.7142	0.0253
323.0	41.0179	1238.38	6.3506	0.2984	12.7157	0.6664	0.0248
333.0	46.2616	1538.30	6.1681	0.2899	13.9853	0.6701	0.0263

N2 PULSE (0.5 CC) HE CARRIER 5A-ZEOLITE (673 K - 24 H)

LEN	DIAM	EPS	DIAMP	THETA	RDE	MU :
11.50	0.63	0.37	0.0602	0.3300	0.000156	0.000200

TEMP (K)	MEAN	VARIANCE	I.V.	RE.	KP	DISPERSION	1/(I.V)**2
	SECS	SEC**2	CM/SEC				
273.0	134.6515	660.90	6.2764	0.2950	42.5732	0.0334	0.0254
283.0	104.3826	396.80	6.2610	0.2942	32.7886	0.0334	0.0255
293.0	100.9433	394.69	6.2282	0.2927	31.5198	0.0358	0.0258
313.0	51.1796	95.39	6.2792	0.2951	15.8249	0.0333	0.0254
323.0	41.6942	64.85	6.2575	0.2941	12.7369	0.0343	0.0255
333.0	36.4975	47.52	6.0582	0.2847	10.7046	0.0339	0.0272

CO PULSE (0.5 CC) HE CARRIER 5A-ZEOLITE (673 K - 24 H)

LEN	DIAM	EPS	DIAMP	THETA	ROE	MU :
11.50	0.63	0.37	0.0602	0.3300	0.000156	0.000200

TEMP (K).	MEAN SECS	VARIANCE SEC**2	I.V. CM/SEC	RE.	KP	DISPERSION	1/(I.V)**2
303.0	364.5471	4909.62	6.2854	0.2954	116.4302	0.0338	0.0253
313.0	265.7144	2700.03	6.3141	0.2967	85.0944	0.0348	0.0251
323.0	191.0793	1339.07	6.2660	0.2945	60.5589	0.0337	0.0255
333.0	152.2732	858.02	6.0806	0.2858	46.6988	0.0350	0.0270

CH4 PULSE (0.5 CC) HE CARRIER 5A-ZEOLITE (673 K - 24 H)

LEN	DIAM	EPS	DIAMP	THETA	ROE	MU :
11.50	0.63	0.37	0.0602	0.3300	0.000156	0.000200

TEMP (K)	MEAN	VARIANCE	I.V.	RE.	KP	DISPERSION	1/(I.V)**2
	SECS	SEC**2	CM/SEC				
273.0	183.9386	1555.94	6.2372	0.2931	58.0034	0.0424	0.0257
283.0	137.5863	779.14	6.2237	0.2925	43.1432	0.0380	0.0258
293.0	107.1817	457.81	6.2187	0.2922	33.4524	0.0368	0.0259
303.0	85.0077	294.87	6.2242	0.2925	26.4338	0.0377	0.0258
313.0	73.3375	210.84	6.2627	0.2943	22.8687	0.0360	0.0255
323.0	61.9531	151.86	6.3077	0.2964	19.3697	0.0361	0.0251
333.0	49.1267	92.17	6.0582	0.2847	14.6119	0.0362	0.0272

N2 PULSE (0.5 CC) HE CARRIER CHABAZITE (673 K - 24 H)

LEN	DIAM	EPS	DIAMP	THETA	ROE	MU :
11.50	0.63	0.37	0.0602	0.3300	0.000156	0.000200

TEMP (K)	MEAN	VARIANCE	I.V.	RE.	KP	DISPERSION	1/(I.V)**2
	SECS	SEC**2	CM/SEC				
263.0	53.1078	2769.46	6.2149	0.2921	16.2686	0.9065	0.0259
273.0	38.0923	1039.07	6.3489	0.2984	11.7636	0.6485	0.0248
283.0	36.1886	883.31	6.2752	0.2949	11.0101	0.6180	0.0254
293.0	39.1279	1087.31	6.2342	0.2930	11.8703	0.6550	0.0257
303.0	39.2685	909.01	6.2924	0.2957	12.0317	0.5387	0.0253
313.0	32.9137	498.33	6.2536	0.2939	9.9244	0.4230	0.0256
323.0	30.4447	373.80	6.2172	0.2922	9.0792	0.3730	0.0259
333.0	28.6483	258.57	6.2310	0.2928	8.5290	0.2907	0.0258

N2 PULSE (0.5 CC) HE CARRIER CHABAZITE (673 K - 24 H)

LEN	DIAM	EPS	DIAMP	THETA	ROE	MU :
11.50	0.63	0.37	0.0602	0.3300	0.000156	0.000200

TEMP (K)	MEAN	VARIANCE	I.V.	RE.	KP	DISPERSION	1/(I.V)**2
313.0	40.9133	749.49	2.9907	0.1405	5.6624	0.8606	0.1119
313.0	32.9659	554.79	3.6691	0.1724	5.5899	0.8000	0.0743
313.0	29.7656	586.00	4.2423	0.1994	5.8617	0.8964	0.0556
313.0	27.1351	469.85	4.7140	0.2215	5.9453	0.7784	0.0450
313.0	25.9817	490.00	5.1054	0.2399	6.1889	0.8175	0.0384
313.0	21.3524	249.59	5.4940	0.2582	5.4037	0.5730	0.0331
313.0	17.6800	173.73	6.0727	0.2854	4.8958	0.5262	0.0271
313.0	16.7540	161.97	6.4909	0.3050	4.9664	0.5112	0.0237
313.0	15.5412	135.71	6.8237	0.3209	4.8825	0.4731	0.0214
313.0	15.2162	148.67	7.3142	0.3437	5.0965	0.5048	0.0187

N2 PULSE (0.5 CC) HE CARRIER CHABAZITE (673 K - 24 H)

LEN	DIAM	EPS	DIAMP	THETA	ROE	MU :
11.50	0.63	0.37	0.0602	0.3300	0.000156	0.000200

TEMP (K)	MEAN	VARIANCE	I.V.	RE.	KP	DISPERSION	1/(I.V)**2
	SECS	SEC**2	CM/SEC				
293.0	34.7558	987.78	4.3290	0.2034	7.0965	1.0861	0.0534
293.0	31.8337	781.76	4.7843	0.2248	7.1063	0.9271	0.0437
293.0	26.4091	506.57	5.5470	0.2372	6.2196	0.8275	0.0393
293.0	25.0075	562.30	5.6182	0.2640	6.5878	0.9202	0.0317
293.0	20.7686	405.68	6.6205	0.3111	6.4347	0.8169	0.0228
293.0	15.2327	157.02	6.8469	0.3218	4.7391	0.5683	0.0213

N2 PULSE (0.3 CC) HE CARRIER CHABAZITE (673 K - 24 H)

LEN	DIAM	EPS	DIAHP	THETA	RDF	MU :
11.50	0.63	0.37	0.0602	0.3300	0.000156	0.000200

TEMP (K)	MEAN	VARIANCE	I.V.	RE.	KP	DISPERSION	1/(I.V)**
	SECS	SEC**2	CM/SEC				
273.0	40.2437	1319.53	4.0335	0.1896	7.7024	1.1615	-0.0615
273.0	35.7738	1022.28	4.5608	0.2143	7.7451	1.0071	0.0481
273.0	28.6467	687.02	4.7862	0.2249	6.4149	1.0057	0.0437
273.0	18.3893	157.65	5.3248	0.2502	4.4134	0.5034	0.0353
273.0	18.5666	212.08	6.1533	0.2892	5.2469	0.5750	0.0264
273.0	16.2190	138.20	6.4826	0.3046	4.7822	0.4660	0.0238

N2 PULSE (0.5 CC) -- HE CARRIER -- CHABAZITE (673 K - 24 H)

LEN	DIAM	EPS	DIAMP	THETA	ROE	MU :
11.50	0.63	0.37	0.0602	0.3300	0.000156	0.000200

TEMP (K)	MEAN SECS	VARIANCE SEC**2	I.V. CM/SEC	RE.	KP	DISPERSION	1/(I.V)**2
263.0	42.7628	1438.07	3.8857	0.1826	7.8987	1.1637	0.0662
263.0	38.7471	1436.90	4.3519	0.2045	8.0242	1.2646	0.0528
263.0	33.9717	1045.91	4.6109	0.2167	7.4123	1.1302	0.0470
263.0	15.6785	83.05	5.1298	0.2411	3.5201	0.3787	0.0380
263.0	25.7272	559.80	5.4393	0.2556	6.5592	0.8941	0.0338
263.0	18.6110	221.19	5.7883	0.2720	4.9142	0.6344	0.0298
263.0	16.6111	178.00	6.2451	0.2935	4.7106	0.5940	0.0256

CO PULSE (0.5 CC) HE CARRIER CHABAZITE (673 K - 24 H)

LEN	DIAM	EPS	DIAMP	THETA	ROE	MU :
11.50	0.63	0.37	0.0602	0.3300	0.000156	0.000200

TEMP (K)	MEAN	VARIANCE	I.V.	RE.	KP	DISPERSION	1/(I.V)**2
	SECS	SEC**2	CM/SEC				
273.0	6.5774	14.02	6.3095	0.2965	1.5321	0.2953	0.0251
283.0	8.1991	22.57	6.3036	0.2962	2.0522	0.3062	0.0252
303.0	24.0103	195.47	6.3282	0.2974	7.1723	0.3081	0.0250
313.0	31.4832	339.58	6.3136	0.2967	9.5640	0.3120	0.0251
323.0	25.9353	225.33	6.3677	0.2993	7.8468	0.3025	0.0247
333.0	20.3306	131.46	6.1102	0.2871	5.7568	0.2993	0.0268

CH4 PULSE (0.5 CC) HE CARRIER CHABAZITE (673 K - 24 H)

LEN	DIAM	EPS	DIAMP	THETA	ROE	HU :
11.50	0.63	0.37	0.0602	0.3300	0.000156	0.000200

TEMP (K)	MEAN SECS	VARIANCE SEC**2	I.V. CM/SEC	RE.	KP	DISPERSION	1/(I.V)**2
263.0	19.8916	142.38	6.2149	0.2921	5.7261	0.3329	0.0259
273.0	9.6608	16.18	6.2797	0.2951	2.5109	0.1587	0.0254
283.0	9.6719	15.86	6.2593	0.2942	2.5044	0.1557	0.0255
293.0	9.4811	15.49	6.2610	0.2942	2.4443	0.1583	0.0255
303.0	10.5358	42.50	6.3282	0.2974	2.8176	0.3479	0.0250
313.0	11.4474	61.82	6.2453	0.2935	3.0638	0.4343	0.0256
323.0	9.5568	15.55	6.2420	0.2933	2.4592	0.1569	0.0257
333.0	9.2690	9.06	6.2310	0.2928	2.3622	0.0973	0.0258

CO PULSE (1.D=0.63CM) HE-CO CARRIER 5A ZEOLITE (673 K - 24 H)

LEN	DIAM	EPS	DIAMP	THETA	ROE	MU
11.50	0.63	0.37	0.0602	0.2800	0.000156	0.000200

TEMP (K)	PERC	MEAN	VARIANCE	I.V.	RE.	KP	DISPERSION	1/(I.V)**2
		SECS	SEC**2	CM/SEC				
313.0	0.0	91.7450	789.93	16.9099	0.7947	78.6423	0.0319	0.0035
313.0	10.0	55.2647	412.89	16.6054	0.7804	46.2791	0.0468	0.0036
313.0	20.0	35.2100	185.79	16.6054	0.7804	29.2720	0.0519	0.0036
313.0	35.0	23.7906	94.28	18.3984	0.8646	21.7663	0.0521	0.0030
313.0	65.0	16.0721	32.87	18.3984	0.8646	14.5140	0.0398	0.0030
313.0	76.0	13.0065	25.25	19.3256	0.9082	12.2495	0.0444	0.0027
313.0	85.0	9.4536	6.51	19.0855	0.8969	8.6270	0.0219	0.0027
313.0	94.0	6.5941	3.53	19.0855	0.8969	5.8399	0.0245	0.0027

CO PULSE (I.D=0.63CM) HE-CO CARRIER 5A ZEOLITE (673 K - 24 H)

LEN	DIAM	EPS	DIAMP	THETA	ROE	MU :
11.50	0.63	0.37	0.0602	0.2800	0.000156	0.000200

TEMP (K)	PERC	MEAN	VARIANCE	I.V.	RE.	KP	DISPERSION	1/(I.V)**2
		SECS	SEC**2	CM/SEC				
293.0	0.0	169.7560	3060.80	18.0808	0.8502	147.0098	0.0381	0.0031
293.0	13.0	80.0198	1167.45	17.9117	0.8418	72.6103	0.0585	0.0031
293.0	28.0	45.0090	291.04	16.9515	0.7966	38.3773	0.0487	0.0035
293.0	56.0	22.1639	56.80	16.6243	0.7813	18.2298	0.0400	0.0036
293.0	72.0	16.4854	44.88	17.2228	0.8094	13.9126	0.0551	0.0034
293.0	88.0	9.9799	11.69	16.9515	0.7966	8.0524	0.0398	0.0035
293.0	97.0	6.6296	3.29	16.3099	0.7665	4.9348	0.0264	0.0038

CH4 PULSE (1.0-0.63CM) HE-CH4 CARRIER 5A ZEOLITE (673 K - 24 H)

LEN	DIAM	EPS	DIAMP	THETA	ROE	MU :
11.50	0.63	0.37	0.0602	0.2800	0.000156	0.000200

TEMP (K)	PERC	MEAN	VARIANCE	I.V.	RE.	KP	DISPERSION	1/(I.V)**2
	.	SECS	SEC**2	CM/SEC				
313.0	0.0	28.5961	58.03	19.5731	0.9198	27.9970	0.0208	0.0026
313.0	24.0	19.1104	52.20	19.9981	0.9398	18.9301	0.0411	0.0025
313.0	35.0	12.5571	23.43	19.9981	0.9398	12.2372	0.0427	0.0025
313.0	50.0	11.6166	10.29	19.9981	0.9398	11.2767	0.0219	0.0025
313.0	57.0	9.7481	7.27	19.9981	0.9398	9.3684	0.0220	0.0025
313.0	63.0	9.2415	6.64	19.9981	0.9398	8.8510	0.0224	0.0025
313.0	76.0	7.2036	4.15	19.9981	0.9398	6.7697	0.0230	0.0025
313.0	83.0	6.1279	3.99	23.7090	1.1142	6.8324	0.0257	0.0018
313.0	92.0	4.0766	0.48	25.5535	1.2009	4.7327	0.0065	0.0015

CH4 PULSE (I.D=0.63CM) HE-CH4 CARRIER 5A ZEOLITE (673 K - 24 H)

LEN	DIAM	EPS	DIAMP	THETA	ROE	MU
11.50	0.63	0.37	0.0602	0.2800	0.000156	0.000200

TEMP (K)	PERC	MEAN	VARIANCE	I.V.	RE.	KP	DISPERSION	1/(I.V)**2
		SECS	SEC**2	CM/SEC				
293.0	0.0	53.0020	186.34	14.3044	0.6722	38.1317	0.0267	0.0049
293.0	23.0	34.1681	76.02	15.2146	0.7150	25.9614	0.0246	0.0043
293.0	37.0	22.4905	58.97	16.7534	0.7873	18.6554	0.0400	0.0036
293.0	52.0	18.7187	51.49	16.5605	0.7783	15.2439	0.0510	0.0036
293.0	64.0	15.3963	23.87	17.8660	0.8396	13.4605	0.0324	0.0031
293.0	75.0	12.6767	31.42	17.9401	0.8431	11.0270	0.0627	0.0031
293.0	87.0	8.6893	4.74	17.7920	0.8361	7.3080	0.0203	0.0032
293.0	93.0	7.1182	3.08	17.6464	0.8293	5.8276	0.0198	0.0032
293.0	98.0	4.2680	1.34	17.7188	0.8327	3.2747	0.0238	0.0032

CO PULSE (I.D=0.63CM) CO-CH4 CARRIER - 5A ZEOLITE (673 K - 24 H)

LEN	DIAM	EPS	DIAMP	THETA	ROE	MU
11.50	0.63	0.37	0.0602	0.2800	0.000156	0.000200

TEMP (K)	PERC	MEAN	VARIANCE	I.V.	RE.	KP	DISPERSION	1/(I.V)**2
		SECS	SEC**2	CM/SEC				
313.0	0.0	190.2369	3937.07	5.8470	0.2748	56.2183	0.1070	0.0293
313.0	5.0	121.0408	1556.39	5.5195	0.2594	33.5316	0.1107	0.0328
313.0	8.0	107.4563	1297.08	5.2067	0.2447	27.9860	0.1241	0.0369
313.0	13.0	91.9705	785.78	5.1975	0.2443	23.8250	0.1028	0.0370
313.0	22.0	88.4944	814.98	5.1975	0.2443	22.9023	0.1151	0.0370
313.0	38.0	75.7109	523.55	5.2270	0.2456	19.6229	0.1005	0.0366
313.0	65.0	74.4085	506.21	4.7744	0.2244	17.5554	0.1101	0.0439
313.0	92.0	67.9416	356.94	5.2067	0.2447	17.4788	0.0854	0.0369
313.0	98.0	60.4400	283.38	5.2371	0.2461	15.5778	0.0852	0.0365

CO PULSE (I.D=0.63CM) CO-CH4 CARRIER 5A ZEOLITE (673 K - 24 H)

LEN	DIAM	EPS	DIAMP	THETA	ROE	MU :
11.50	0.63	0.37	0.0602	0.2800	0.000156	0.000200

TEMP (K)	PERC	MEAN	VARIANCE	I.V.	RE.	KP	DISPERSION	1/(I.V)**2
		SECS	SEC**2	CM/SEC				
293.0	2.0	223.0968	4944.61	5.3890	0.2533	60.8122	0.1060	0.0344
293.0	5.0	157.2066	3050.40	5.5130	0.2591	43.6738	0.1287	0.0329
293.0	10.0	129.6260	1581.67	5.3821	0.2529	35.0421	0.1006	0.0345
293.0	14.0	120.6271	1579.92	5.2702	0.2477	31.8790	0.1185	0.0360
293.0	45.0	94.4097	778.63	5.0712	0.2383	23.8636	0.0990	0.0389
293.0	60.0	86.9921	636.52	5.1384	0.2415	22.2409	0.0941	0.0379
293.0	96.0	87.0275	510.68	4.7733	0.2243	20.6274	0.0812	0.0439

CH4 PULSE (I.D=0.63CM) CO-CH4 CARRIER 5A ZEOLITE (673 K - 24 H)

LEN	DIAM	EPS	DIAMP	THETA	ROE	MU :
11.50	0.63	0.37	0.0602	0.2800	0.000156	0.000200

TEMP (K)	PERC	MEAN	VARIANCE	I.V.	RE.	KP	DISPERSION	1/(I.V)**2
		SECS	SEC**2	CM/SEC				
293.0	0.0	164.7700	1515.58	2.3001	0.1081	18.7675	0.1396	0.1890
293.0	6.0	163.1910	1645.92	2.6170	0.1230	21.2231	0.1358	0.1460
293.0	15.0	131.3962	1438.75	3.0235	0.1421	19.7012	0.1585	0.1094
293.0	25.0	123.9740	1172.47	4.2213	0.1984	26.1391	0.1039	0.0561
293.0	34.0	111.6763	1236.30	5.2762	0.2480	29.5043	0.1080	0.0359
293.0	53.0	96.3412	1372.13	6.1511	0.2891	29.6769	0.1382	0.0264
293.0	76.0	70.8163	879.24	8.4762	0.3983	30.0674	0.1189	0.0139

CH4 PULSE (I.D=0.63CM) CO-CH4 CARRIER 5A ZEOLITE (673 K - 24 H)

LEN	DIAM	EPS	DIAMP	THETA	ROE	MU :
11.50	0.63	0.37	0.0602	0.2800	0.000156	0.000200

TEMP (K)	PERC	MEAN	VARIANCE	I.V.	RE.	KP	DISPERSION	1/(I.V)**2
		SECS	SEC**2	CM/SEC				
313.0	0.0	35.8040	138.06	8.3777	0.3837	14.7313	0.0739	0.0142
313.0	4.0	36.2602	142.65	9.1992	0.4323	16.4477	0.0678	0.0118
313.0	13.0	45.2538	239.71	9.2176	0.4332	20.7154	0.0730	0.0118
313.0	28.0	49.2566	266.56	8.4246	0.3959	20.6050	0.0760	0.0141
313.0	45.0	52.7661	278.12	8.4007	0.3948	22.0504	0.0684	0.0142
313.0	56.0	60.7932	312.75	8.2875	0.3895	25.1429	0.0587	0.0146
313.0	75.0	65.5260	395.81	8.2627	0.3883	27.0629	0.0642	0.0146